ABSTRACT

Title of Thesis: INVESTIGATION OF FUEL-AIR MIXING IN A MICRO-FLAMEHOLDER FOR MICRO-POWER AND SCRAMJET APPLICATIONS

Kiran Hamilton Jeffrey Dellimore,
Master of Science, 2005

Thesis Directed By: Assistant Professor Christopher P. Cadou
Department of Aerospace Engineering

This thesis presents a first principles model of the fuel-air mixing process in a micro-flameholder. This model is used to identify key design parameters involved in fuel-air mixing and to characterize how mixing performance scales with the Reynolds number. The results of this analysis show that fuel-air mixing in micro-flameholders occurs primarily at low Reynolds numbers ($1<Re<5x10^3$) traditionally associated with the laminar to transitional flow regime. Mixing lengths in micro-flameholders based solely on molecular diffusion are also predicted using a modified Burke-Schumann model. The predicted mixing lengths indicate that less distance is required for fuel-air mixing as micro-flameholders get smaller. Axisymmetric CFD simulations are performed to validate the predictions of the Burke-Schumann model, and to investigate the importance of axial diffusion and viscous effects. The results of these simulations suggest that viscous shear at the wall and at the fuel-air interface can significantly impact mixing lengths in micro-flameholders.

INVESTIGATION OF FUEL-AIR MIXING IN A MICRO-FLAMEHOLDER FOR MICRO-POWER AND SCRAMJET APPLICATIONS

By

Kiran Hamilton Jeffrey Dellimore

Thesis submitted to the Faculty of the Graduate School of the
University of Maryland, College Park, in partial fulfillment
of the requirements for the degree of
Master of Science
2005

Advisory Committee:
Assistant Professor Christopher Cadou, Chair
Associate Professor Andre Marshall
Associate Professor Kenneth Yu

Dedication

For my parents who sacrificed so much in order give me a first class education. I hope this work in some small way can show you that your efforts were not all in vain. This thesis is also dedicated to the memory of my college roommate, Kevin Mark Khan, who took his own life on July 28th, 2003. His death has served as a cautionary reminder for me not to take life too seriously.

Acknowledgements

This work has been sponsored by the Space Vehicles Technology Institute, grant NCC3-989, one of the NASA University Institutes, with joint sponsorship from the Department of Defense. Appreciation is expressed to Claudia Meyer of the NASA Glenn Research Center, program manager of the University Institute activity, and to Dr. John Schmisseur and Dr. Walter Jones of the Air Force Office of Scientific Research.

Table of Contents

List of Tables

List of Figures

Nomenclature

D: diffusivity *(m^2/sec)*

D_{ab}: binary diffusion coefficient *(m^2/sec)*

d_j: Injector port diameter *(m)*

D_h: Hydraulic diameter *(m)*

f: Fuel-air ratio

H: Height of mixing passage *(m)*

i: Number of molecules of oxygen which combine with one molecule of fuel

J: Momentum flux ratio

Kn: Knudsen number

L: Length of mixing passage, characteristic length scale (m)

ℓ_κ: Kolmogorov length scale

$\dot{m}$: Mass flow rate *(kg/sec)*

M: Mach number

N: Number of fuel injectors

P: Static pressure (Pa)

Pe: Peclet number

P_f: Fuel power *(W)*

P_0: Total pressure *(Pa)*

Q_R: Lower heating value *(J/kg)*

R: Gas constant (J/kgK)

Re: Reynolds number

Re_D: Crossflow Reynolds Number

Re_j: Jet Reynolds Number

Re_{ji}: Jet- interface Reynolds Number

Sc: Schmidt number

St: Strouhal number

t: time *(sec)*

T: Static temperature (*K*)

T_0: Total temperature *(K)*

U: Characteristic velocity (*m/sec*)

U_c: Crossflow velocity *(m/sec)*

U_j: Jet velocity *(m/sec)*

W: Width of mixer *(m)*

W/H: Aspect ratio of the passage

Y: species mass fraction

Y_{max}: Maximum jet penetration depth *(m)*

Greek

α: Jet to crossflow velocity ratio

γ: Ratio of specific heats

η: Efficiency, Kolmogorov length scale

λ: Taylor length scale

μ: Dynamic viscosity ($Nsec/m^2$)

ν: Kinematic viscosity (m^2/sec)

ϕ: Equivalence ratio

Π: Pressure ratio

ρ: Density (kg/m^3)

τ_{conv}: Convective mixing time *(sec)*

τ_{dif}: Diffusive mixing time *(sec)*

ζ: Ratio of the diffusive mixing time to the convective mixing time

Subscripts

a: Air

c: Crossflow

conv: Convective

d: Hydraulic diameter

dif: Diffusive

E: Enhanced

f: Fuel

j: Fuel jet

ji: Jet-crossflow interface

κ: Kolmogorov

m: Mixed

ME: Mixing Enhancement

UE: Un-enhanced

Acronyms

AIAA: American Institute of Aeronautics and Astronautics

ASCE: American Society of Civil Engineers

ASME: American Society of Mechanical Engineers

BS: Burke-Schumann

CFD: Computational Fluid Dynamics

FTIR: Fourier Transform Infra-Red

IC: Internal Combustion

IEEE: Institute of Electrical and Electronics Engineers

IR: Infra-Red

MEMS: Micro Electro Mechanical Systems

PLIF: Planar Laser Induced Fluorescence

UAV: Unmanned Air Vehicle

Abbreviations

2-D: two dimensional

3-D: three dimensional

Ann.: Annular

Cann.: Cannular

CO_2: Carbon dioxide

G-G: Gas-Gas

L-G: Liquid-Gas

L-L: Liquid-Liquid

NOx: nitrogen oxides

psi: pounds per square inch

rms: root mean squared

scramjet: supersonic combustion ramjet

Chapter 1: Introduction

1.1 Motivation

Recently, interest in both supersonic combustion and micro-scale combustion has been spurred by efforts to develop scramjet engines and combustion-based micro-power systems. Combustion in both of these situations is made challenging by the inherently short times available for fuel-air mixing and burning [1 & 2]. In the case of supersonic combustion, the situation is further complicated by difficulties associated with holding a flame at supersonic speeds, which makes achieving stable and sustained combustion extremely difficult [3]. In addition, because of NOx emissions concerns and material limitations it is also desirable to operate scramjet and micro-power devices at extremely lean equivalence ratios [4], which adds a further dimension of difficulty to initiating and sustaining combustion, in both scramjets and micro-combustors. In light of these tremendous technical challenges, new techniques must be developed in order to efficiently and rapidly mix fuel and air, so as to create an environment suitable for stable and efficient combustion. The aforementioned provide the motivation for this thesis, which is the investigation of fuel-air mixing in a micro-flameholder that is suitable for combustion initiation and stabilization in scramjet engines or micro-power systems.

A micro-flameholder designed for achieving ignition and flameholding in a scramjet combustor has been previously built and tested experimentally by Mitani et al. in 2001 [5]. The micro-igniter was constructed from copper and measured 15cm in length and 5mm in width, with injector port diameters of 1.4mm and 2.5mm. Using a

hydrogen-oxygen, mixture Mitani et al. showed experimentally that the micro-flameholder could successfully promote ignition in a Mach 2.5 air crossflow. The ignition performance of the micro-flameholder was found to be comparable to that of an oxygen plasma ignition torch; however, a much larger energy input was required for the operation of the micro-igniter.

This thesis seeks to extend the flameholding concept proposed by Mitani et al. by distributing micro-flameholders throughout the scramjet combustion chamber. One possible arrangement is shown below in Figure1-1, where an array of micro-flameholders is integrated into the upper portion of a rearward facing step or 'dump'. The idea is to create a locally well-mixed nearly stoichiometric region near the top of the 'dump' that burns stably and serves as a low-drag pilot to ignite and stabilize combustion in the bulk combustor flow. The micro-burner array consists of three layers: a top layer, which acts as a cover plate; a middle layer, in which fuel and air streams mix; and a bottom layer containing the fuel and air reservoirs.

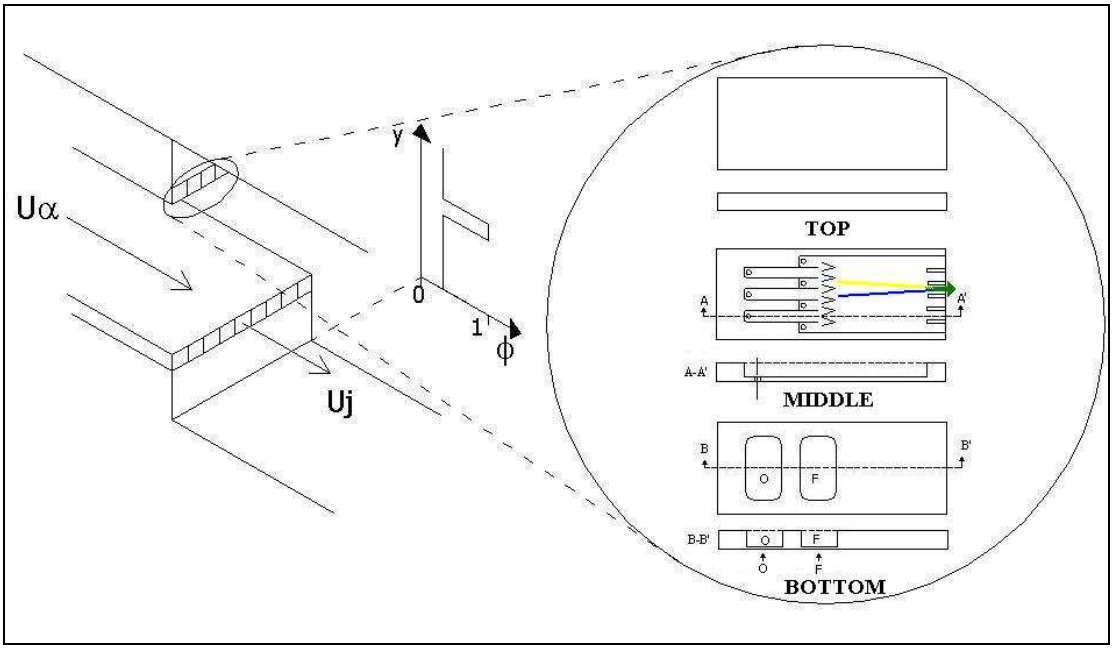

Figure 1-1: Schematic of scramjet micro-flameholder design concept.

An analogous flameholding concept could also be applied to combustion-based micro-power systems. A schematic of a micro-flameholder suitable for use in a micro-power device is illustrated below in Figure 1-2. Mixing is accomplished by the transverse injection of fuel into an air crossflow through multiple, opposed fuel injection ports integrated into a rearward facing step, 'dump' combustor configuration.

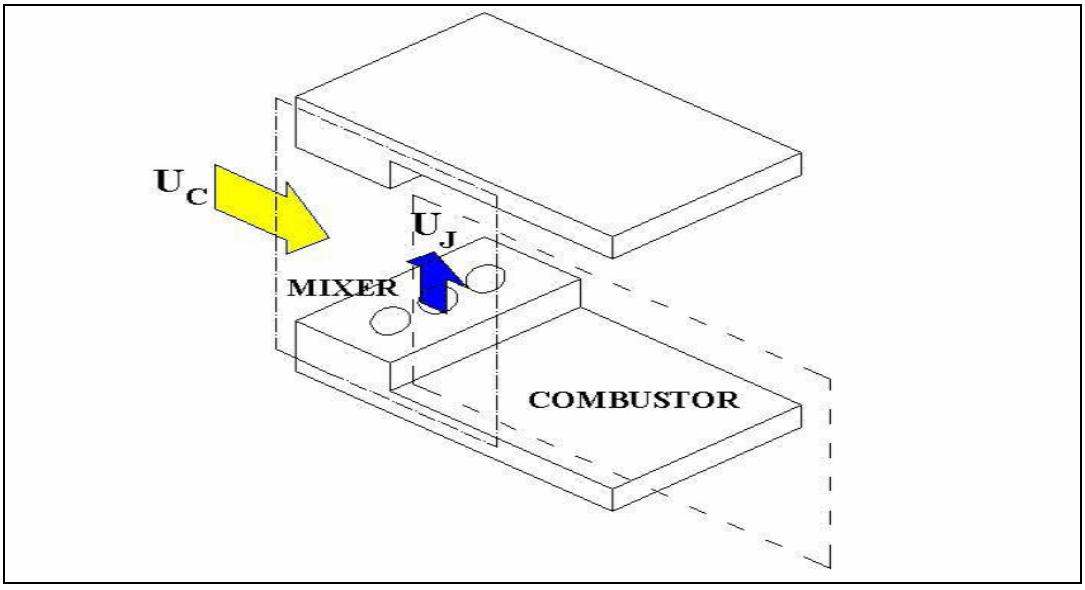

Figure 1-2: Schematic of micro-power system micro-flameholder design concept.

Despite the different appearance of the two micro-flameholder designs shown in Figure 1-1 and Figure 1-2, it is important to recognize that the physical problem is essentially the same in each case. In both concepts mixing is achieved via the injection of fuel into an airflow, inside a passage with small dimensions. The major difference, however, between the scramjet and micro-power system flameholder designs, is in their function. In the former case, the aim of the mixing process is to ignite and stabilize a pilot flame which in turn stabilizes combustion in the bulk flow of the combustor. In contrast, in the latter case the fuel-air mixture leaving the

flameholder is directly burned in the micro-combustor. These similarities and differences present analogous as well disparate design challenges which are discussed in the next section.

1. 2 Micro-flameholder Design Considerations

1.2.1 Basic design challenges for micro-flameholder concept

The design and operation of a micro-flameholder for micro-power or scramjet combustor applications is governed by the following considerations:

1. *Residence time limitations*: In both micro-power systems and in scramjet engines the time available for fuel and air to mix and burn is severely limited. In the case of micro-power systems this is due to their inherently small dimensions and the need to have minimum flow velocities greater than or equal to the laminar flame speed [6]. In the case of scramjet engines, this is due to extremely high velocities, on the order of 1-2km/s, associated with the supersonic flow through the engine and the short combustor lengths, often less than 3m, needed to avoid thermal 'choking' [7].
2. *Fuel-air mixing challenges:* Due to the intrinsically small dimensions associated with a micro-flameholder, it is expected that the Reynolds number of the flow through such a device will be in the laminar flow regime [8]. As a result, a successful micro-flameholder must be able to provide efficient and rapid mixing of fuel and air in the absence of strong inertial forces. This may make mixing difficult because weaker inertial forces will not sustain large concentration gradients, which means molecular diffusion will be slow.

3. *Fabrication and integration issues*: Complex micro-flameholder geometries will need to be avoided in order to ensure that the flameholder is easy to fabricate and in particular, for scramjet applications, also light weight. Simplicity will also make it easier to integrate a micro-flameholder into a micro-combustion system or a scramjet combustor. In the scramjet case, especially, this will simplify the overall combustion system design and will reduce the number of in-stream components that introduce additional frictional and wave drag, as well as heating effects [9] & [10].
4. *Materials limitations:* Gas temperatures in many conventional combustors can approach 2000K [11]. However, most of the current processes used to micro-fabricate MEMS devices are based on silicon which is not an ideal high temperature material since it exhibits creep problems at temperatures above 900K [12] and melts at 1680K [13]. Therefore, it may be necessary to shield or actively cool any micro-fabricated micro-flameholder components from the high temperature combustor environment. Some cooling can come from the fuel, but steps will need to be taken to prevent coking and auto-ignition of the mixture before it leaves the micro-flameholder [8].
5. *Flame stabilization issues*: Using micro-flameholders to stabilize a flame in micro-combustion systems or scramjet combustors presents different challenges. In the case of a scramjet combustor, flame stabilization will be difficult because the flow through the combustor is supersonic. This means that the heat flux from the micro-flameholder will need to be very large in order to initiate and maintain combustion. In addition, it will also be necessary

to stabilize the flame in such a way as to minimize total pressure losses in the combustor, which has a significant effect on the combustor efficiency [9] & [14]. The issues are somewhat different in a micro-combustor. Heat conduction to the combustor walls can lead to quenching but it can also lead to heat recirculation which has a beneficial stabilizing effect [15].

6. *Fuel and air delivery issues:* In order to effectively operate a micro-flameholder, a continuous supply of fuel and air must be provided. In the case of the scramjet combustor application this will require a delivery system which utilizes very little power and which doesn't impair the high speed flow of air through the combustor.

1.2.2 Design Focus

A broad spectrum of micro-flameholder design challenges were identified in the preceding section. However, due to the technical complexity involved, not all of these design considerations can be adequately addressed in this thesis. The main issue is to understand how fuel and air mix at low Reynolds numbers. As a result, the main focus of this study will be to address the challenge of mixing fuel and air in a micro-flameholder by thoroughly characterizing this process.

1.3 Review of Previous Flameholding Research

1.3.1 Introduction:

This section reviews the existing literature on flameholding in an effort to place the current work in the context of what has been previously done. Since flameholding relies on both efficient mixing of fuel and air and efficient as well as stable combustion, we divide the preceding work into two broad categories; fuel-air mixing and combustion stabilization. Further, we make a distinction between work examining these two processes at the 'micro' (length scales < 1mm) and 'conventional' scales (length scales > 10 mm).

1.3.2 Conventional-scale fuel-air mixing:

Fuel-air mixing at the conventional-scale is an extremely complicated process which can be accomplished in many ways using a wide variety of technologies. One of the most common and extensively investigated means of achieving mixing is via the transverse injection of a fuel jet into a crossflow of air (usually air). In this approach, mixing is achieved by the shearing and subsequent breakup of the jet as it penetrates into the crossflow; however, the physics governing this process is extremely complex and is still being actively researched. In general, due to the relatively large characteristic dimensions associated with conventional-scale devices, mixing at the conventional-scale invariably occurs at high Reynolds numbers ($>10^4$) where the flow is inertially-dominated [16]. Accordingly, there is a vast literature describing convectively-dominated (or high Reynolds number) turbulent jet-in-crossflow mixing processes [17-37].

In 1959, Gordier [17] investigated the discharging of turbulent liquid jets into a liquid crossflow. This work was soon followed by several empirical studies involving turbulent gas-gas (G-G) and liquid-gas (L-G) mixing conducted by Keffer et al (1962) [18], Alderberg (1967)[19], Pratte et al. (1967) [20], Margason (1967) [21], Patrick (1967) [22], and Greber et al. (1972 & 1974) [23] & [24]. These studies concentrated on very basic aspects of mixing such as jet trajectory, jet breakup and jet concentration profiles. More recently, numerous, experimental L-L and L-G mixing studies have been carried out by Kelso et al. (1995) [25], Nejad et al. (1996) [26], Faeth et al. (1998) [27], Gonçalves et al. (1999) [28], Johari et al. (1999) [29] and Jackson et al. (2001) [30]. These have focused primarily on the empirical aspects of liquid jet breakup, liquid jet penetration and horseshoe vortex formation, associated with the injection of liquid jets into subsonic air crossflows.

Mixing in supersonic crossflows has also been extensively investigated in the context of supersonic combustion. Over the years a myriad of fuel injection schemes such as flush wall injection and strut injection, among others, have been experimentally and numerically explored for scramjet combustor applications. In 1997 Aso et al. [31] computationally and experimentally studied the supersonic mixing flow-field associated with swept ramped injectors. Based on their results they concluded that strong, longitudinal vortices generated by the sweep angle of the injector, may play a significant role in supersonic mixing. Their results also suggested that an optimum injector sweep angle may lie between 10^0 and 20^0. More recently, in 2000, Mathur et al. [32] conducted experiments to compare the performance of an aerodynamic ramp fuel injector with a 15^0 flush wall injector, in a combustor

simulating Mach 5 flight. Their results showed that the flush wall injection scheme had superior mixing efficiency over the entire range of combustor inlet conditions when compared to the ramp injector. They also found that the aerodynamic ramp injector operated over a narrower range of equivalence ratios ($0.60 < \Phi < 0.80$) compared with the flush wall injector ($0.26 < \Phi < 0.84$) for the same combustor conditions.

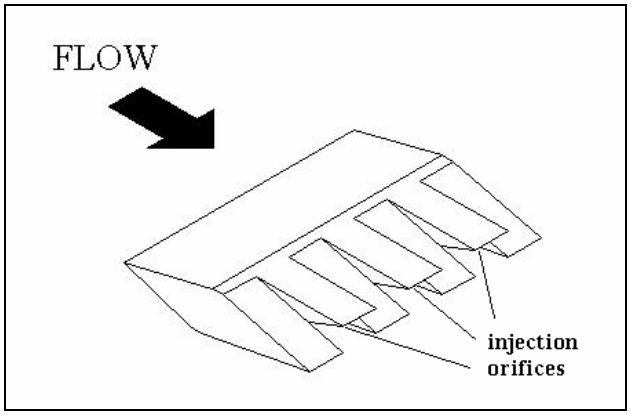

Figure 1-3: Sketch of an alternating double-wedge strut for supersonic mixing enhancement (Adapted from Nishioka et al. (1998) [33])

Many studies have also focused on mixing enhancement in supersonic flows. In 1998, Nishioka et al. [33] performed experiments and numerical simulations to investigate supersonic mixing enhancement using streamwise vortices generated by an alternating, double-wedge strut which is shown above in Figure 1-3. Their results showed that the vortices produced by the alternating wedge strut effectively enhanced mixing by producing a more uniform local equivalence ratio distribution at the exit of the combustor when compared with a multiple orifice injection strut. Further, Chen et al. [34] (1996) experimentally investigated mixing enhancement by comparing the mixing performance of an aerodynamic ramp injection scheme with that of a wall ramp injector in a Mach 2 air crossflow. From their results they concluded that the

aero-ramp injector exhibited a significant increase in jet penetration and mixing efficiency when compared to the wall ramp injector under identical flow conditions. Chen et al. attributed this enhanced mixing to multiplicative fuel-vortex interactions observed near the injection orifices of the aero-ramp.

Several supersonic mixing studies have also investigated cavity-induced mixing enhancement. In 2000 Burnes et al. [35], conducted a series of experiments to determine the physical mechanisms associated with fuel-air mixing enhancement in various acoustically open wall cavity configurations in Mach 2 airflow. Their results showed that for certain cavity aspect ratios, large coherent structures, which may enhance mixing, are periodically generated by a flapping shear layer that covers the entire cavity. Moreover, in 2002, Yu et al [36] examined the effect of duct confinement on cavity-induced supersonic mixing enhancement at various stagnation pressures, ranging from 35 psi to 120 psi. The results of this study demonstrated that flow-induced cavity resonance can be used to enhance supersonic mixing by producing large-amplitude coherent fluctuations. A thorough review of fuel-air mixing enhancement strategies applicable to supersonic flows has been compiled by Seiner et al. [37] (1999). This review provides a detailed discussion of a broad range of passive and active mixing enhancement strategies that have been successfully employed in supersonic flows.

1.3.3 Microscale fuel-air mixing:

Most of the existing work on microscale mixing involves liquid-liquid (L-L) mixing in very low Reynolds number flows (Re < 100). There has been a lot of work focused on mixing very small amounts of liquid, usually on the order of micro- or

nano-liters, for 'lab-on-a-chip' biochemical applications [38-42]. In contrast, there is comparatively little work in microscale gas-gas mixing or liquid-gas mixing that is relevant to micro-flameholders and micro-igniters. A review of the previous microscale liquid-liquid mixing work, while not directly applicable to fuel-air mixing in micro-flameholders, is presented here in order to place the current problem in context.

In 1993 Miyake et al. [38] developed a L-L micro-mixer using plumes to increase the contact area between the liquid components and thus achieve faster mixing via diffusion. This device operates at very low Reynolds numbers on the order of 1. More recently Whitesides et al (2002) [39], developed a chaotic micro-mixer with a staggered 'herringbone' structure for enhancing mixing which works in a flow regime of $0.1 < Re < 100$.

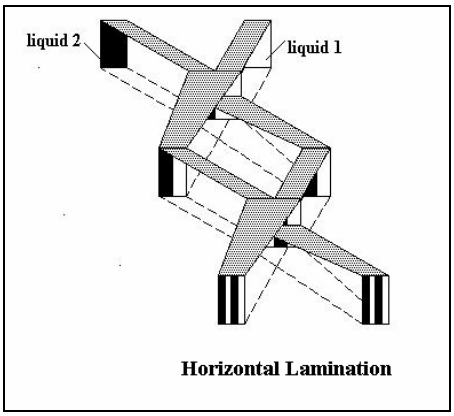

Figure 1-4: Illustration of the concept of mixing by lamination (Adapted from Branebjerg et al. (1996) [42])

Generally, mixing at low Reynolds numbers has been achieved via passive and active strategies or some combination of these two approaches. Beebe et al. [40] have demonstrated passive mixing in a 3-D serpentine micro-channel by using a 'C-shaped' repeating unit to generate chaotic advection. It operated in the range of $6 <$

Re < 70. Chaotic advection has also been employed by Liepmann et al. [41] in the development of a planar laminar mixer for use when Re<5. Branebjerg et al. [42], have used multi-layer lamination to passively mix liquids at Reynolds numbers in range of 2< Re<100. This technique is illustrated in Figure 1-4 and works by increasing the contact area between the liquid components, thereby decreasing the diffusion length required for mixing.

Active L-L mixing techniques such as micro-stirring and cross-stream lamination have been explored by Betz [43] in 2001. In the former, stirring is accomplished by oscillating a 200μm stirrer at low frequencies (10<ν<100 Hz), at the convergence of the two liquid components being mixed. In the latter active mixing occurs since the laminated streams flow perpendicular to each other, in such a way as to continuously stretching and mixing as they propagate along the channel.

G-G microscale mixing of hydrogen and air, as well as propane and air, has been investigated by Mehra [6] (2000) in experimental tests of the MIT micro-engine combustor. This device was designed to achieve fuel-air mixing by employing a jet-in-crossflow mixing strategy based on turbulent correlations by Margason [21] (1968). Although the primary focus of this work was to achieve microscale combustion, Mehra encountered many difficulties in mixing fuel and air, and it was only possible to achieve stable combustion when fuel was injected at the farthest possible point (~10mm) upstream of the combustor. More recent experimental work on pre-mixed flames in a micro-jet burner by Choudhuri et al. [44] (2002) suggested that difficulties in achieving good fuel-air mixing impacted the burner's stability limits. Subsequent 2-D and 3-D CFD simulations at low Reynolds numbers (500 <

Re < 1300), by Anchondo et al. [45-46] (2003&2004) showed that adequate mixing and flame stability could only be achieved at low fuel-air flow rates (<2m/s). Spatial variations in equivalence ratio were relatively large and these led to a narrowing of the overall flammability limits in the simulated burner. This latter work suggests that diffusion may govern fuel-air mixing when the Reynolds number is low.

1.3.4 Conventional-scale combustion stabilization:

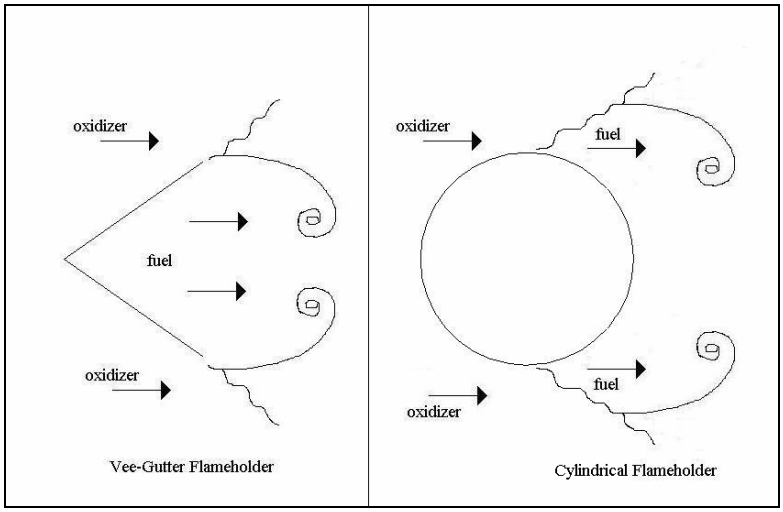

Figure 1-5: Schematic of conventional-scale bluff-body flameholders.

There is an extremely large body of work investigating combustion stabilization in conventional combustors in both subsonic and supersonic flows. The low velocity associated with subsonic flows favors the formation of very steady recirculation zones, where hot products can heat the incoming fuel-air mixture, and in so doing provide conditions conducive to stable combustion. Bluff bodies such as vee-gutters and cylinders, illustrated above in Figure 1-5, are commonly used to generate these recirculation zones.

Much of the early combustion stabilization research was conducted in the 1950's. In 1956, Cornell et al. [47] investigated the flow behind a vee-gutter cascade

in a gas turbine combustor. They compared their experimental results with the predictions of a theoretical model was able to successfully predict the wake shape, the total pressure loss, and the drag force of high blockage cascades of vee-gutter profiles. In the same year, Ames et al. [48] investigated interference effects between multiple bluff-body flameholders, and showed that the maximum blow-off velocity decreased as the number of flameholders increased due to increase in the blockage ratio.

This work was soon followed by Potter et al. [49], in 1958, who conducted experiments to study the effect of pressure and duct geometry on bluff body flame stabilization. Potter et al. found that the variation of blow-off velocity with flameholder size and duct geometry is mainly due to changes in the recirculation zone length. They also found that the variation of blow-off velocity with pressure was the result of the change in the critical time (i.e. the ratio of recirculation-zone length to blow-off velocity) with pressure.

More recently, in 1996, Bardon et al. [50] investigated bluff body flame stabilization tailored to ramjet and afterburner combustors by employing direct fuel injection in the recirculation zone behind the bluff body. Their study showed that this flameholding technique produced significant reductions in unburned hydrocarbons and therefore resulted in improved combustion efficiency. Further, Roquemoore et al. [51] in 2002 developed a new combustion stabilization technique which employs high swirl to enhance the burning rate. Among the advantages of this method are extremely short flame lengths, stable operation at relatively low pressure drop,

improved fuel-air mixing, and high combustion efficiency over a wide operating range ($0.7 < \Phi < 1.7$).

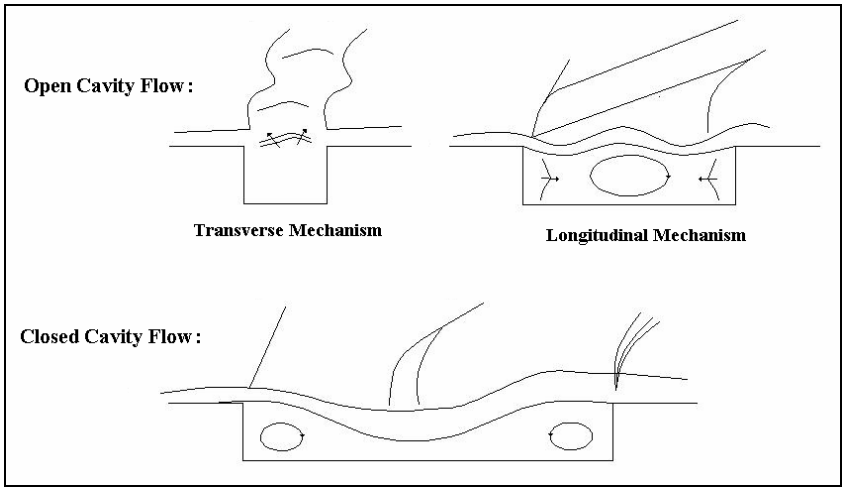

Figure 1-6: Flame stabilization mechanisms associated with cavity flameholders (Adapted from Hanson et al. (1999) [52]).

In recent years, due to renewed interest in scramjet engines for hypersonic flight, supersonic combustion stabilization has become an extremely active area of research. A wide range of both intrusive and non-intrusive flame stabilization techniques including ramps, pylons, and wall-cavities have been experimentally and numerically explored. Particular attention has been given to cavity-based supersonic flameholding, due to the relatively small total pressure losses associated with this form of flame stabilization.

In 1999, Hanson et al. [52] conducted experiments to investigate the influence of cavity flameholder geometry on the combustion of a hydrogen jet in a supersonic combustor simulating a flight Mach number of 10. Using OH-PLIF and schlieren imaging, Hanson et al. observed differences in shockwave structures for various open and closed cavity geometries. From their results they identified three distinct cavity-related flame stabilization mechanisms which are illustrated above in Figure 1-6. In

the same year, Mathur et al. [53] experimentally studied the performance of a cavity flameholder in a direct-connect supersonic combustor simulating flight conditions between Mach 4 and 5. Mathur et al. successfully achieved ignition and sustained combustion inside the cavity using ethylene fuel over a wide range of equivalence ratios ($0.25 < \phi < 0.75$). Their results also indicated that a combustion efficiency of approximately 80% was achieved. Further, in 2001 Sung et al. [54] studied the enhancement and stabilization of liquid kerosene supersonic combustion using various pilot flame and cavity-based flameholder configurations. Their experiments demonstrated that cavity configurations with combined open-closed cavities exhibited better combustion performance than single closed cavity configurations.

Several numerical supersonic combustion stabilization studies have also been performed recently. In 1997, Bowersox et al. [55] numerically investigated the flammability limits of cavity flame holders in supersonic flow using a perfectly stirred reactor model. They found that an important property for flameholding is the lower limit residence time, which is the minimum residence time required to sustain combustion within the reactor. Bowersox et al. also concluded that heat loss significantly reduces flameholding limits by increasing the ignition delay time and the upper limit residence time- the minimum residence time required for auto-ignition. Moreover, in 2002, Mohieldin et al. [56] numerically studied the ignition and flame characteristics of propane combustion in a scramjet engine. Their results suggested that using a swept, rearward-facing step configuration allows for enhanced fuel-air mixing and combustion by creating a low-pressure recirculation region near the base of the step.

1.3.5 Microscale combustion stabilization:

Combustion stabilization on the micro-scale is an emerging field of research which is currently being aggressively investigated. One of the best known micro-combustion research efforts is associated with M.I.T.'s micro-turbojet engine [6]. Ignition and stable micro-combustion has been achieved using both hydrogen and propane fuel, however this has been at the expense of efficiency and has been demonstrated only over a relatively narrow range of operating conditions. Micro-combustion research is also being pursued by Fernandez-Pello et al. [57] in the development of a rotary (Wankel) micro-engine at UC Berkley. Similar efforts have also been undertaken by Dahm et al [58] at the University of Michigan, who are developing a micro-swing engine and by Faulkner et al. [59] at Georgia Tech, who are developing a micro-scale combustor. Although all of these have achieved ignition on the micro-scale, none of them have realized the goal of achieving sustained and efficient microscale combustion under a wide range of operating conditions. In 2002, Gollahalli et al. [60] experimentally investigated the characteristics of micro-jet diffusion flames by measuring flame lengths produced in micro-burners and comparing their results with theoretically predicted flame lengths. They found that the predicted flame lengths did not agree well with the measured values and that micro-burners exhibited very narrow flame stability limits.

In addition to these empirical micro-combustion studies numerous theoretical and numerical investigations have also been pursued. In 2002, Lee et al. [61] theoretically investigated flame propagation in a micro-combustor with non-negligible heat loss at the combustor walls. Their results showed that strong heat loss

at the combustor walls had an adverse effect on the combustion efficiency with this effect being most pronounced at small combustor passage heights. Lee et al. also found that preheating as well as raising the combustor inlet pressure increased both the thermal and combustion efficiency of the micro-combustors being studied.

In 2004, Leach et al. [62] studied the effect of structural heat conduction and heat loss on the power density of silicon micro-combustors using a one-dimensional numerical model with full chemistry which incorporates the heat exchange to and within the combustor walls. The results of this study suggest that axial heat transfer widens combustion stability limits, increases the burning rate, and may enable the construction of smaller, higher power density combustors. Leach et al. also found that heat loss to the environment places a lower bound on the volume of a micro-combustor.

1.4 Organization of the Thesis

This chapter has introduced the concept of a micro-flameholder and identified the main challenges in its design and operation for both micro-power and scramjet applications. It has stated the main focus of this thesis which is to identify the conditions associated with good fuel-air mixing in micro-flameholders, and has presented a brief review of the previous work done in the area of mixing and flameholding.

Chapter two attempts to characterize the fuel-air mixing process in micro-flameholders using simple, first-order models. An analytical model is developed to identify the Reynolds number range expected in micro-flameholders. Next, a simple model based on diffusion flame theory is used to estimate the basic physical size of

micro-flameholders. The chapter concludes by exploring the effect of varying different flameholder operating parameters on fuel-air mixing and by presenting worst-case estimates of the size of micro-flameholders.

Chapter three presents the results of low Reynolds number, two-dimensional, axisymmetric and planar, CFD simulations of fuel-air mixing in micro-flameholders. These results are used to characterize the fuel-air mixing process in a micro-flameholder in greater detail.

Chapter four describes different techniques that can be used to enhance fuel-air mixing in micro-flameholders. This is prefaced by a concise introduction to the basic physics involved in fuel-air mixing and by a simple first order analysis to identify the dominant mixing mechanism in micro-flameholders. The chapter concludes with a brief discussion on how to quantify mixing enhancement.

Chapter five presents a series of experiments that can be used to verify the numerical and analytical results presented in chapters two and three. These experiments are also designed to test the mixing enhancement strategies proposed in chapter four.

Chapter six summarizes the major conclusions of this thesis.

Chapter seven presents recommendations for future work.

Chapter 2: Characterization of Fuel-air Mixing in a Micro-flameholder

2.1 Introduction

The mixing of fuel and air is often an extremely complex process which is accomplished using a variety of technologies. At the most basic level mixing can be characterized using the Reynolds number [63]**.** Physically, the Reynolds number describes the ratio of inertial forces to viscous forces in a fluid flow. It is defined in terms of a characteristic length scale, l, a characteristic velocity, U, the density, ρ, and the dynamic viscosity, μ, of the fluid:

$$Re_l = \frac{\rho U l}{\mu} \tag{2.1}$$

Reynolds numbers less than approximately 2,000 generally indicate that an internal flow is laminar, while Reynolds numbers above approximately 4,000 indicate that an internal flow is fully turbulent [64]. However, it should be pointed out that these limits are somewhat arbitrary since they depend on the geometry and surface properties of the flow channel. For instance, if very smooth channels are used it is possible to delay the transition to turbulence until Reynolds numbers on the order of 10^5 or even 10^6 are reached [64]. Moreover, recent work by Morini et al. [65], Peng et al. [66] and Choi et al. [67] suggests that the laminar-to-turbulent transition in micro-channels may in fact occur at much lower Reynolds numbers than predicted by classical theory (on the order of 1,000 to 2,000).

The Reynolds number is an important parameter because it provides an indication of the nature of the processes governing transport, and consequently mixing. When the Reynolds number is large ($>10^5$), inertial forces are much larger

than viscous forces and fuel-air mixing is dominated by convective transport [63]. Conversely, when the Reynolds number is small (<1), diffusive transport dominates [68 & 69].

Fuel-air mixing in conventional-scale flameholders occurs at relatively large Reynolds numbers (>10^4) where mixing is dominated by convective transport. Accordingly, there is extensive literature describing turbulent (or convectively dominated) mixing processes [17-30, 70-74]. In contrast, there is relatively little work in the open literature that addresses gaseous fuel-air mixing at low Reynolds numbers [6 & 60] where one might expect micro-flameholders to operate. However, since there are currently no operating micro-flameholders it is difficult to say exactly what the appropriate Reynolds number range is in these devices. Therefore, the goal of this chapter is to attempt to characterize fuel-air mixing in a micro-flameholder by identifying the approximate Reynolds number ranges that can be expected and by evaluating the applicability of the existing mixing literature to the prediction of fuel-air mixing performance in these devices.

2.2 Reynolds Number Scaling in Micro-flameholders: Basic Model

2.2.1 Generic Fuel-air Mixing Configuration

A generic representation of the fuel-air mixing process in a micro-flameholder is illustrated in Figure 2-1. The figure shows a fuel jet of velocity U_j, issuing transversely into an air crossflow with velocity U_c. This configuration has the advantage of being simple while still capturing the basic characteristics of mixing in a

micro-flameholder. It is also a mixing scheme that has been extensively investigated [17-30 & 70-74].

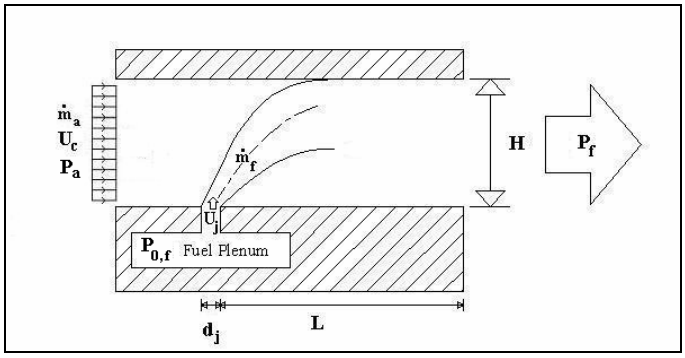

Figure 2-1: Generic configuration for a fuel-air mixing in a micro-flameholder.

Three Reynolds numbers are typically used to characterize fuel-air mixing in this arrangement: the air cross-flow Reynolds number Re_D, the fuel jet Reynolds number Re_j, and the fuel jet-to-air crossflow interface Reynolds number Re_{ji}. The length and velocity scales associated with each are summarized in Table 2.1. Note that D_h is the hydraulic diameter of the cross-flow passage and d_j is the diameter of the fuel jet, injector orifice.

	U	L
Re_D	U_c	D_h
Re_j	U_j	d_j
Re_{ji}	U_c	d_j

Table 2.1: Summary of Reynolds numbers used to characterize fuel-air mixing which are assumed to be common to all configurations.

The viscosity is a property of the working fluid, so Eq. (2.1) indicates that there are two free parameters U and L, which set the Reynolds number in a flameholder. Therefore, determining the Reynolds number range in micro-flameholders requires that we establish how the Reynolds numbers associated with fuel-air mixing, scale with U and L. This is equivalent to establishing how U and L scale with power output.

2.2.2 Constraints on Mixing in a Micro-flameholder

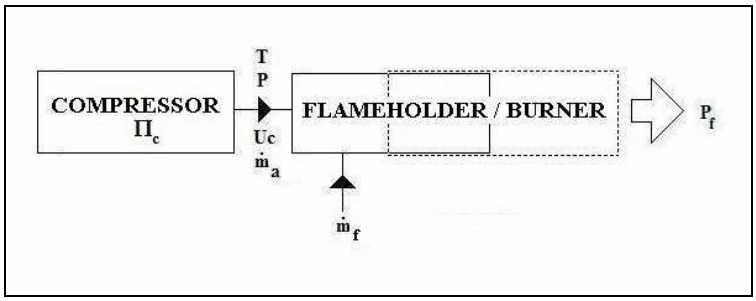

Figure 2-2: Schematic of a generic combustion system.

Constraints on U and L arise in part from the conditions imposed by power system components located upstream and downstream of the flameholder. These components are represented schematically in Figure 2-2. It is assumed that flow is introduced to the mixing section via a compressor which raises its temperature and pressure. Assuming the process is isentropic, the pressure and temperature of the air entering the flameholder are given by:

$$p = p_o \Pi_c \tag{2.2}$$

$$T = T_o \Pi_c^{\gamma-1/\gamma} \tag{2.3}$$

where P_0 and T_0, are the inlet total pressure and temperature respectively, Π_c, is the compression ratio and γ, is the ratio of specific heats.

The velocity of the fluid exiting the mixing section is constrained by the burning rate in the combustor; however, predicting this burning rate in a generic manner is difficult because the achievable burning rate depends on stoichiometry, fuel type and flameholder geometry. A further complication arises from the fact that in many engines the mixing and combustion regions are co-incident (i.e. fuel-injected

spark ignition, compression ignition, and gas turbine engines). However, in all situations the temperature of the reactants gets raised before combustion begins.

In light of these complexities, a more generally applicable limitation is that mixing and combustion process occur in a flow regime free of shock waves and other disturbances where compressibility is negligible:

$$0.01 \leq \frac{U}{\sqrt{\gamma RT}} \leq 0.3 \tag{2.4}$$

The final constraint involves the geometry of the mixing passage. Since we are primarily interested in a micro-scale device that will have to be fabricated using planar photolithography and etching techniques, we assume the flow passages are rectangular in cross-section as illustrated in Figure 2-3.

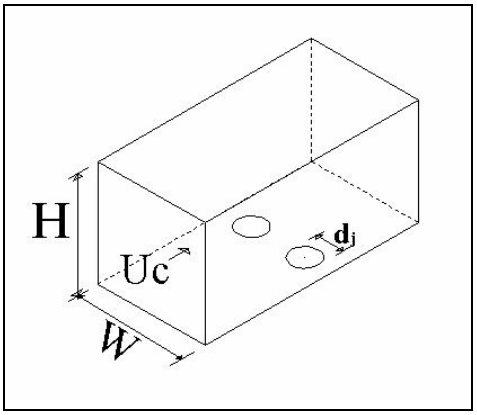

Figure 2-3: Geometry of the fuel-air mixing passage in a micro-flameholder.

In addition, in order to keep the devices in the micro-scale regime, it is assumed that the maximum characteristic dimension of the passage is not greater than 10 mm and not less than 10 micro meters. The latter ensures that the continuum assumption always holds at atmospheric pressure.

$$\begin{aligned} 10x10^{-6}\,m \leq H \leq 10^{-2}\,m \\ 10x10^{-6}\,m \leq W \leq 10^{-2}\,m \end{aligned} \tag{2.5}$$

We are now in a position to compute U and l (and hence Re_D, the first entry in Table 2.1) as a function of device power. Note that in the proceeding sections, power refers to the power associated with the combustion of the fuel. The actual output of the power system depends on the system's overall efficiency. Predicting how the overall efficiency scales with the size of the device is beyond the scope of this work.

2.2.3 Calculation Method

The hydraulic diameter of a flow passage is defined as four times its cross sectional area divided by its perimeter. For the rectangular channels considered here, the hydraulic diameter is:

$$D_h = \frac{4HW}{2(W+H)} \tag{2.6}$$

The velocity scale is the cross-flow velocity, U_c, illustrated in Figure 2-1. It is related to the mass flow rate of air, $\dot{m}_a$, through the engine:

$$U_c = \frac{RT}{P}\frac{\dot{m}_a}{HW} \tag{2.7}$$

where the density is written in terms of the pressure, temperature, and the gas constant for air using the ideal gas law.

The fuel power is the product of fuel's heating value with its mass flow rate, $\dot{m}_f$:

$$P_f = \dot{m}_f Q_R = f\dot{m}_a Q_R \tag{2.8}$$

The fuel-air ratio, f, relates the mass flow rate of fuel to the mass flow rate of air and must lie within a certain range to ensure stable combustion. For the micro-scale power systems considered here, we assume that the fuel is propane burning at an

equivalence ratio of 0.6. This corresponds to $f = 0.038$. Eqs. (2.6), (2.7) and (2.8) can be combined to give an expression for the crossflow Reynolds number that depends on the geometry of the flow passage, and the fuel power:

$$\mathrm{Re}_{Dh} = C_1 \frac{P_f}{(H+W)} \tag{2.9}$$

where the parameters that can be treated as constants are lumped into C_1.

$$C_1 = \frac{2}{\mu_a f Q_R} \tag{2.10}$$

Note that C_1 is not entirely independent of the pressure ratio because the viscosity, μ_a, depends on the mixer inlet temperature. Eqs. (2.9) and (2.10) show how the crossflow Reynolds number scales with the size of the device measured in terms of power output, P_f, and the characteristic dimensions H and W.

So far, we have only considered Reynolds numbers associated with the main air flow through the mixing channel. The next step is to extend this reasoning to develop models for the other two Reynolds numbers that are important for fuel-air mixing: the fuel jet Reynolds number, Re_j, and the jet-interface Reynolds number, Re_{ji}.

The range of possible values of Re_j and Re_{ji} corresponding to a given combination of fuel power, P_f, and crossflow Reynolds number, Re_D, depends on the physical constraints imposed on the fuel injectors. We will begin by assuming that the injectors are round orifices with diameters that are large enough for continuum flow but small enough to fit into the flow channel. This leads to the following constraint on the jet orifice diameter:

$$100\lambda \le d_j \le \frac{W}{2} \tag{2.11}$$

where λ is the mean free path (3.8×10^{-8} m for propane at 1atm. and 300K).

Next, we require that the center-to-center spacing of the injector orifices to be at least twice the orifice diameter, as shown in Figure 2-4. This leads to the following constraint on the number of injectors N:

$$N \le \frac{W}{2d_j} \tag{2.12}$$

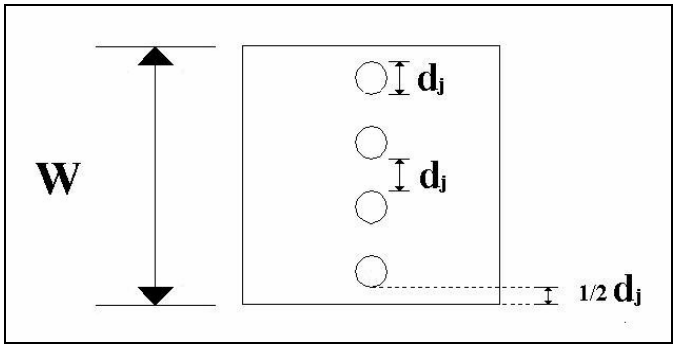

Figure 2-4: Schematic showing the fuel injector spacing in a micro-flameholder.

An additional constraint is that the injectors must be numerous enough and of sufficient size to pass the amount of fuel required to achieve the specified power level. That is:

$$P_f = Nm_f Q_R \tag{2.13}$$

This leads to:

$$U_j = \frac{P_f}{\rho_f Q_R} \frac{4}{N\pi d_j^2} \tag{2.14}$$

Finally, the trajectory of the jet should be such that its maximum penetration depth Y_{max} equals the channel height H. For the purposes of this investigation, the

following expression is used for the maximum penetration depth of a single round jet injected into a circular round duct [75]:

$$Y_{\max} = 1.15 d_j \left(\frac{\rho_f U_j^2}{\rho_a U_c^{\ 2}} \right)^{1/2} \tag{2.15}$$

where the quantity in brackets is the momentum flux ratio, J. Eq. (2.15) is valid for $1 \leq J \leq 10^4$. Applying this constraint to Eq. (2.15), substituting the result into Eq. (2.14), and setting $Y_{max}=H$ (i.e. the jet penetrates the entire channel and just touches the opposite wall) gives the following expression for the jet diameter in terms of the fuel properties, the number of injectors, and the fuel power of the device:

$$d_j = \frac{4.6}{N \pi U_c H} \frac{P_f}{Q_R} \sqrt{\frac{1}{\rho_a \rho_f}} \tag{2.16}$$

Using Eqs. (2.14) and (2.16) to compute the jet Reynolds number gives:

$$\mathrm{Re}_j = C_2 \frac{P_f}{W} \tag{2.17}$$

where the parameters that can be treated as constants are lumped into C_2.

$$\mathrm{C_2} = \frac{0.87}{\mathrm{f Q_R \mu_f}} \sqrt{\frac{\rho_a}{\rho_f}} \tag{2.18}$$

Note, once again that C_2 is not entirely independent of the pressure ratio because the viscosity, μ_f, depends on the flameholder inlet temperature, as do the fuel and air densities, ρ_a and ρ_f. Eqs. (2.17) and (2.18) are solved subject to the additional constraints presented in Eqs. (2.11), and (2.12).

In a similar fashion, Eqs. (2.7) and (2.8) can be combined with Eq. (2.16), to give an expression for the jet-interface Reynolds number, Re_{ji}

$$Re_{ji} = C_3 \frac{P_f}{H} \tag{2.19}$$

where the parameters that can be treated as constants are lumped into C_3.

$$C_3 = \frac{1.46}{N \mu_a Q_R} \sqrt{\frac{\rho_f}{\rho_a}} \tag{2.20}$$

2.2.4 Results

2.2.4.1 Crossflow Reynolds number

Eqs. (2.9) and (2.10) are solved subject to the constraints presented in Eqs. (2.4) and (2.5), to give the range of possible crossflow Reynolds numbers that are associated with fuel-air mixing in micro-flameholders of various sizes (as measured by the overall combustion power, P_f).

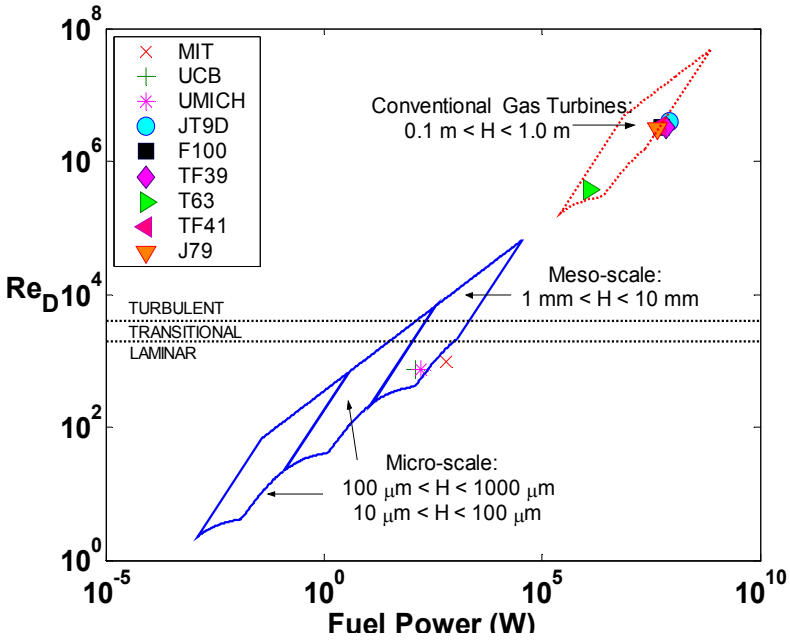

Figure 2-5: Crossflow Reynolds number, Re_D, associated with fuel-air mixing, as a function of power, P_f, associated with complete combustion of propane fuel. The first three symbols correspond to various micro-engines in development [6 & 57-58]; the remaining open symbols correspond to various gas turbine engine combustors [76].

The solid curves in Figure 2-5 bound three regions in (P_f, Re_D) space where fuel-air mixing can be expected to occur in three different size classes of micro-flameholders. The region bounded by the dotted curve shows the model's prediction of the (P_f, Re_D) space associated with fuel-air mixing in conventional-scale gas turbine engines having compression ratios of approximately twenty.

The first three symbols in the figure correspond to the fuel-air mixing regimes found in three micro-engines currently being developed [6 & 57-58]. The remaining solid, symbols correspond to conventional gas turbine combustors [76]. Note that the results appear reasonable as most of the symbols corresponding to micro-engines lie in the micro-area while the symbols corresponding to conventional engines fall in the conventional area. The MIT micro-engine falls slightly outside the boundary because of its cylindrical geometry, which corresponds to a very high W/H in our model. The gas turbine combustor and micro-engine data used in creating Figure 2-5 are summarized in Tables 2.2 and 2.3.

The overall message of Figure 2-5 is that crossflow Reynolds numbers associated with fuel-air mixing in micro-flameholders are generally lower than in conventional systems. As a result, achieving good fuel-air mixing could be proportionally more difficult in micro-flameholders because it will have to rely more on molecular diffusion and less on inertial entrainment.

However, it is also interesting to note that the Reynolds numbers in all but the very smallest devices are not so low that mixing will be completely dominated by molecular diffusion. Instead, Figure 2-5 indicates that mixing in most micro-flameholders will occur in the transitional region where laminar and turbulent

behavior is possible. This makes modeling and predicting the mixing process much more difficult because both molecular and inertial transport will need to be considered.

	JT9D	F100	TF39	T63	TF41	J79	
$\dot{m}_f$	*2.03*	*1.33*	*1.62*	*0.03*	*1.26*	*1.05*	*kg/s*
Uc	*15.1*	*16.8*	*12.0*	*35.1*	*21.1*	*22.8*	*m/s*
L	*0.97*	*0.64*	*0.85*	*0.14*	*0.61*	*0.81*	*M*
F	*0.02*	*0.02*	*0.02*	*0.02*	*0.02*	*0.01*	
Пc	*20*	*20*	*20*	*20*	*20*	*20*	
Type	*ann.*	*ann.*	*ann.*	*can*	*can.*	*can.*	

Table 2.2: Conventional gas turbine combustor data at 796K and 20atm, based on kerosene fuel (Q_R=42.0 MJ/kg), from [76].

	MIT	UCB	UM	
Fuel	*H_2*	*H_2*	*C_4H_{10}*	
Q_R	*120.0*	*120.0*	*45.7*	*MJ/kg*
$\dot{m}_f$	*5.22*	*1.20*	*3.71*	*10^{-6} kg/s*
Uc	*16.0*	*1.46*	*5.73*	*m/s*
L	*0.8*	*9.0*	*2.0*	*Mm*
F	*0.029*	*0.011*	*0.137*	
Пc	*3*	*1*	*1*	
Type	*Gas Turbine*	*Wankel*	*Swing*	

Table 2.3: Existing micro-engine data at 300K and 1atm, estimated from [6 & 57-58].

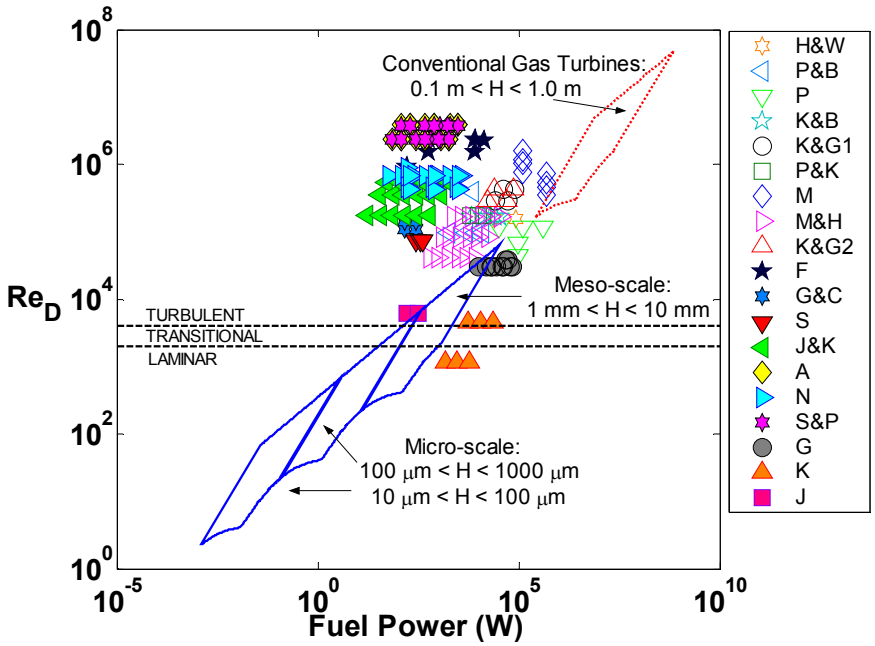

Figure 2-6: Crossflow Reynolds number, Re_D, associated with fuel-air mixing as a function of power, P_f, associated with complete combustion of propane fuel. The open symbols correspond to previous experimental investigations of G-G mixing [18], [20-24] & [70-72] and the solid symbols correspond to L-G [19], [26-28], [30] & [73-74] and L-L [17], [25] & [29] mixing studies.

Figure 2-6 compares the microscale flow regimes to those explored in several well-known investigations [17-30 & 70-74] of the mixing of gaseous and liquid jets in a cross-flow. The solid symbols correspond to experimental investigations of liquid-gas (L-G) and liquid-liquid (L-L) mixing while the open symbols correspond to gas-gas (G-G) mixing. The data corresponding to each study, along with the abbreviations used in the figure, are summarized in Table 2.4. It is important to note that all of these studies involved non-reacting jets. A power was computed for the purpose of comparison with our model by multiplying the stated mass flow rate of injectant by the heating value of propane, Q_R = 46.2 MJ/kg, which serves as a representative fuel for all of the results presented here. The fact that the Reynolds numbers associated with fuel-air mixing in micro-flameholders appear to lie in the region where transitional and laminar behavior is expected, and the fact that very little

previous work has addressed this Reynolds number regime, suggest that additional experiments may be necessary to characterize fuel-air mixing in micro-flameholders.

Symbol	*Ref.*	*Type*	d_j	U_c	U_j	D_h	T	P
K&G1	*[23]*	*G-G*	*4.0*	*0.9-3.7*	*4.6-32.0*	*1.6*	*293.0*	*1.0*
K&B	*[18]*	*G-G*	*3.3-10.0*	*3.0-7.6*	*39.3-409.7*	*0.2*	*340.0*	*1.0*
M	*[21]*	*G-G*	*6.4*	*15.0*	*25.0-85.0*	*0.2*	*600.0*	*1.0*
P	*[22]*	*G-G*	*9.5*	*1.52*	*3.0 - 15.2*	*1.6*	*293.0*	*1.0*
P&K	*[70]*	*G-G*	*6.4*	*1.58*	*6.4-13.1*	*1.6*	*293.0*	*1.0*
P&B	*[20]*	*G-G*	*25.4*	*3.2-9.5*	*7.9-30.8*	*1.6-2.5*	*293.0*	*1.0*
M&H	*[71]*	*G-G*	*2.0-3.3*	*1.3-5.0*	*6.3-62.5*	*0.5*	*293.0*	*1.0*
K&G2	*[24]*	*G-G*	*6.4*	*6.0-9.0*	*27.6-82.6*	*0.7*	*450.0*	*1.0*
H&W	*[72]*	*G-G*	*6.4*	*6.0-9.0*	*17.0-76.4*	*0.7*	*293.0*	*1.0*
F	*[27]*	*L-G*	*0.8-7.0*	*9.7-24.2*	*8.4-11.8*	*1.4*	*297.0*	*1.0*
G&C	*[28]*	*L-G*	*1.0*	*58.3-74.6*	*6.1-11.9*	*0.03*	*303.0*	*1.0*
S	*[73]*	*L-G*	*2.24*	*38.0*	*2.3-3.5*	*0.03*	*300.0*	*1.0*
J&K	*[30]*	*L-G*	*0.5-2.0*	*28.1-84.4*	*2.9-18.4*	*0.1*	*197*	*1.4*
A	*[19]*	*L-G*	*0.8-3.2*	*154.4-257.4*	*4.7-12.8*	*0.2*	*293.0*	*1.0*
N	*[26]*	*L-G*	*0.5-2.0*	*69.2-142.0*	*9.8-37.9*	*0.1*	*306.0*	*1.4*
S&P	*[74]*	*L-G*	*0.8-3.2*	*151.4-244.0*	*4.7-12.9*	*0.2*	*293.0*	*1.0*
G	*[17]*	*L-L*	*9.5-12.7*	*1.2-1.5*	*4.6-24.1*	*0.4*	*293.0*	*1.0*
K	*[25]*	*L-L*	*25.4*	*0.05-0.2*	*0.1-1.5*	*0.4*	*293.0*	*1.0*
J	*[29]*	*L-L*	*3.0*	*0.2*	*0.8-1.5*	*0.6*	*300.0*	*1.0*
		-	*mm*	*m/s*	*m/s*	*m*	*K*	*atm.*

Table 2.4: Experimental data from several well-known non-reacting mixing studies [17-30 & 70-74].

2.2.4.2 Jet Reynolds number

Using similar methods to those used to generate Figures 2-5 and 2-6, Eqs. (2.17) and (2.18) can be solved subject to the constraints given in Eqs. (2.11), (2.12) and (2.15), to obtain the range of possible jet Reynolds numbers that are associated with fuel-air mixing in micro-flameholders of various sizes (as measured by the overall combustion power, P_f).

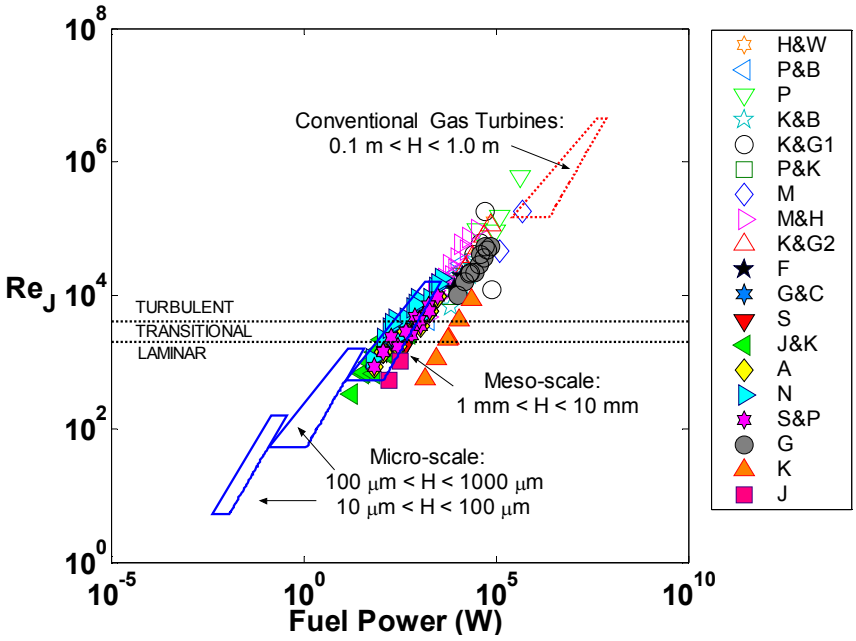

Figure 2-7: Jet Reynolds numbers, Re_j, associated with fuel-air mixing as a function of power, P_f, associated with complete combustion of propane fuel at 300K. The open symbols correspond to previous experimental investigations of G-G mixing [18], [20-24] & [70-72] and the solid symbols correspond to L-G [19], [26-28], [30] & [73-74] and L-L [17], [25] & [29] mixing studies.

Figure 2-7 shows the ranges of jet Reynolds numbers that one would expect in various size classes of micro-flameholders. As with the cross-flow results, the Reynolds numbers for meso-scale flameholders lie in the transitional regime while those associated with micro-scale devices lie mostly in the laminar regime. Note that in spite of the small size of the fuel jets ($2.5\ \mu m \leq d_j \leq 750\mu m$) the Reynolds numbers remain fairly large. This is because even though the diameter of the fuel jets is small,

the jet velocities can be relatively large. The symbols correspond to various experimental investigations [17-30 & 70-74]. While many of these studies extend into the mesoscopic range, the figure shows that the majority of the space associated with micro-flameholders is unexplored.

2.2.4.3 Jet-interface Reynolds number

Finally, we can determine how the jet-interface Reynolds number scales with micro-flameholder size (as measured by the overall combustion power, P_f) by solving Eqs. (2.19) and (2.20), using the same constraints that were applied previously for the jet Reynolds number.

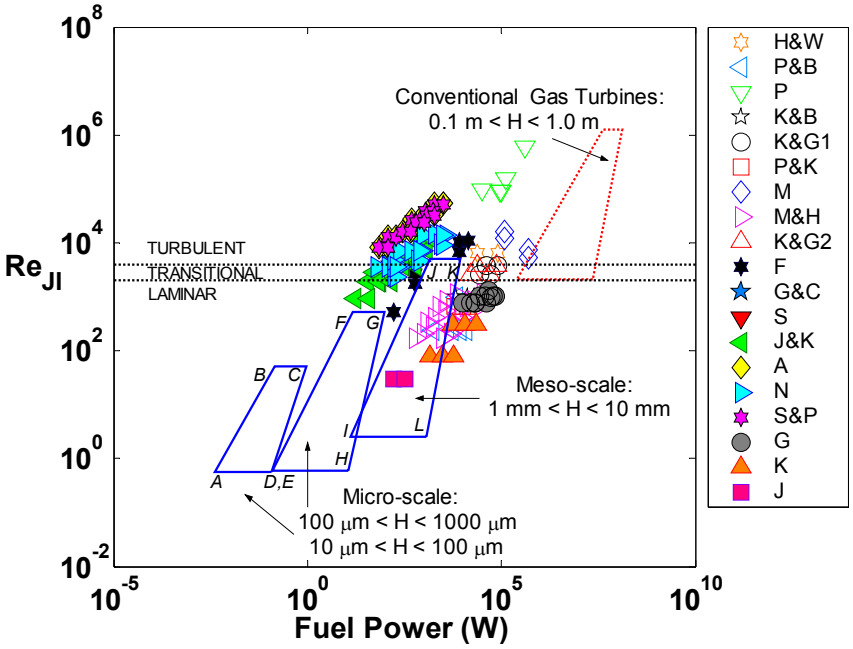

Figure 2-8: Jet-interface Reynolds numbers, Re_{ji}, associated with fuel-air mixing as a function of power, P_f, associated with complete combustion of propane fuel. The open symbols correspond to previous experimental investigations of G-G mixing [18], [20-24] & [70-72] and the solid symbols correspond to L-G [19], [26-28], [30] & [73-74] and L-L [17], [25] & [29] mixing studies.

Figure 2-8 shows the ranges of jet-interface Reynolds numbers that one would expect in various size classes of micro-flameholder. Note that the jet-interface Reynolds numbers are much smaller than the jet and cross-flow Reynolds numbers

because the jets are very small in diameter (2.5 μm ≤ d_j ≤750μm) and the cross-flow velocity is much slower than the jet velocity. The low Reynolds numbers suggest that the flow is predominantly laminar at the jet-crossflow interface and molecular mixing processes are likely to be dominant there. Again, the solid markers show the disconnect between regimes explored in existing literature [17-30 & 70-74] and the regimes associated with micro-power systems.

2.2.4.4 Possible Configuration Variations in Each Mixing Regime

While it is only possible to display two design parameters on the charts, each outlined space encompasses a wide range of passage heights, passage widths, jet diameters, number of jets, etc., that satisfy the imposed constraints. To help provide a sense of the range of parameter combinations that are possible across the spaces corresponding to microscale and meso-scale flameholders, the values of the various flameholder design parameters at the 'corners' of the spaces (labeled A-L) in Figure 2-8 are presented in Table 2.5.

	Re_D	Re_j	Re_{ji}	N	J	H	W	d_j
A	8.6×10^{1}	8.0×10^{1}	1.7×10^{1}	*1*	*2.9*	3.1×10^{1}	1.3×10^{1}	*4.0*
B	1.9×10^{0}	2.7×10^{0}	6.0×10^{-1}	*1*	*2.9*	5.0×10^{0}	5.4×10^{0}	*2.5*
C	1.1×10^{1}	2.7×10^{0}	6.0×10^{-1}	*8*	*1.3*	5.0×10^{1}	5.0×10^{1}	*2.9*
D	$3.1 10^{2}$	8.0×10^{1}	2.7×10^{1}	*8*	*1.8*	5.0×10^{1}	4.7×10^{1}	*2.5*
E	6.8×10^{2}	8.0×10^{2}	104.8	*1*	*7.6*	1.9×10^{2}	1.1×10^{2}	*15.8*
F	1.1×10^{1}	2.7×10^{1}	8.0×10^{-1}	*1*	*132.5*	5.0×10^{1}	5.0×10^{1}	*3.7*
G	1.0×10^{2}	2.7×10^{1}	7.0×10^{-1}	*8*	*1.2*	4.5×10^{2}	4.3×10^{2}	*3.0*
H	3.3×10^{3}	8.0×10^{2}	2.5×10^{2}	*10*	*6.4*	5.0×10^{2}	5.0×10^{2}	*37.8*
I	6.8×10^{3}	8.0×10^{3}	1.1×10^{3}	*1*	*7.3*	2.0×10^{3}	1.0×10^{3}	*16.0*
J	1.1×10^{2}	2.7×10^{2}	1.4×10^{0}	*6*	*132.5*	5.0×10^{2}	5.0×10^{2}	*6.3*
K	2.0×10^{4}	2.7×10^{2}	5.4×10^{0}	*82*	*1.1*	8.8×10^{3}	8.1×10^{3}	*24.7*
L	6.0×10^{4}	8.0×10^{3}	2.8×10^{3}	*29*	*8.4*	1.0×10^{4}	9.2×10^{3}	*42.4*
units	-	-	-	-	-	*μm*	*μm*	*μm*

Table 2.5: Summary of key parameters used to characterize mixing, corresponding to the boundaries of the micro- and meso-scale regions, shown in Figure 2-8.

One of the things that the table illustrates is that comparing devices based on a single parameter can be problematic. For example, flameholders that have similar Re_D, can have very different Re_j and Re_{ji}. As a result, the fuel-air mixing process and performance could vary considerably among micro-flameholders having the same crossflow Reynolds number.

2.2.5 Influence of Micro-flameholder Operating Parameters on the Reynolds Number Range

2.2.5.1 Introduction

In this section we explore how the Reynolds number range is influenced by varying different micro-flameholder operating parameters such as the inlet temperature, the equivalence ratio and the fuel type used. Understanding how each of these parameters affects fuel-air mixing in the micro-flameholder is important in determining an optimum flameholder design. In addition, since the mixing model contains many assumptions, this serves as an additional method of checking that the model's predictions are reasonable.

2.2.5.2 Effect of Preheating on Fuel-air mixing

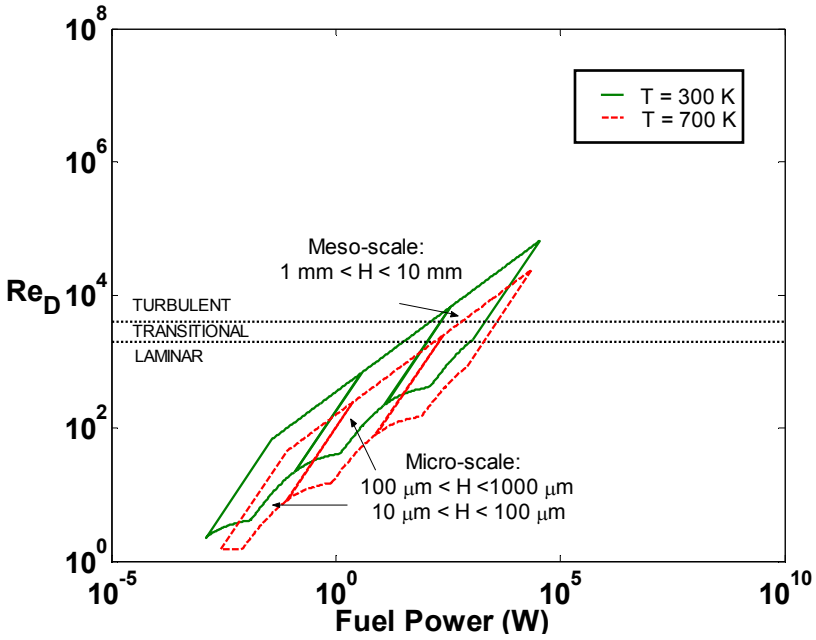

Figure 2-9: Effect of preheating on the crossflow Reynolds number, Re_D, associated with fuel-air mixing as a function of power, P_f, associated with complete combustion of propane fuel.

Preheating of the fuel-air mixture might occur if the flameholder is not well insulated from the hot combustor gases. This is more and more likely as the size of the flameholder is reduced. If the inlet temperature increases, then the viscosity of the gaseous flow entering the flameholder increases. This lowers the Reynolds number, which leads to degraded mixing performance (the reverse would be true for liquid flows, for which viscosity decreases with increasing temperature).

The effect of preheating the fuel-air mixture on the crossflow, jet and jet-interface Reynolds number are shown in Figures 2-9 through 2-11, respectively. Two gas temperatures are compared in the figures: 700K corresponding to a pre-heated micro-flameholder inlet (indicated by the dashed lines), and 300K (indicated by the solid lines), corresponding to a well insulated, un-pre-heated inlet. As expected, pre-

heating significantly lowers the Reynolds number range expected in micro-flameholders.

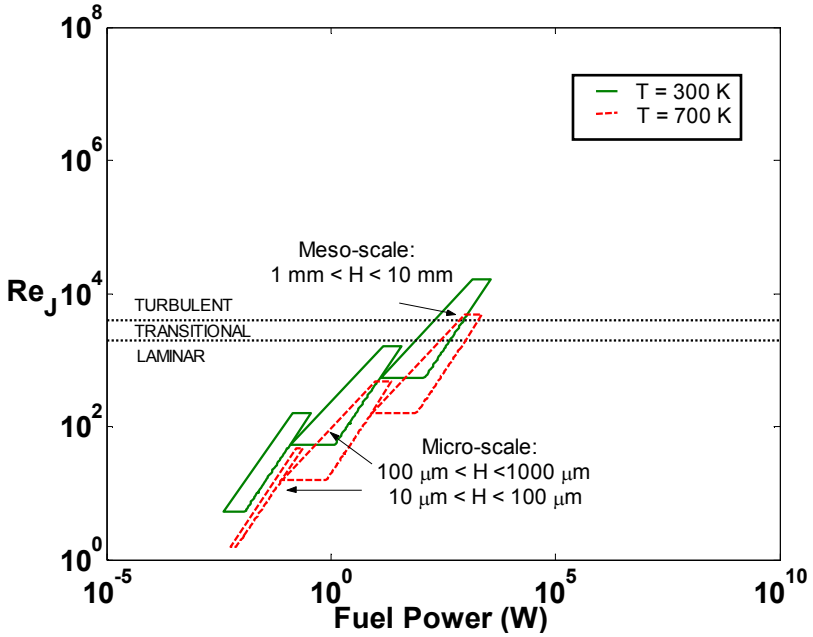

Figure 2-10: Effect of preheating on the jet Reynolds, Re_j, numbers associated with fuel-air mixing as a function of power, P_f, associated with complete combustion of propane fuel.

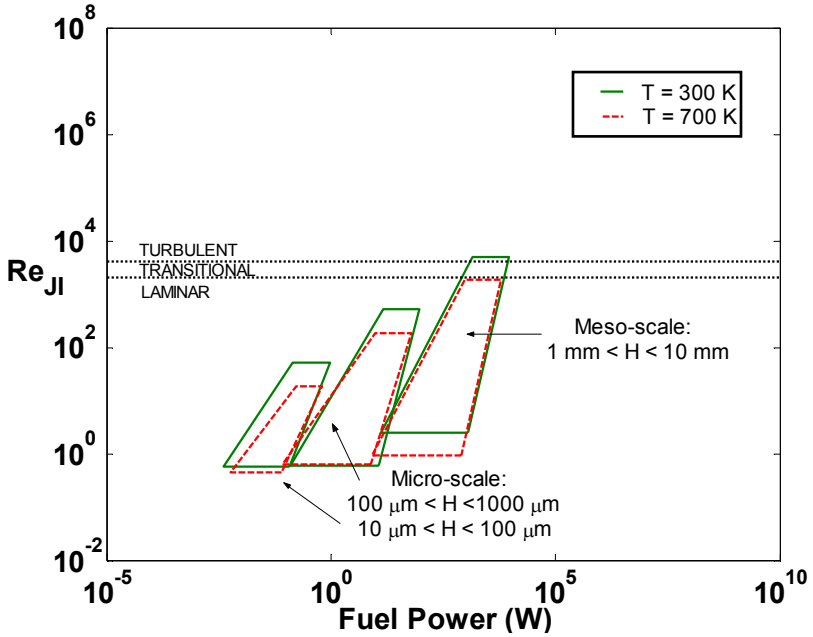

Figure 2-11: Effect of preheating on the jet-interface Reynolds number, Re_{ji}, associated with fuel-air mixing as a function of power, P_f, associated with complete combustion of propane fuel.

2.2.5.3 Effect of Variation in the Equivalence Ratio on Fuel-air Mixing

Figures 2-12 to 2-14 show the effect of varying the equivalence ratio on the crossflow, jet and jet-interface Reynolds numbers respectively. The dashed lines correspond to an equivalence ratio, $\Phi = 0.5$, while the solid lines correspond to $\Phi = 1.0$. The figures show that the equivalence ratio has a relatively small effect on the Reynolds number range. This is expected because the mass flow rate of hydrocarbon fuels is usually very small compared to the air flow rate. It should be noted, however, that increasing the equivalence ratio, increases the overall energy release rate of the device (i.e. P_f) which results in the regions being shifted slightly to the right.

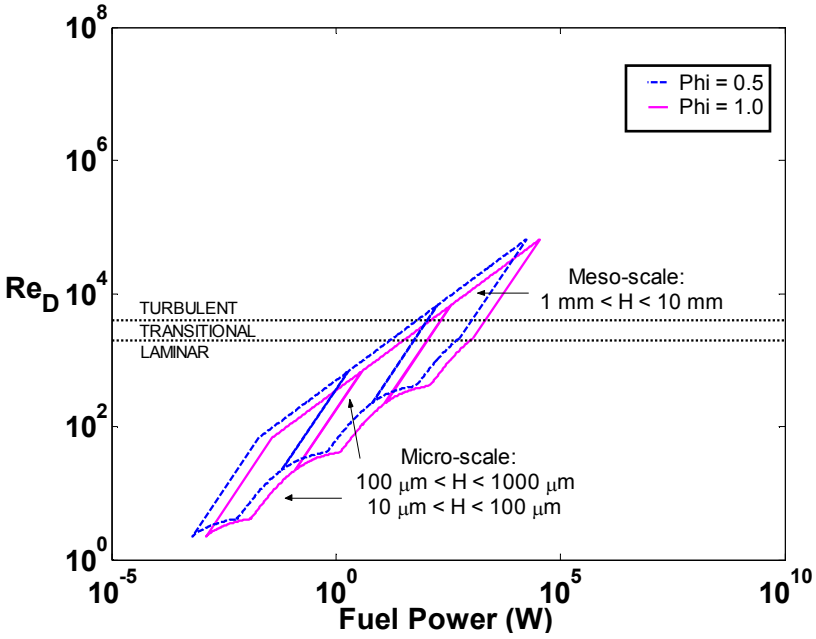

Figure 2-12: Effect of equivalence ratio on the crossflow Reynolds number, Re_D, associated with fuel-air mixing as a function of power, P_f, associated with complete combustion of propane.

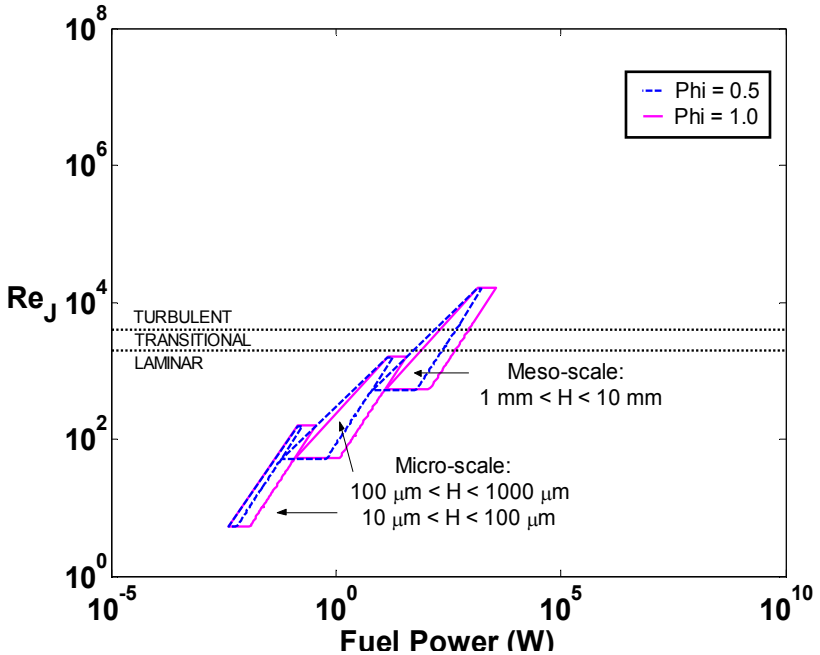

Figure 2-13: Effect of equivalence ratio on the jet Reynolds number, Re_j, associated with fuel-air mixing as a function of power, P_f, associated with complete combustion of propane fuel.

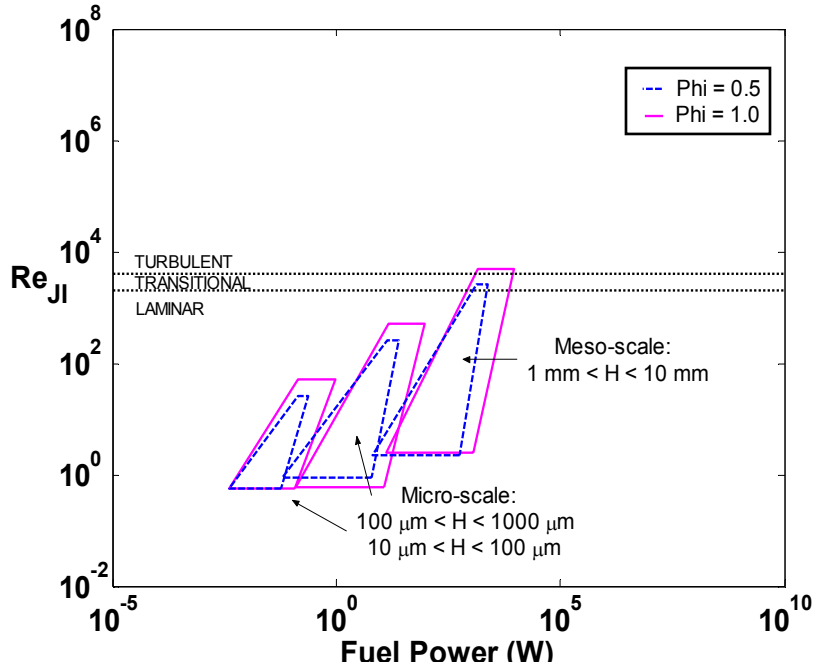

Figure 2-14: Effect of equivalence ratio on the jet-interface Reynolds number, Re_{ji}, associated with fuel-air mixing, as a function of power, P_f, associated with complete combustion of propane fuel.

2.2.5.4 Effect of Fuel Type on Fuel-air Mixing

Changing the fuel type is expected to have a negligible effect on the Reynolds number range associated with mixing in micro-flameholders because hydrocarbon fuels have similar stoichiometric fuel air ratios (around ~0.06). The largest difference in the Reynolds number range should arise when low molecular weight fuels like hydrogen, which has a stoichiometric fuel-air ratio that is roughly half that of most hydrocarbon fuels (0.029) are used. Since, the jet Reynolds number depends on the fuel properties it is reasonable to assume that this Reynolds number will be most sensitive to changes in fuel type.

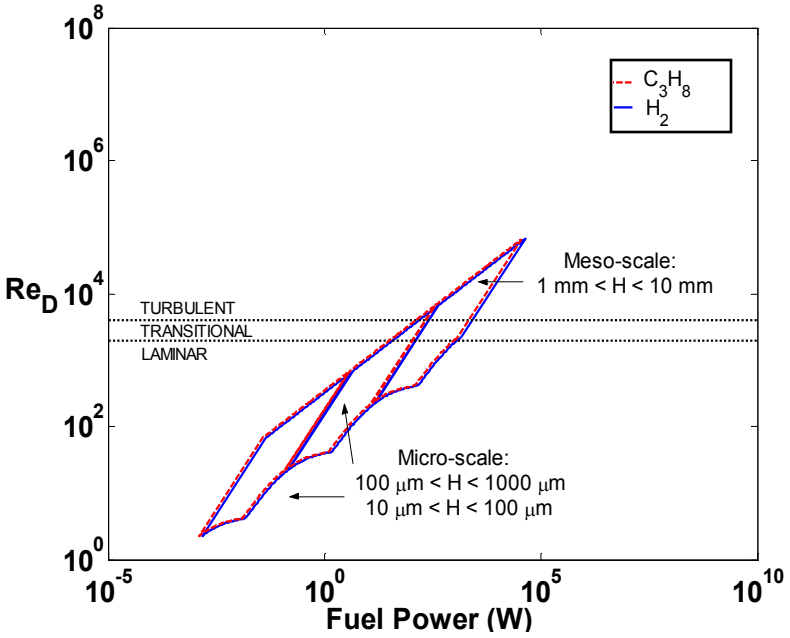

Figure 2-15: Effect of fuel type on the crossflow Reynolds number, Re_D, associated with fuel-air mixing as a function of power, P_f, associated with complete combustion of each fuel.

Figures 2-15 through 2-17, for hydrogen and propane, confirm the assertions of the previous paragraph by showing that the effects of fuel type on the Reynolds number range expected in micro-flameholders are generally negligible. As expected, Figure 2-16 suggests that fuel-air mixing will likely be more difficult in hydrogen-

fueled devices because the Reynolds number range is somewhat lower. Nevertheless, it is also clear that regardless of fuel type used, parts of the Re_j range will still span both the laminar and transitional flow regimes.

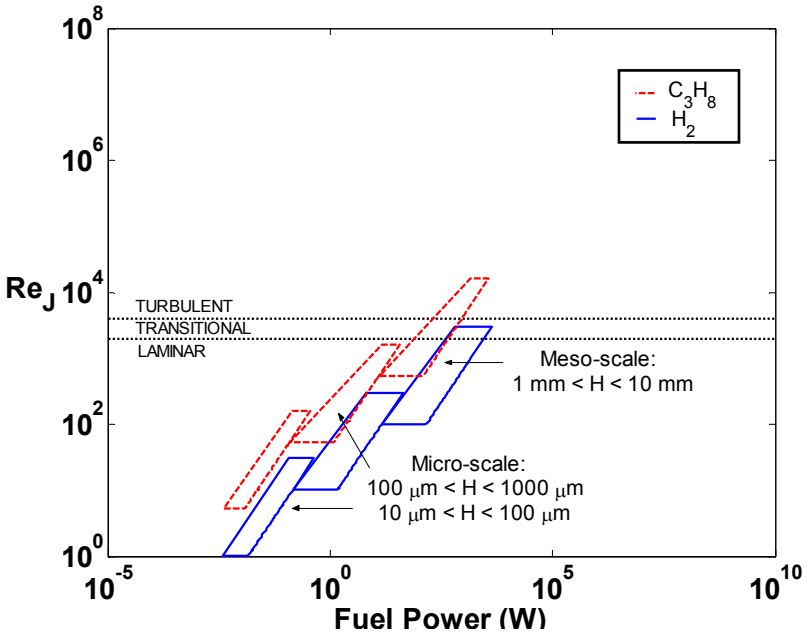

Figure 2-16: Effect of fuel type on the jet Reynolds number, Re_j, associated with fuel-air mixing as a function of power, P_f, associated with complete combustion of each fuel.

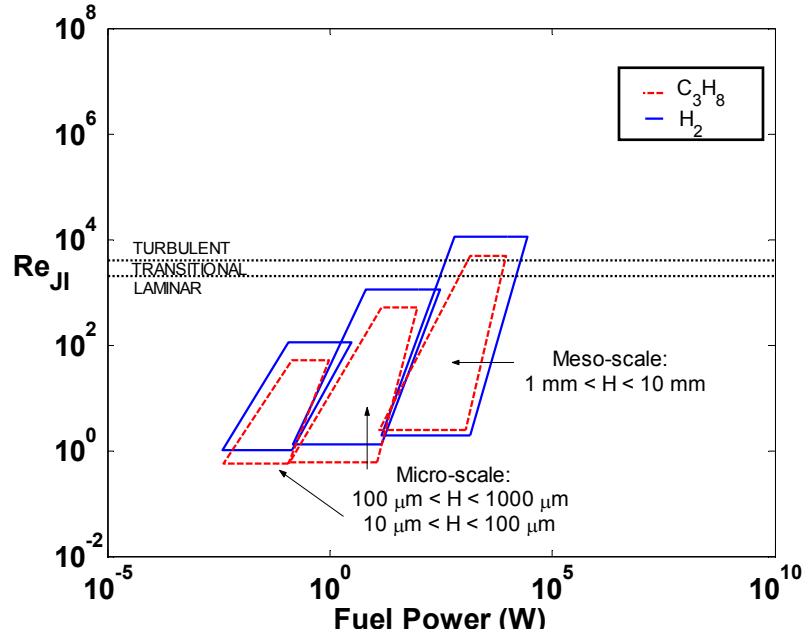

Figure 2-17: Effect of fuel type on the jet-interface Reynolds number, Re_{ji}, associated with fuel-air mixing as a function of power, P_f, associated with complete combustion of each fuel.

2.3 Estimating Mixing Lengths in Micro-flameholders

2.3.1 Introduction

Having identified the relevant Reynolds number ranges for micro-flameholders, the next challenge is to determine how the Reynolds number is related to mixing performance. One useful measure of flameholder mixing performance is the mixing length which is defined as the distance (measured from the point of fuel injection) required for the fuel and air to mix in stoichiometric proportion. The mixing length is also important because it influences the overall size/length of the flameholder. The purpose of this section, therefore, is to develop simple models and scaling laws for predicting the range of mixing lengths that can be expected in micro-flameholders and to use these as indicators of the device size required to achieve a particular level of mixing performance.

2.3.2 Scaling of Mixing Lengths in Micro-flameholders

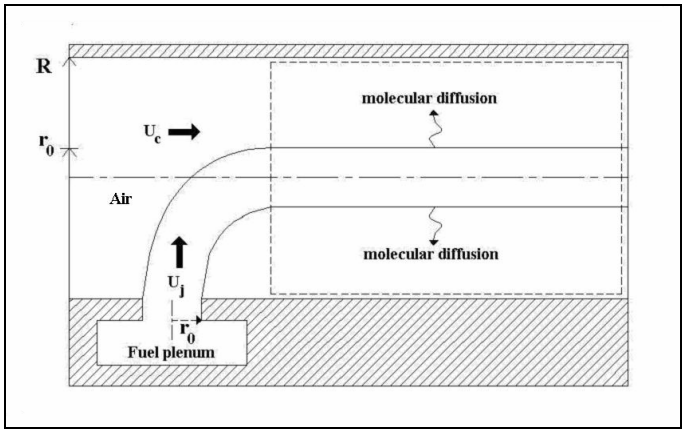

Figure 2-18: Schematic of the jet-in-crossflow mixing configuration

Referring once again to the 'generic,' jet-in-crossflow mixing configuration, reproduced here in Figure 2-18, it is possible to break the flow into two distinct

regions: A near-field region where the jet turns, which is dominated by a horseshoe vortex stabilized at the jet exit, and a far-field region where the jet is parallel to the mixing passage walls and spreads via molecular diffusion.

In a micro-flameholder, it is reasonable to expect that the far-field region will be much larger than the near-field turning region because the extremely small passage dimensions will force the jet to turn in a relatively short distance. As a result the present analysis focuses on understanding the mixing process occurring in the far-field region denoted by the dashed box in Figure 2-18. Mixing in this region is assumed to take place solely through molecular diffusion, and hence we focus on developing a simple model based on diffusion. This assumption is supported by the results of the preceding sections which suggest that Reynolds numbers in micro-flameholders fall in the laminar-transitional flow regime. It is also supported by previous experimental and numerical studies by Choudhuri et al. [45] and Anchondo et al. [45-46], (summarized in section 1.3 in Chapter one), which suggest that molecular diffusion may govern fuel-air mixing when the Reynolds number is low.

2.3.3 Axisymmetric Mixing Length Model

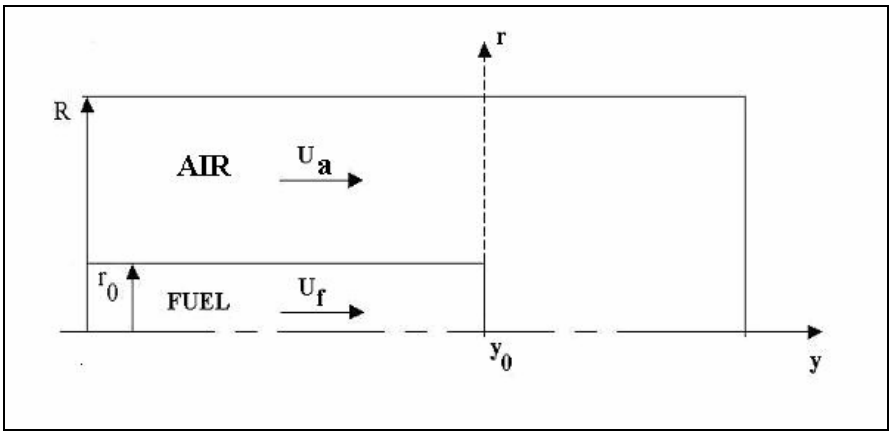

Figure 2-19: Schematic of the axisymmetric Burke-Schumann diffusive mixing model.

The mixing process occurring in the far-field region outlined in Figure 2-18 can be thought of as the diffusion of a cylindrical fuel volume with radius r_0 (equal to the radius of the fuel injection port) into a cylindrical air crossflow with radius, R, that completely surrounds the fuel stream. This is illustrated in Figure 2-19 where the velocity of the fuel core is U_f, the velocity of the air cross-flow is U_a and the fuel first encounters the air steam at the downstream location indicated by y_0. Assuming that transport is purely diffusive and occurs only in the radial direction leads to the following expressions for conservation of mass in the core and cross-flow regions [77]:

$$\frac{\partial Y_f}{\partial t} = D_{fo}\left(\frac{\partial^2 Y_f}{\partial r^2} + \frac{1}{r}\frac{\partial Y_f}{\partial r}\right) \tag{2.21}$$

$$\frac{\partial Y_o}{\partial t} = D_{fo}\left(\frac{\partial^2 Y_o}{\partial r^2} + \frac{1}{r}\frac{\partial Y_o}{\partial r}\right) \tag{2.22}$$

where Y_f is the mass fraction of fuel, Y_o is the mass fraction of oxygen, D_{fo} is the binary diffusion coefficient, r is the radial distance from the axis of symmetry, and t is the time. Viscous effects are neglected.

A well-known solution to this set of equations for the special case when $U_f = U_a$ was proposed by Burke and Schumann in 1928 [78]. Following the approach outlined by Kuo [79], Eqs. (2.21) and (2.22) can then be solved by applying a simple transformation that couples the fuel and oxygen mass fractions into a single variable, β, defined as follows:

$$\beta = \alpha_f - \alpha_o \tag{2.23}$$

where $\alpha_f = -\frac{Y_f}{MW_f}$ and $\alpha_o = -\frac{Y_o}{MW_o i}$; MW_f is the molecular weight of fuel, MW_o is the molecular weight of oxygen, and i is the number of molecules of air necessary to combine stoichiometrically with one molecule of fuel.

Using this transformation and applying the assumption that the velocity of the fuel and air streams is a constant value, U, Eqs. (2.21) and (2.22) collapse into a single expression in terms of β:

$$\frac{\partial \beta}{\partial y} = \frac{D_{fo}}{U}\left(\frac{\partial^2 \beta}{\partial r^2} + \frac{1}{r}\frac{\partial \beta}{\partial r}\right) \tag{2.24}$$

where y is the distance in the axial direction, and U is the flow velocity.

The initial conditions for this transformed diffusion equation are:

$$\begin{aligned} \beta_1 &= -\frac{Y_1}{MW_f} \quad for\ 0 \le r \le r_0\ at\ y = 0, \\ \beta_2 &= \frac{Y_2}{MW_o i} \quad for\ r_0 \le r \le R\ at\ y = 0, \end{aligned} \tag{2.25}$$

where Y_1 and Y_2, are the initial fuel and oxygen mass fractions respectively. ($Y_1 = 1$ and $Y_2 = 0.232$ in the present work).

The boundary conditions are:

$$\frac{\partial \beta}{\partial r} = 0 \quad at\ r = 0,\ for\ y > 0$$
$$\frac{\partial \beta}{\partial r} = 0 \quad at\ r = R,\ for\ y > 0 \tag{2.26}$$

The solution to Eq. (2.24) which satisfies these initial and boundary conditions is given by:

$$\beta = \beta_0 \frac{r_0^2}{R^2} - \beta_2 + \frac{2 r_0 \beta_0}{R} \sum \mu^{-1} \frac{J_1\left(\mu \frac{r_0}{R}\right) J_0\left(\mu \frac{r}{R}\right)}{\left[J_0(\mu)\right]^2} exp\left[- \frac{D_{ab} \mu^2 y}{U R^2} \right] \tag{2.27}$$

where μ is the positive root of the equation $J_1(\mu) = 0$. J_1 and J_0 are Bessel functions of the first kind and $\beta_0 = \beta_2 - \beta_1$.

While this expression was originally developed by Burke and Schumann to predict the lengths of diffusion flames, it is useful for estimating the approximate order of magnitude of diffusive mixing lengths in micro-flameholders. The diffusive mixing length, L_m, is given by the y-value in Eq. (2.27) for which β=0, when: (i) $r = 0$ (i.e. the centerline of the annulus) for fuel-lean mixtures, or (ii) $r = R$ (i.e. the outer radius of the annulus), for fuel-rich mixtures.

2.3.4 Results from the Axisymmetric Model

2.3.4.1 Mixing Lengths and Stoichiometric Contours

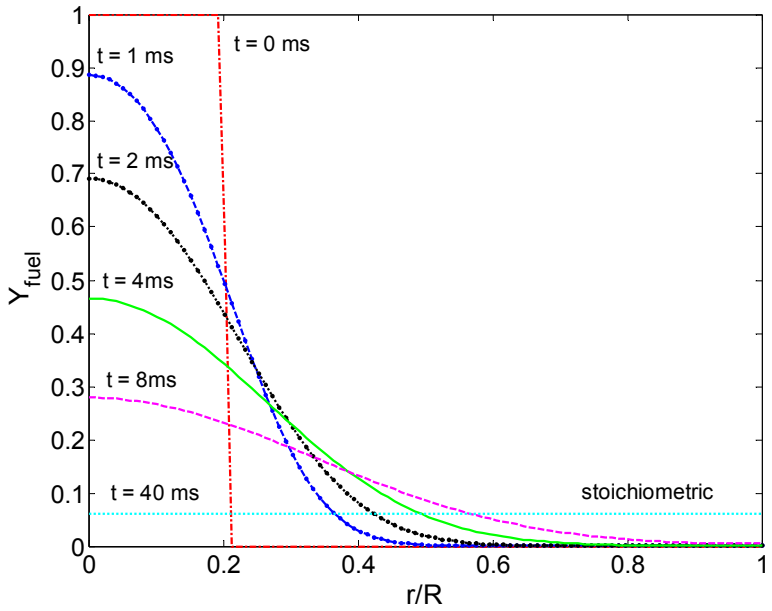

Figure 2-20: Fuel mass fraction, *Y*, as a function of non-dimensional radial distance, *r/R*, associated with the stoichiometric mixing of propane and air based on the axisymmetric Burke-Schumann model of diffusive fuel-air mixing (*R*= 1 mm, r_0/R = 1/5, *U*= 10m/s, *T* = 300K).

Figure 2-20 shows a typical result for the evolution of fuel mass fraction with time as predicted by Eq. (2.27) for the diffusive mixing of propane and air. The rate of mixing is seen to be very rapid initially because of the steep concentration gradient at the fuel-air interface. However, the figure shows that as time progresses, the mixing rate steadily decreases until a "mixed" state is reached when the fuel mass fraction at the fuel-air interface is stoichiometric (i.e. when $\beta = 0$). As time advances, the radial position of the stoichiometric contour moves from r_0/R=0.2 to r_0/R=1. Eventually, as time goes to infinity, the fuel becomes uniformly distributed throughout the domain and the fuel air ratio approaches a constant value equal to the

overall equivalence ratio of the problem. In this case, since the overall equivalence ratio of the system is stoichiometric, the fuel mass fraction everywhere in the domain approaches the stoichiometric fuel mass fraction.

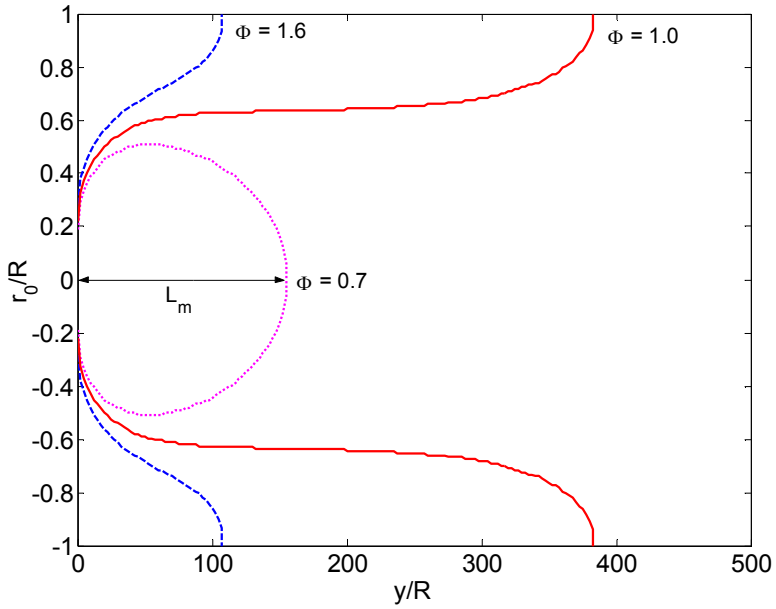

Figure 2-21. Stoichiometric (β=0) contours corresponding to overall equivalence ratios that are Φ>1 (rich), Φ=1 (stoichiometric), and Φ<1 (lean) determined using the axisymmetric Burke-Schumann model. The gas temperature is 300K, the flow velocity is 10m/s, the mixing passage radius is 1mm and the ratio of the fuel jet radius to outer annuls radius is ≈1/5.

Since the velocities of the fuel and oxidizer streams are equal, the overall equivalence ratio is determined by the ratio of the fuel jet radius to the outer annulus radius r_0/R. This leads to:

$$\Phi = \frac{1}{f}\left[\left(\frac{r_0}{R}\right)^2 \Big/ \frac{\rho_{ox}}{\rho_f}\left(1-\left(\frac{r_0}{R}\right)^2\right)\right]; \quad \text{where } 0 \le \frac{r_0}{R} < 1 \tag{2.28}$$

The corresponding stoichiometric (β=0) mixing contour for this situation is shown in Figure 2-21 along with contours for rich (Φ =1.6) and lean (Φ =0.7), overall equivalence ratios. In the rich case indicated by the dashed lines in Figure 2-21, fuel is in excess and therefore the stoichiometric contour extends from r_0/R=0.33 to

r_0/R=1. In contrast, in the lean case indicated by the dotted lines, the air is in excess and hence the stoichiometric contour passes through the centerline of the mixing passage. The diffusive mixing length, L_m, for this latter case is also illustrated in Figure 2-21. Another way to understand this is that the stoichiometric contour (or fuel-air interface) moves towards the deficient reactant.

The effects of varying different flow and geometric, parameters on the diffusive mixing lengths predicted by the axisymmetric mixing model are explored in the following subsections.

2.3.4.2 Effect of Varying the Flow Velocity and the Overall Equivalence Ratio

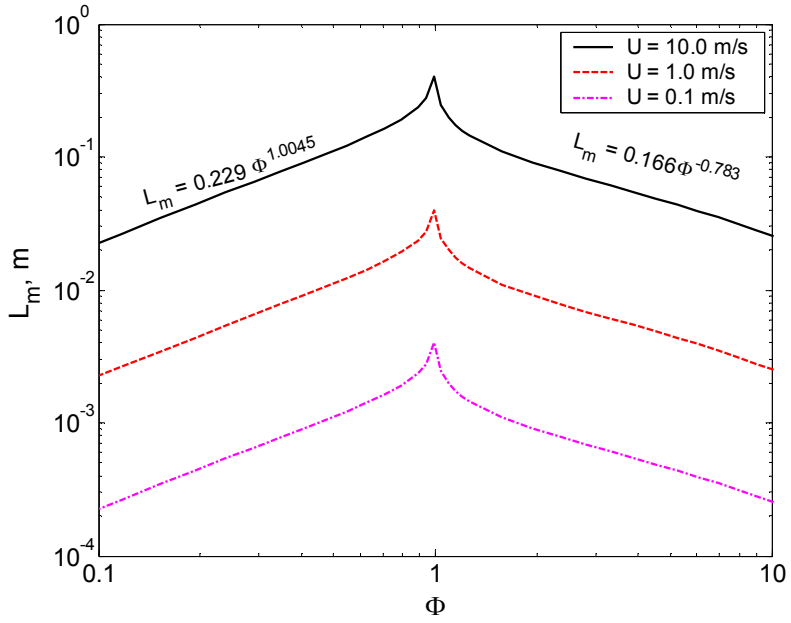

Figure 2-22: Diffusive mixing length, L_m, as a function of equivalence ratio, Φ, for the diffusive mixing of propane and air in an annular mixing passage of outer radius, R=1mm, for various flow velocities at a temperature, T=300K, as determined by the axisymmetric Burke-Schumann model.

Figure 2-22 shows how the mixing length varies with equivalence ratio for three different flow velocities. The outer annulus radius is fixed at R = 1mm and the gas temperature is 300K. The figure shows that mixing length is maximized when the

overall equivalence ratio is 1 and decreases when the overall equivalence ratio becomes either lean or rich. The mixing length peaks at an equivalence ratio of one because neither reactant is in excess. This, in turn, maximizes the distance over which molecular diffusion must occur. Power laws describe the variation of mixing length with equivalence ratio for most of the space. For lean mixtures and U=10 m/s, L_m= $0.229\Phi^{1.0045}$ whereas for rich mixtures and u=10 m/s L_m= $0.166\Phi^{-0.783}$. The mixing length is linearly proportional to the flow velocity i.e. increasing the flow velocity increases the mixing length by the same factor. Overall, Figure 2-22 shows that diffusive mixing in micro-power systems can be improved by operating at low flow rates and at overall equivalence ratios that are as far from stoichiometric as possible.

2.3.4.3 Effect of Varying the Mixing Passage Dimensions

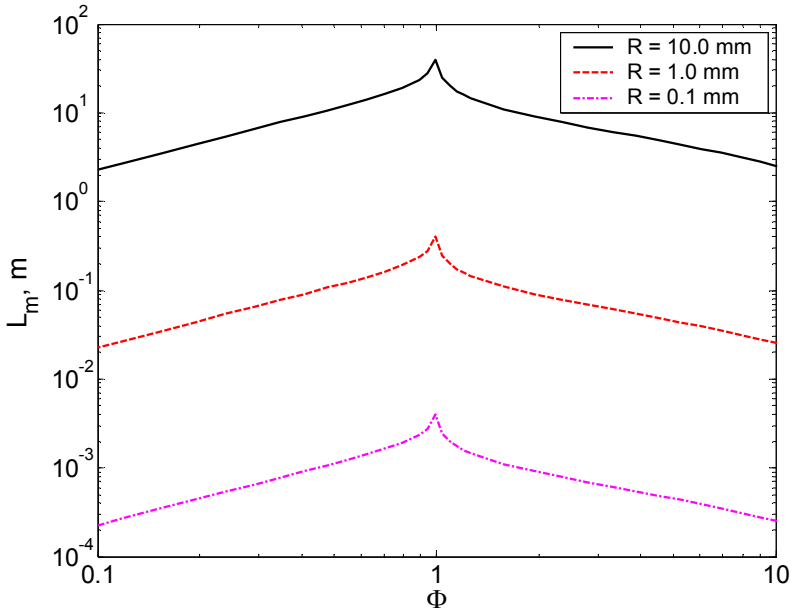

Figure 2-23: Diffusive mixing length, L_m, as a function of equivalence ratio, Φ, for the diffusive mixing of propane and air in a 10 m/s flow through annular mixing passages of various outer radii, at a temperature, T=300K, as determined by the axisymmetric Burke-Schumann model.

Figure 2-23 shows how the mixing length varies with equivalence ratio and the outer annulus radius, *R*. The mixing length increases as the outer annulus radius increases because the reactants must diffuse farther. A careful look at the plot shows that the diffusive mixing length is proportional to the square of the outer annulus radius so that if the outer annulus radius is increased by an order of magnitude, the mixing length increases by two orders of magnitude. This suggests that mixing performance could actually be improved by reducing the passage size. This result can be explained by the fact that the gradients driving diffusive transport become steeper as the device size is reduced.

2.3.4.4 Effect of Preheating the Fuel and Air

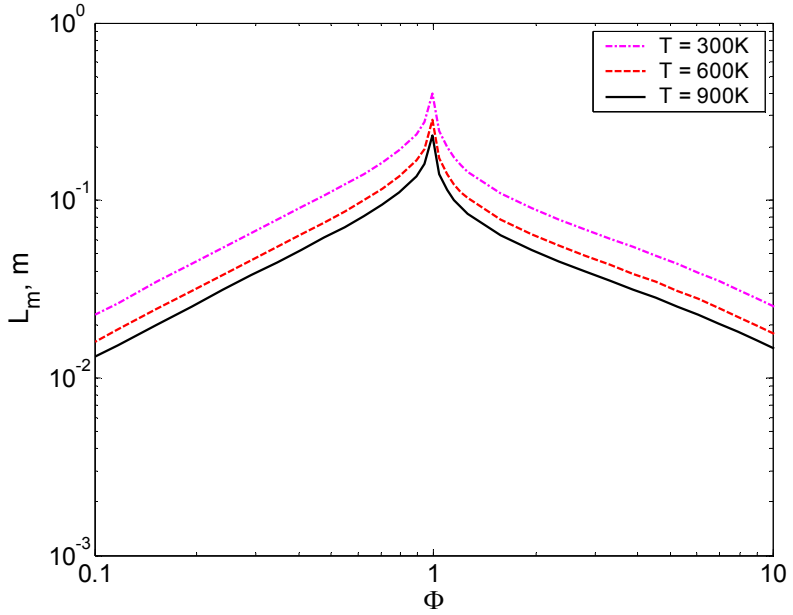

Figure 2-24: Diffusive mixing lengths, L_m, predicted using the axisymmetric Burke-Schumann model, as a function of equivalence ratio, Φ, for three different mixing pre-heating temperatures. The mixing passage radius is 1mm and the flow velocity (before pre-heating) is 10m/s.

Increasing the gas temperature by pre-heating has two effects. It increases the value of the diffusion coefficient and it decreases the density which, in turn increases

the flow velocity. Figure 2-24 shows that the net effect is that the diffusive mixing length is inversely proportional to the square root of the pre-heating temperature. This can be explained by the fact that the diffusion lengths scales linearly with velocity, while it scales with the inverse three-halves power with diffusivity. Overall, this result suggests that mixing lengths in micro-power systems can be minimized by pre-heating the fuel-oxidizer mixture.

2.3.4.5 Range of Mixing Lengths Predicted by the Axisymmetric Model

The preceding figures have shown that a wide range of mixing lengths are possible in axisymmetric, meso- and micro-scale flameholders depending upon the mixing passage diameter, and the flow conditions (i.e. velocity and temperature). To help provide a better quantitative sense of the wide range of mixing lengths that are possible, mixing lengths corresponding to a single (stoichiometric) equivalence ratio are summarized below in Table 2.6, for various passage sizes, flow velocities and flow temperatures.

Φ	T [K]	R [m]	U [m/s]	L_m [m]
0.1	300	1.0×10^{-3}	10.0	2.3×10^{-2}
1	300	1.0×10^{-3}	10.0	3.8×10^{-1}
10	300	1.0×10^{-3}	10.0	2.5×10^{-2}
1	300	1.0×10^{-3}	10.0	3.8×10^{-1}
1	300	1.0×10^{-3}	1.0	3.8×10^{-2}
1	300	1.0×10^{-3}	0.1	3.8×10^{-3}
1	300	1.0×10^{-2}	10.0	3.8×10^{1}
1	300	1.0×10^{-3}	10.0	3.8×10^{-1}
1	300	1.0×10^{-4}	10.0	3.8×10^{-3}
1	300	1.0×10^{-3}	10.0	3.8×10^{-1}
1	600	1.0×10^{-3}	10.0	2.7×10^{-1}
1	900	1.0×10^{-3}	10.0	2.2×10^{-1}

Table 2.6: Summary of mixing lengths associated with the stoichiometric, diffusive mixing of propane and air in an infinitely wide, planar mixing passage under various flow and geometric conditions, as determined by the axisymmetric Burke-Schumann model.

2.3.5 Planar Mixing Length Model

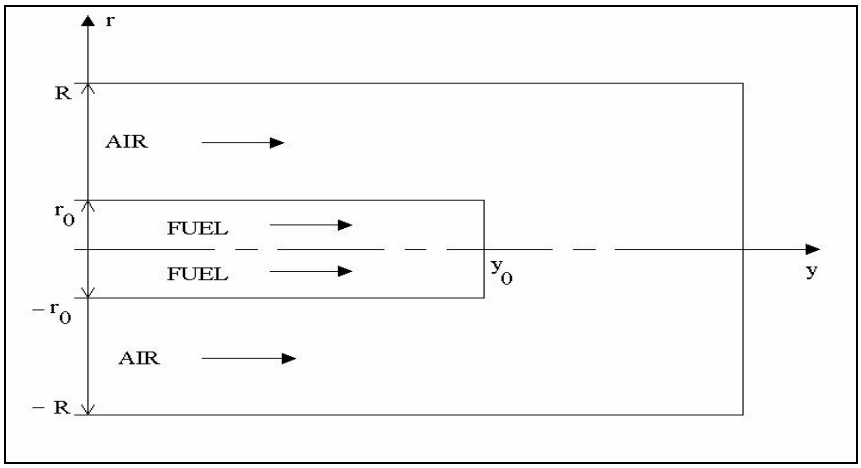

Figure 2-25: Schematic of the planar Burke-Schumann diffusive mixing model.

A planar analysis analogous to the axis-symmetric analysis of section 2.3.3 can also be performed by considering the flow of fuel through a duct bounded by two parallel walls separated by a distance $2r_0$. As before, the fuel jet encounters the air flow at y_0 and mixing is initiated. In this case the air is assumed to flow parallel to the fuel jet through an outer duct bounded by two parallel walls, set a distance $2R$ apart, which completely surround the fuel jet. Based on this mixing configuration and once again using the first assumption that the velocity at the fuel-air interface is a constant value, U, we can write the diffusion equations for the fuel and oxidizer streams as follows:

$$\frac{\partial Y_f}{\partial y} = \frac{D_{fo}}{U}\left(\frac{\partial^2 Y_f}{\partial x^2}\right) \tag{2.29}$$

$$\frac{\partial Y_o}{\partial y} = \frac{D_{fo}}{U}\left(\frac{\partial^2 Y_o}{\partial x^2}\right) \tag{2.30}$$

where x is the distance, from the centerline of the mixing passage, perpendicular to the flow direction and y is the distance in the streamwise direction.

Using the same transformation as before to couple the fuel and air mass fractions into a single variable, β, Eqs. (2.29) and (2.30) can be combined into a single equation:

$$\frac{\partial \beta}{\partial y} = \frac{D_{fo}}{U}\left(\frac{\partial^2 \beta}{\partial x^2}\right) \tag{2.31}$$

The initial conditions for this transformed equation are:

$$\begin{aligned} \beta_1 &= -\frac{Y_1}{MW_f} \quad for\ -r_0 \le x \le r_0\ at\ y = 0 \\ \beta_2 &= \frac{Y_2}{MW_o i} \quad for\ -R \le x \le -r_0\ and\ r_0 \le x \le R\ at\ y = 0 \end{aligned} \tag{2.32}$$

and the boundary conditions are:

$$\begin{aligned} \frac{\partial \beta}{\partial r} &= 0 \quad at\ x = 0,\ for\ y > 0 \\ \frac{\partial \beta}{\partial r} &= 0 \quad at\ x = R\ and\ x = -R,\ for\ y > 0 \end{aligned} \tag{2.33}$$

The solution of Eq. (2.31) that satisfies these boundary and initial conditions is:

$$\beta = \beta_0 \frac{r_0}{R} - \beta_2 + \frac{2\beta_0}{\pi} \sum_{n=1}^{\infty} n^{-1} sin\left(\frac{n\pi r_0}{R}\right) cos\left(\frac{n\pi x}{R}\right) exp\left[-\frac{D_{fo} n^2 \pi^2 y}{UR^2}\right] \tag{2.34}$$

where $\beta_0 = \beta_2 - \beta_1$.

Once again, the equation for the stoichiometric contour is obtained by setting β=0. The diffusive mixing length, L_m, is given by the y-value in Eq. (2.34) for which β=0, when: (i) $r = 0$ (i.e. the centerline of the mixing passage) for fuel-lean mixtures, or (ii) $r = R$ (i.e. the outer walls of the mixing passage), for fuel-rich mixtures.

2.3.6 Results from the Planar Model

2.3.6.1 Mixing Lengths and Stoichiometric Contours

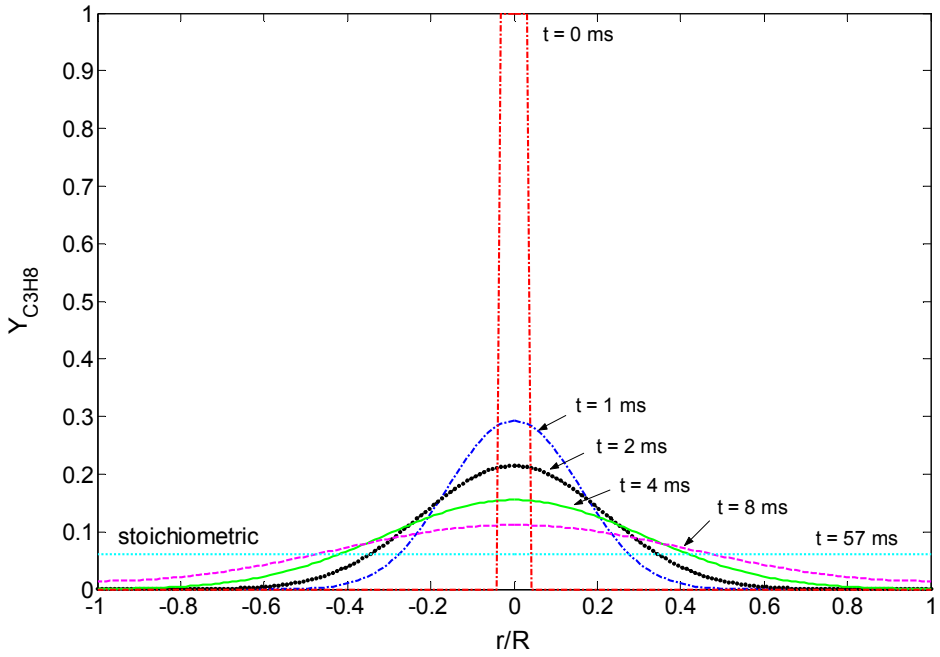

Figure 2-26: Fuel mass fraction, Y, as a function of non-dimensional displacement from the mixing passage centerline, r/R, associated with the mixing of propane and air based on the planar Burke-Schumann model of diffusive fuel-air mixing (R = 1 mm, $r_0/R \approx 1/25$, U = 10m/s, T = 300K).

A typical result for the evolution of fuel mass fraction with time as predicted by Eq. (2.34) for the diffusive mixing of propane and air is shown in Figure 2-26. The rate of mixing is seen to be very rapid initially because of the steep concentration gradient at the fuel-air interface. However, the figure shows that as time progresses, the mixing rate steadily decreases, until a "mixed" state is reached when the fuel mass fraction at the fuel-air interface is stoichiometric (i.e. when $\beta = 0$). In this case, since the overall equivalence ratio of the system is stoichiometric, the fuel mass fraction everywhere in the domain approaches the stoichiometric fuel mass fraction as time advances to infinity. The radial position of the stoichiometric contour also moves

outwards radially from $r_0/R=0.04$ to $r_0/R=1$ and from $r_0/R=-0.04$ to $r_0/R=-1$ as time advances.

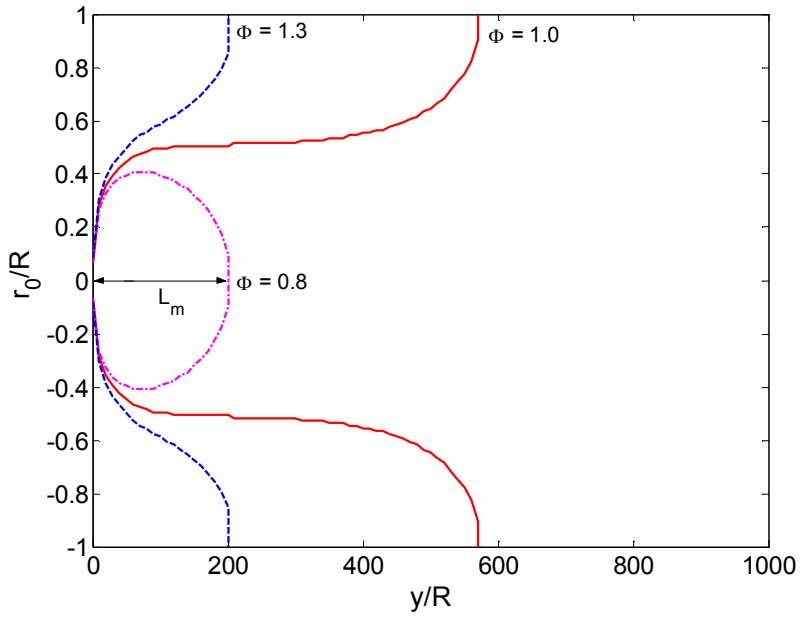

Figure 2-27 Stoichiometric (β=0) contours corresponding to overall equivalence ratios that are Φ>1 (rich), Φ=1 (stoichiometric), and Φ<1 (lean) determined using the planar Burke-Schumann model. The gas temperature is 300K, the flow velocity is 10m/s, the mixing passage radius is 1mm and the ratio of the fuel jet radius to outer annuls radius is ≈1/25.

Since the velocities of the fuel and oxidizer streams are identical, the overall equivalence ratio is determined by the ratio of the fuel jet radius to the outer annulus radius r_0/R. This leads to:

$$\Phi = \frac{1}{f}\left[\left(\frac{\rho_f}{\rho_{ox}}\right)\left(\frac{r_0/R}{1-r_0/R}\right)\right]; \quad \text{where } 0 \le \frac{r_0}{R} < 1 \tag{2.35}$$

It is important to note that this planar formulation corresponds to an *infinitely* wide, mixing passage.

The corresponding stoichiometric (β=0) mixing contour for this situation is shown in Figure 2-27 along with contours for rich ($\Phi=1.3$) and lean ($\Phi=0.8$), overall

equivalence ratios. In the rich case, indicated by the dashed lines in Figure 2-27, fuel is in excess, and therefore the stoichiometric contour extends radially outwards towards the mixing passage walls. In contrast, in the lean case, indicated by the dotted lines, the air is in excess and hence the stoichiometric contour passes through the centerline of the mixing passage. The diffusive mixing length, L_m, for this latter case is also illustrated in Figure 2-27.

The effects of varying different flow and geometric, parameters on the diffusive mixing lengths predicted by the axisymmetric mixing model are explored in the following subsections.

2.3.6.2 Effect of Varying the Flow Velocity and the Equivalence Ratio

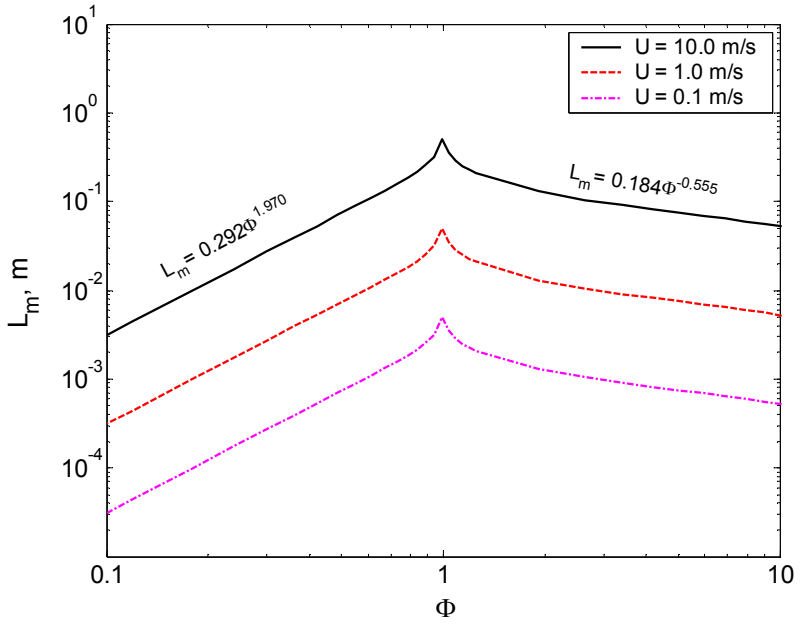

Figure 2-28: Diffusive mixing length, L_m, as a function of equivalence ratio, Φ, for the diffusive mixing of propane and air in an annular mixing passage of height, H=2mm, for various flow velocities at a temperature, T=300K, as determined by the planar Burke-Schumann model.

A plot showing how the mixing length varies with equivalence ratio for three different flow velocities is shown in Figure 2-28. The passage height is fixed at H =

2mm and the gas temperature is 300K. The figure shows that mixing length is maximized when the overall equivalence ratio is 1 and decreases when the overall equivalence ratio becomes either lean or rich. The mixing length peaks at an equivalence ratio of one because neither reactant is in excess and therefore the distances over which diffusive transport can occur are maximized. Power laws describe the variation of mixing length with equivalence ratio for most of the space. For lean mixtures at a flow velocity of 10 m/s, $L_m = 0.292\Phi^{1.970}$ whereas for rich mixtures at the same flow velocity, $L_m = 0.184\Phi^{-0.555}$. As in the asymmetric case, the mixing length is linearly proportional to the flow velocity i.e. increasing the flow velocity increases the mixing length by the same factor. However, comparison with the results of the axisymmetric model also reveals that the mixing lengths predicted in the planar case are longer than in the axisymmetric situation, for equivalence ratios near one, while for very lean or very rich equivalence ratios the reverse is true. It is also important to note that mixing lengths in the planar case are more sensitive to changes in the equivalence ratio. This is due to the fact that in the axis-symmetric case, the area which sets the equivalence ratio increases with the square of the radius of the mixing passage. Hence a smaller change in the diffusive mixing length is associated with a particular change in the equivalence ratio, in the axis-symmetric case relative to the planar case. Overall, Figure 2-28 shows that diffusive mixing in micro-power systems can be improved by operating at low flow rates and at overall equivalence ratios that are as far from stoichiometric as possible.

2.3.6.3 Effect of Varying the Mixing Passage Dimensions

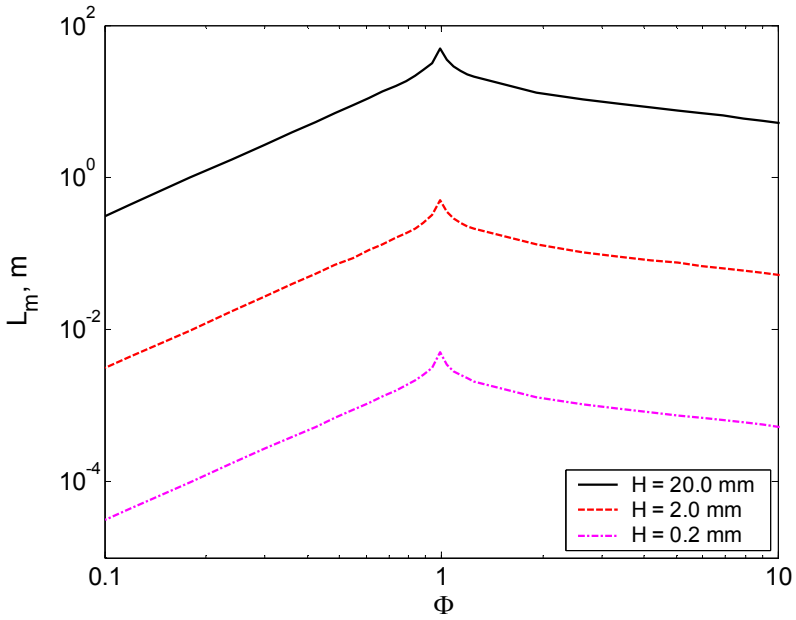

Figure 2-29: Diffusive mixing length, L_m, as a function of equivalence ratio, Φ, for the diffusive mixing of propane and air in a 10 m/s flow through planar mixing passages of various heights, at a temperature, T=300K, as determined by the planar Burke-Schumann model

Figure 2-29 shows how the mixing length varies with equivalence ratio and the height of the mixing passage, *H,* at a flow velocity of 10 m/s and a temperature of 300K. As in the axisymmetric case, the mixing length increases as the passage height increases because the reactants must diffuse farther. Careful examination of the plot shows that the diffusive mixing length is proportional to the square of the height of the mixing passage. This means that if the mixing passage height is increased by an order of magnitude, the mixing length increases by two orders of magnitude. This is the same dependence as in the axisymmetric case and suggests that mixing performance could be improved by reducing the passage size. Again, this result can be explained by the fact that the gradients driving diffusive transport become steeper as the device size is reduced.

2.3.6.4 Effect of Preheating the Fuel and Air

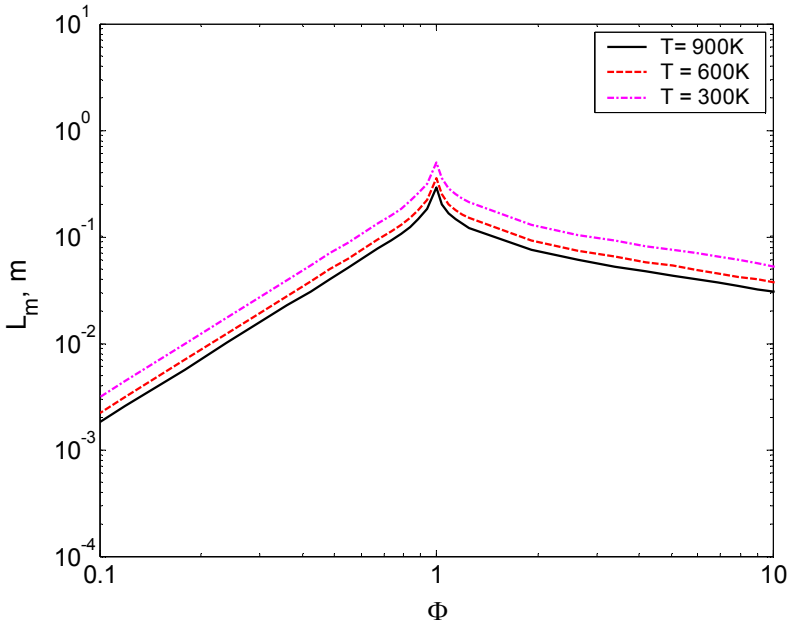

Figure 2-30: Diffusive mixing lengths, L_m, predicted using the planar Burke-Schumann model, as a function of equivalence ratio, Φ, for three different mixing pre-heating temperatures. The mixing passage height is 2mm and the flow velocity (before pre-heating) is 10m/s.

As explained previously, increasing the gas temperature through pre-heating has two effects. It increases the value of the diffusion coefficient and it decreases the density which, in turn increases the flow velocity. Figure 2-30 shows that the net effect of pre-heating is that the diffusive mixing length is inversely proportional to the square root of the pre-heating temperature. Overall, this result suggests that mixing lengths in micro-power systems can be minimized by pre-heating the fuel-oxidizer mixture.

2.3.6.5 Range of Mixing Lengths Predicted by the Planar Model

The preceding figures have shown that a wide range of mixing lengths are possible in planar, meso- and micro-scale, flameholders depending upon the mixing passage diameter, and the flow conditions (i.e. velocity and temperature). The figures also show that the mixing lengths predicted by the planar model are longer than in the axisymmetric model, for equivalence ratios near one, while for very lean or very rich equivalence ratios, shorter mixing lengths are observed. To help provide a better quantitative sense of the wide range of mixing lengths that are possible, mixing lengths corresponding to stoichiometric fuel-air mixtures and various geometric and flow conditions, are summarized below in Table 2.7.

Φ	T [K]	$H = 2R$ [m]	U [m/s]	L_m [m]
0.1	300	2.0×10^{-3}	10.0	3.1×10^{-3}
1	300	2.0×10^{-3}	10.0	5.7×10^{-1}
10	300	2.0×10^{-3}	10.0	5.2×10^{-2}
1	300	2.0×10^{-3}	10.0	5.7×10^{-1}
1	300	2.0×10^{-3}	1.0	5.7×10^{-2}
1	300	2.0×10^{-3}	0.1	5.7×10^{-3}
1	300	2.0×10^{-2}	10.0	5.7×10^{1}
1	300	2.0×10^{-3}	10.0	5.7×10^{-1}
1	300	2.0×10^{-4}	10.0	5.7×10^{-3}
1	300	2.0×10^{-3}	10.0	$5.7x\ 10^{-1}$
1	600	2.0×10^{-3}	10.0	4.0×10^{-1}
1	900	2.0×10^{-3}	10.0	3.3×10^{-1}

Table 2.7: Summary of mixing lengths associated with the stoichiometric, diffusive mixing of propane and air in an infinitely wide, planar mixing passage under various flow and geometric conditions, as determined by the planar Burke-Schumann model.

2.4 Conclusions

The basic analyses conducted in this chapter have provided some simple but useful insights into the fundamental characteristics of fuel-air mixing in micro-flameholders.

1) The Reynolds number boundary analysis show that fuel-air mixing in micro-flameholders occurs in the laminar to transitional range and that Reynolds numbers are much lower than those associated with mixing in conventional-scale power systems. Pre-heating of the fuel-air mixture, which is likely at small scales, further, reduces the Reynolds number range in these systems.
2) There is a dearth of experimental work in the literature that has investigated this Reynolds number range.
3) The results from the purely diffusive mixing models suggest that:
    a. Less distance is required for fuel-air mixing as micro-flameholders get smaller.
    b. The shortest mixing lengths are required for mixing at very lean and very rich overall equivalence ratios ($\Phi << 1$ and $\Phi >> 1$).
    c. Preheating reduces fuel-air mixing lengths.
    d. Lowering the flow velocity reduces mixing lengths in micro-flameholders.

So far we have used somewhat limited one-dimensional models that neglect convective processes to investigate fuel-air mixing in micro-flameholders. These are inadequate, however, because mixing is an inherently multi-dimensional process [80]. The next step, therefore, is to develop higher fidelity models capable of accounting

for different effects like convective transport, interface instability and multi-dimensionality.

Chapter 3: Numerical Modeling of Fuel-air Mixing in a Micro-flameholder

3.1 Introduction

Chapter 3 presents the results of CFD simulations of fuel-air mixing in micro-flameholders at low Reynolds numbers, made using CFD-ACE+ [81], a commercial Navier-Stokes solver. Effectively 'inviscid' (to be explained later), numerical simulations are performed first, to provide basic physical understanding of the fuel-air mixing process in micro-flameholders that can be compared directly to the results of the previous section. These are then followed by more realistic viscous simulations which capture the effects of shear at the fuel-air interface and at the walls of the mixing passage.

The main objective in performing low Reynolds number, CFD simulations was to understand the reliability of the predictions made using the simple Burke-Schumann, diffusive mixing model developed in Chapter two. While this model is compact and uncomplicated, it does not include axial diffusion or viscous shear at interfaces, which may be important to the fuel-air mixing process in a micro-flameholder. Using CFD simulations we can explore these effects individually, which allows us to understand their impact on the overall mixing problem. Moreover, for simplicity and to facilitate easy comparison with the Burke-Schumann model only axisymmetric micro-flameholder geometries are considered here.

3.2 Axisymmetric CFD Simulations

3.2.1 Quantifying Mixing

In order to compute mixing lengths based on the CFD simulation results for comparison with the Burke-Schumann model predictions, it is necessary to first devise a means of quantitatively determining the extent of fuel-air mixing in a particular computational domain. One very convenient way to do this is to use the β-parameter, which was introduced as Eq. (2.23) in Chapter two, and is reproduced here, as Equation (3.1):

$$\beta = \alpha_f - \alpha_o \tag{3.1}$$

where $\alpha_f = -\frac{Y_f}{MW_f}$, $\alpha_o = -\frac{Y_o}{MW_o i}$, Y_f is the mass fraction of fuel, Y_o is the mass fraction of oxygen, MW_f is the molecular weight of fuel, MW_o is the molecular weight of oxygen, and i is the number of molecules of air necessary to combine stoichiometrically with one molecule of fuel.

When β = 0, fuel and air are present in exact stoichiometric proportion and are considered to be 'mixed'. The stoichiometric contour corresponding to β=0 can be computed from the species concentration fields returned by the CFD simulations. The mixing length, L_m, is determined by finding the maximum streamwise distance, along either the centerline of the mixing passage (for fuel-lean mixtures) or along the outer wall of the mixing passage (for fuel-rich mixtures), for which β = 0.

3.2.2 Governing Equations and Solution Method

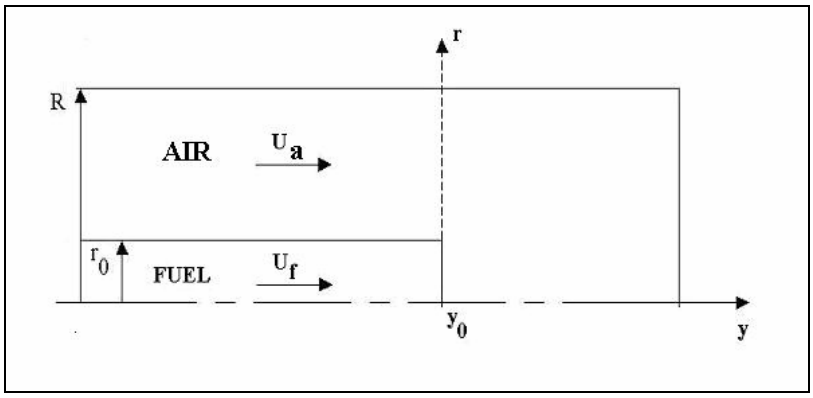

Figure 3-1: Schematic of the axisymmetric micro-flameholder geometry.

The fuel-air mixing process in a micro-flameholder is governed by the steady, transport of mass, momentum, and energy equations [77, 81&82], written below:

$$\rho\left(v_r\frac{\partial v_r}{\partial r}+u\frac{\partial v_r}{\partial y}\right)=-\frac{\partial P}{\partial r}+\mu\left(\frac{\partial^2 v_r}{\partial r^2}+\frac{1}{r}\frac{\partial v_r}{\partial r}-\frac{v_r}{r^2}+\frac{\partial^2 v_r}{\partial y^2}\right) \tag{3.2}$$

$$\rho\left(v_r\frac{\partial u}{\partial r}+u\frac{\partial u}{\partial y}\right)=-\frac{\partial P}{\partial y}+\mu\left(\frac{\partial^2 u}{\partial r^2}+\frac{1}{r}\frac{\partial u}{\partial r}+\frac{\partial^2 u}{\partial y^2}\right) \tag{3.3}$$

$$0=D_{ab}\left(\frac{\partial^2 Y_k}{\partial r^2}+\frac{1}{r}\frac{\partial Y_k}{\partial r}+\frac{\partial^2 Y_k}{\partial y^2}\right) \tag{3.4}$$

$$\rho C_v\left(v_r\frac{\partial T}{\partial r}+u\frac{\partial T}{\partial y}\right)=-T\left(\frac{\partial p}{\partial T}\right)\left(\frac{1}{r}\frac{\partial(rv_r)}{\partial r}+\frac{\partial u}{\partial y}\right)-\left(\nabla\cdot\tau\cdot\vec{V}\right) \tag{3.5}$$

where r is the distance in the radial direction, y is the distance in the axial direction, v_r and u are the radial and axial velocity components respectively, ρ is the density, P is the pressure, μ is the dynamic viscosity , Y is the mass fraction of species k and $\vec{V}$ is the velocity vector.

Equations (3.2)-(3.5) are solved using CFD-ACE+ (a commercial CFD package by ESI U.S. R&D Inc.), over two-dimensional (axis-symmetric) structured computational grids based on the axisymmetric micro-flameholder geometry illustrated schematically in Figure 3-1. They are solved subject to various boundary and initial conditions, which are applied at the inlets, outlets and walls of two-dimensional, 0.5mm x 0.25m, structured computational grids containing 31,122 cells. A representative computational grid containing two domains (one for fuel and one for oxidizer) is illustrated below in Figure 3-2.

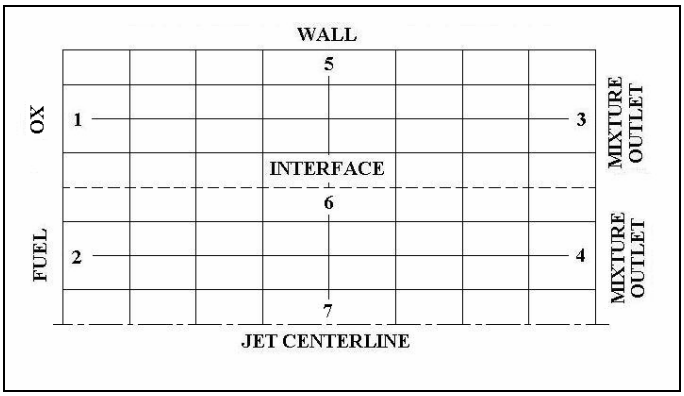

Figure 3-2: Representative computational grid.

Air, with initial mass fraction of oxygen $Y_o = 0.232$, is injected at boundary 1 while fuel, with initial mass fraction $Y_f = 1.0$, is injected at boundary 2. Mixture outlets are located at boundaries 3 and 4. The outer wall of the mixing passage is shown by boundary 5, and the jet centerline is given by boundary 7. Boundary 6 is the interface between the two domains along which momentum, mass and energy transport occur.

A blended quasi-second order spatial differencing method comprising 90% upwinding and 10% backwards Euler is used for all simulations [81]. In addition, a conjugate-gradient-squared (CGS) solver, with preconditioning is used to solve for the

pressure, velocity, and mass fractions. A numerical simulation is considered converged if the l2norm of all residuals was reduced to at least $1.0x10^{-5}$.

Once a converged solution is obtained, the computed mass fractions of propane and oxygen were used to estimate the diffusive mixing length, L_m. This is accomplished by using Eq. (3.1) to determine the axial distance at which $\beta = 0$ at either the centerline of the mixing passage (for fuel-lean mixtures), or at the outer wall of the mixing passage (for fuel-rich mixtures).

3.2.3 Grid Convergence and Resolution

Preliminary two-dimensional CFD simulations were performed to determine the minimum number of grid cells needed to provide an accurate solution. To this end, a grid convergence test was performed using the centerline exit velocity (U_{CE}), the centerline exit temperature (T_{CE}) and the centerline exit fuel mass fraction ($Y_{f,CE}$) as indicators of grid convergence.

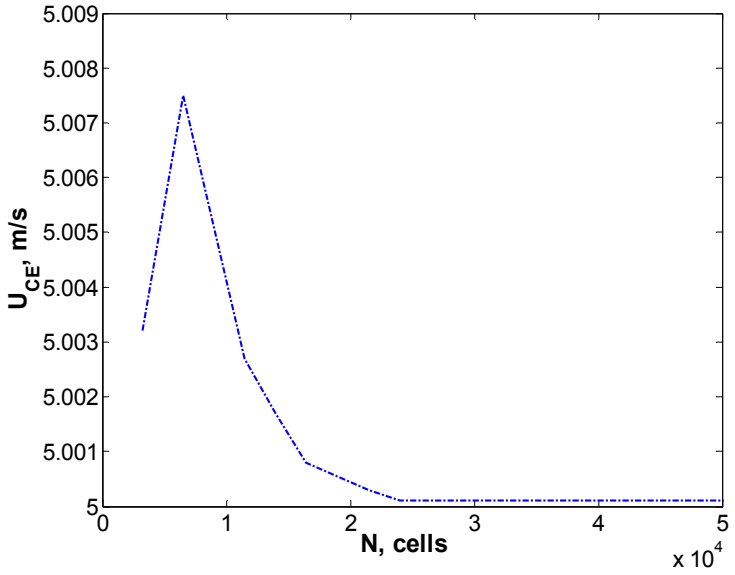

Figure 3-3: Centerline exit velocity associated with the mixing of propane and air in a micro-flameholder plotted as a function of the number of computational grid cells used in an axisymmetric, CFD simulation.

Figure 3-3 shows that the centerline velocity is converged (within <0.5%) by approximately 25,000 cells. However, to be certain that this is a reasonable benchmark for grid convergence the grid convergence test results for the centerline exit fuel mass fraction and centerline exit temperature are plotted in Figures 3-4 and 3-5. In the former case convergence to within 0.5% of the final exit centerline temperature is achieved with just 17,000 cells. In the latter case convergence (within <0.5%) is achieved by roughly 22,000 cells. Based on these results it can be inferred that 25,000 cells is the minimum number grid cells required to ensure that the CFD simulation results are grid independent.

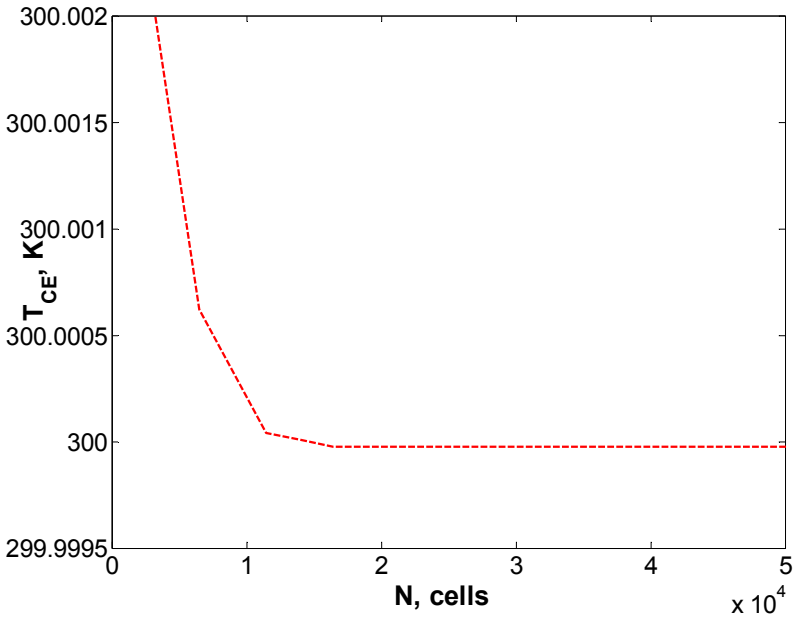

Figure 3-4: Centerline exit Temperature associated with the mixing of propane and air in a micro-flameholder plotted as a function of the number of computational grid cells used in an axisymmetric CFD simulation.

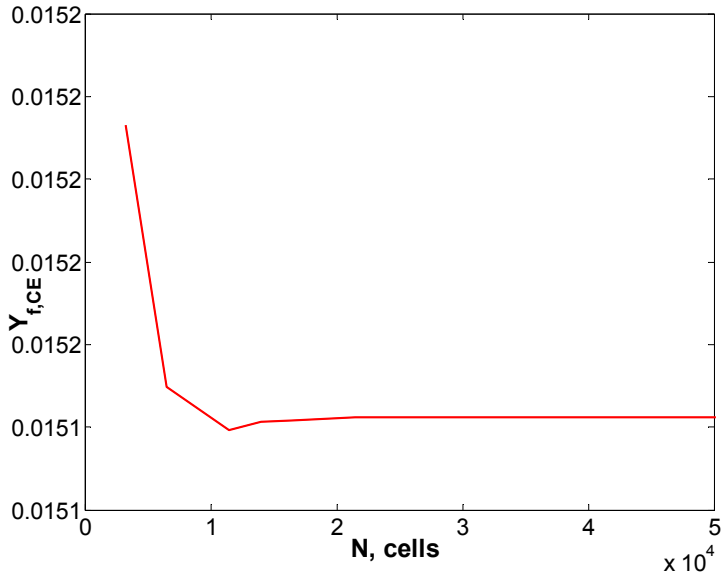

Figure 3-5: Fuel mass fraction at the centerline exit associated with the mixing of propane and air in a micro-flameholder plotted as a function of the number of computational grid cells used in an axisymmetric CFD simulation.

In addition to ensuring that the grids used were sufficiently converged, adequate grid resolution is also an important consideration. To resolve the smallest flow structures it is necessary to ensure that the grid spacing is smaller than or equal to the Kolmogorov length scale (which is the smallest length scale in a flow for which the Re>1, discussed in detail in section 4.2.2). Since the Kolmogorov length scale is dependent on the flow Reynolds number, the ability of a grid to resolve the smallest structures in a flow therefore depends on the Reynolds number. At high Reynolds numbers the Kolmogorov length scale is much smaller than at low Reynolds numbers, as result finer grid spacing is needed to adequately resolve the smallest flow structures. In the present work the grids (which contain 32,000+ cells) can resolve flows with Re≤300 which corresponds to an approximate grid resolution of 6.5 μm. In order to resolve the smallest length scales for Reynolds numbers up to 1000, it would be necessary to have 80,000+ cells, which would give a grid resolution of roughly 2.5 μm.

3.2.4 Numerical Simulation Approach

A step-wise approach was used in performing the CFD simulations in order to isolate the specific effects of axial diffusion and viscous shear.

First, to investigate the purely diffusive mixing problem for comparison with the Burke-Schumann model in Chapter two, the effects of viscous shear were suppressed by imposing slip boundary conditions at the upper wall, by setting $U_f = U_a$ at the inlets, and by enforcing constant pressure boundary conditions at the outlet boundaries. Comparison with the Burke-Schumann results that only include the effects of radial diffusion allowed the effects of axial diffusion to be investigated.

Second, CFD simulations incorporating the effects of viscous shear at the outer wall of the mixing passage were performed. This involved imposing a no slip boundary condition at the outer wall, while maintaining all of the other boundary conditions in the first set of simulations.

Third, numerical simulations designed to investigate the effects of shear at the fuel-air interface were performed by creating a velocity mismatch between the fuel and air streams. In this case U_a was fixed while U_f was varied over a range of velocity ratios, from 1 to 100 (i.e. $1 \leq \alpha \leq 60$). Slip boundary conditions were enforced at the upper wall and constant pressure was enforced at the outlet boundaries. Turning shear at the outer wall of the mixing passage off allowed the effects of shear at the fuel-air interface to be isolated.

For simplicity, all cells in the computational domain were initialized to the flow conditions at the air inlet. In addition, all numerical simulations were performed using air containing (21% oxygen and 79% nitrogen), as the oxidizer and propane as the fuel.

3.3 Axisymmetric CFD Results

3.3.1 Effect of Axial Diffusion and Viscous Wall Shear

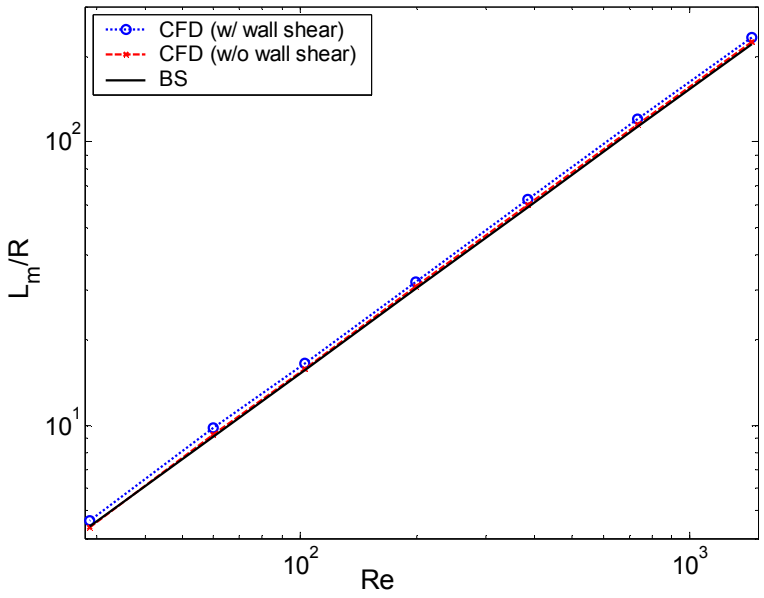

Figure 3-6. Non-dimensional diffusive mixing length, L_m/R, as a function of Reynolds number for the diffusive mixing of propane and air at an equivalence ratio, Φ = 0.8. The mixing passage radius is 0.5mm and the gas temperature is 300K.

Fig. 3-6 compares the variation of non-dimensional mixing length predicted by the Burke-Schumann (BS) diffusive model, to CFD simulations with and without wall slip. The overall equivalence ratio in these simulations is 0.8. Since the velocities of the fuel and oxidizer streams are the same, the case with the slip boundary condition corresponds to an 'effectively inviscid' situation because even though the viscosity is not zero, there is no velocity gradient present to drive the transport of momentum between the fluid and the wall or from one stream to another. In this case, species transport will occur entirely by molecular diffusion and not via entrainment (or vorticity) driven by viscous shear. As a result, in the 'effectively inviscid' situation, the Reynolds number serves only as an indicator of flow velocity. It is retained, however,

so that results may be compared to those corresponding to the ordinary viscous situation with no slip at the walls.

Figure 3-6 shows that the Burke-Schumann model's predictions lie within 2% of those predicted by the effectively inviscid CFD over the entire range of Reynolds numbers explored. This suggests that axial diffusion is negligible even at low Reynolds numbers (at this particular equivalence ratio, Φ=0.8). Including viscous shear at the wall increases the mixing length by approximately 8% percent although this is difficult to see in the figure. This is an initially surprising result. It is caused by viscous shear at the wall slowing the outer (air) flow near the wall. This, in turn, increases the velocity of the fluid in the center of the mixing passage in order satisfy mass conservation. The increase in the flow velocity towards the center of the mixing passage produces the slight increase (8%) in the mixing length.

To justify this claim we can examine some key flow parameters associated with mixing, which will allow us to gain deeper insight into the physics of the mixing process when shear is present at the wall. Figure 3-7 shows inlet u-velocity component, vorticity, and stream function contours for the mixing of propane and air in a passage with and without shear at the wall. The inlet flow velocity in each case is 10m/s, which corresponds to a flow Reynolds number of approximately 320.

In Figure 3-7 a) there is no shear at the wall, the solution is effectively inviscid. Since the velocity field is uniform everywhere. This is confirmed by examining the u-velocity component, vorticity and stream function contours for this situation. The u-velocity component is constant; no vorticity is present in the flow; and the streamlines are all parallel to each other.

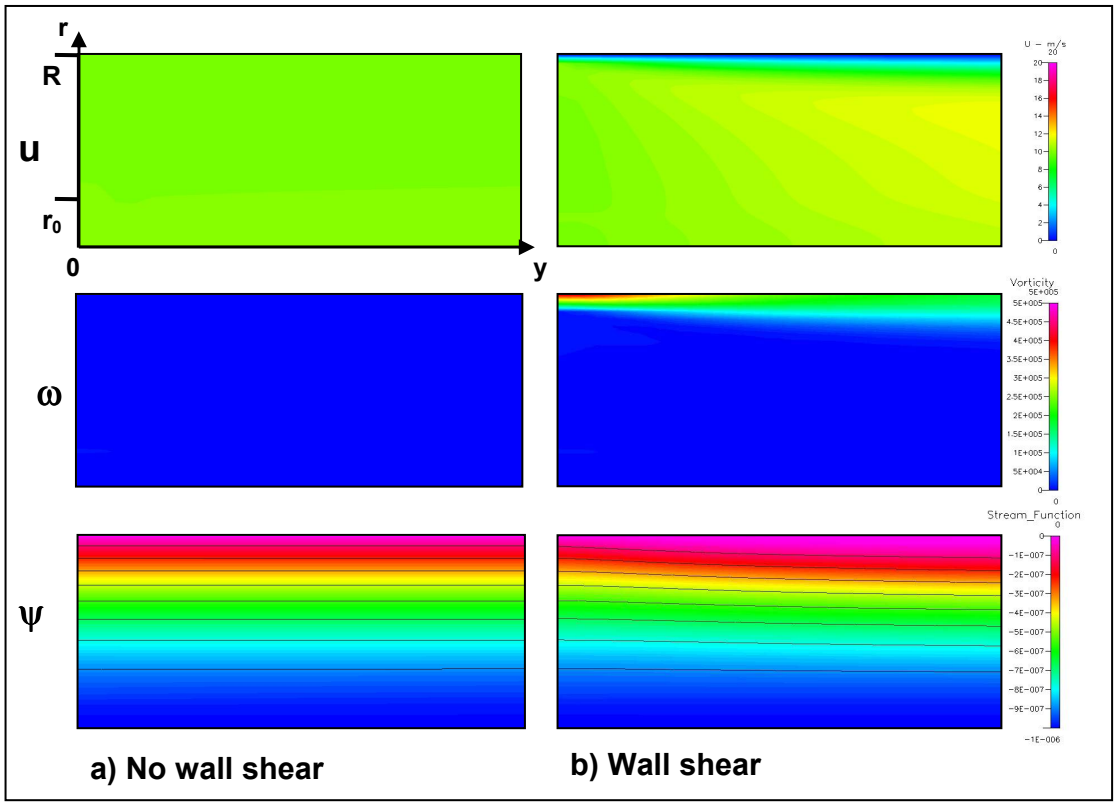

Figure 3-7. U-velocity component, vorticity and stream function contours associated with mixing of propane and air, at an equivalence ratio of 0.8, inside a mixing a passage of radius 0.5mm, for the case of a) no shear at the mixing passage walls and b) shear at the mixing passage walls. The inlet flow velocity in each case is 10 m/s, which corresponds to a flow Reynolds number of ~320. The gas temperature is 300K.

In Figure 3-7 b) shear is present at the outer wall. The u-velocity component contours show that a velocity boundary layer is developing near wall. Associated with this velocity boundary layer is a region of vorticity near the wall. In addition, the streamlines in this case appear to be converging towards the center of the passage, which indicates that the flow is accelerating.

Based on these results we can conclude that the earlier explanation for the increase in mixing length is consistent with what is observed in the flow.

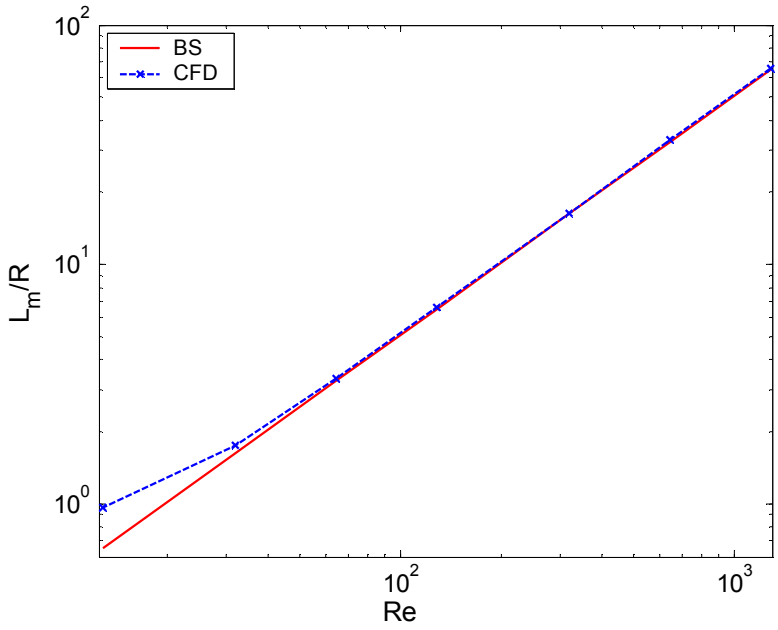

Figure 3-8. Non-dimensional diffusive mixing length, L_m/R, as a function of Reynolds number, *Re*, for the diffusive mixing of propane and air at an equivalence ratio, Φ = 3.0. The mixing passage radius is 1.0mm and the gas temperature is 300K.

Because the mixing length is somewhat sensitive to the overall equivalence ratio, axial diffusion can become important at low Reynolds numbers when the overall equivalence ratio is not unity. Figure 3-8 compares the predictions of the Burke-Schumann model to results from effectively inviscid CFD simulations when the overall equivalence ratio is three. The results show that the Burke-Schumann model's predictions are within 2% of the effectively inviscid CFD predictions for Re>50. However, for Re<50, axial diffusion (which is not accounted for in the Burke-Schumann model) becomes significant and the mixing lengths predicted by the effectively inviscid CFD solutions are larger that those predicted by the Burke-Schumann model. Finally, it should be noted that these results are only presented to show the effect of equivalence ratio on the importance of axial diffusion. An overall equivalence ratio of three is unrealistic for a micro-flameholder.

3.3.2 Effect of Axial Diffusion and Viscous Shear when the Velocities of the Fuel and Air Streams Differ

3.3.2.1 Effect of Viscous Shear at the Fuel-air Interface on the Mixing Length

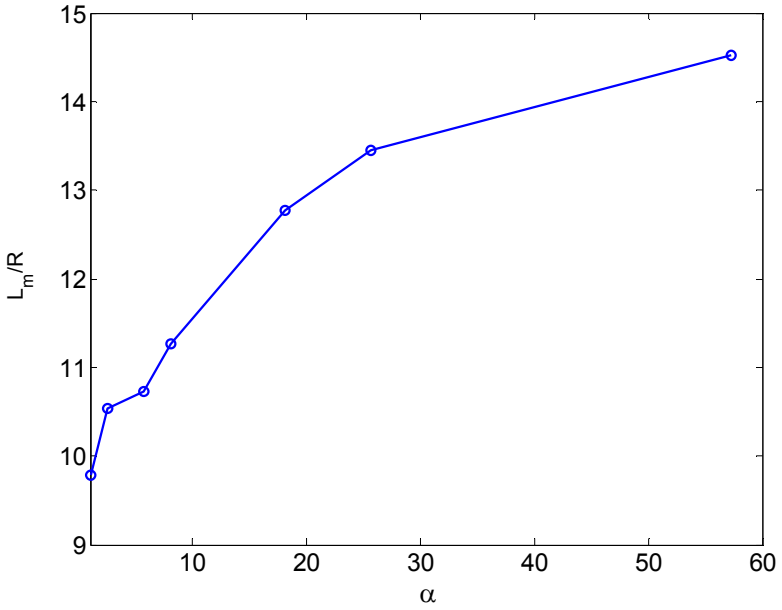

Figure 3-9. Non-dimensional diffusive mixing length, L_m/R, as a function of velocity ratio, α, for the diffusive mixing of propane and oxidizer, at an equivalence ratio, $\Phi = 0.8$. The mixing passage radius is 0.5mm, the gas temperature is 300K and the velocity of the air stream is 1.0 m/s.

Fig. 3-9 shows the variation of the mixing length with velocity ratio, α, predicted using CFD simulations without shear at the mixing passage walls. The velocity ratio is increased by holding the air velocity constant while increasing the velocity of the fuel stream and maintaining the overall equivalence ratio at 0.8. The results indicate that, increasing the velocity ratio while holding all other parameters constant, increases the mixing length. At low to moderate velocity ratios ($\alpha < 10$) the increase in mixing length is as much as 10%, while at higher velocity ratios ($10 < \alpha < 60$), the increase in mixing length can be as great as 50%. These results can be

explained by the fact that increasing the velocity ratio increases the fuel stream velocity, which in turn increases the mixing length, since the stoichiometric contour at this particular equivalence ratio (Φ=0.8) passes through the centerline of the mixing passage. It is important to note, however, that the increase in mixing length is not as great as would be expected if the overall flow velocity was increased to the velocity of the fuel stream. This is because the higher speed fuel stream entrains the slower moving air flow, which results in a deceleration of the fuel flow and an acceleration of the air flow. As the velocity ratio increases the disparity between the fuel and air stream velocities becomes larger, which means that it takes longer for the high speed stream to decelerate and mix through entrainment of the low speed flow. Hence, the increase in mixing length is more pronounced at higher velocity ratios. Overall these results suggest that mixing lengths in micro-flameholders can be minimized by avoiding velocity mismatch between the fuel and air streams.

These results can be explained by considering Figure 3-10 shows inlet, u-velocity component, vorticity and stream function contours for the mixing of propane and air in a passage with and without shear at the fuel-air interface. In the former case the inlet flow velocity is 1m/s, which corresponds to a flow Reynolds number of approximately 30, while in the latter case the air flow velocity is 1m/s and the velocity ratio, $\alpha = 20$.

In Figure 3-10 a) there is no shear at the wall, and thus the solution is effectively inviscid. This is confirmed by examining the u-velocity component, vorticity and stream function contours for this situation. The figure shows that the u-velocity component is constant; no vorticity is present in the flow; and the streamlines are all parallel to each other.

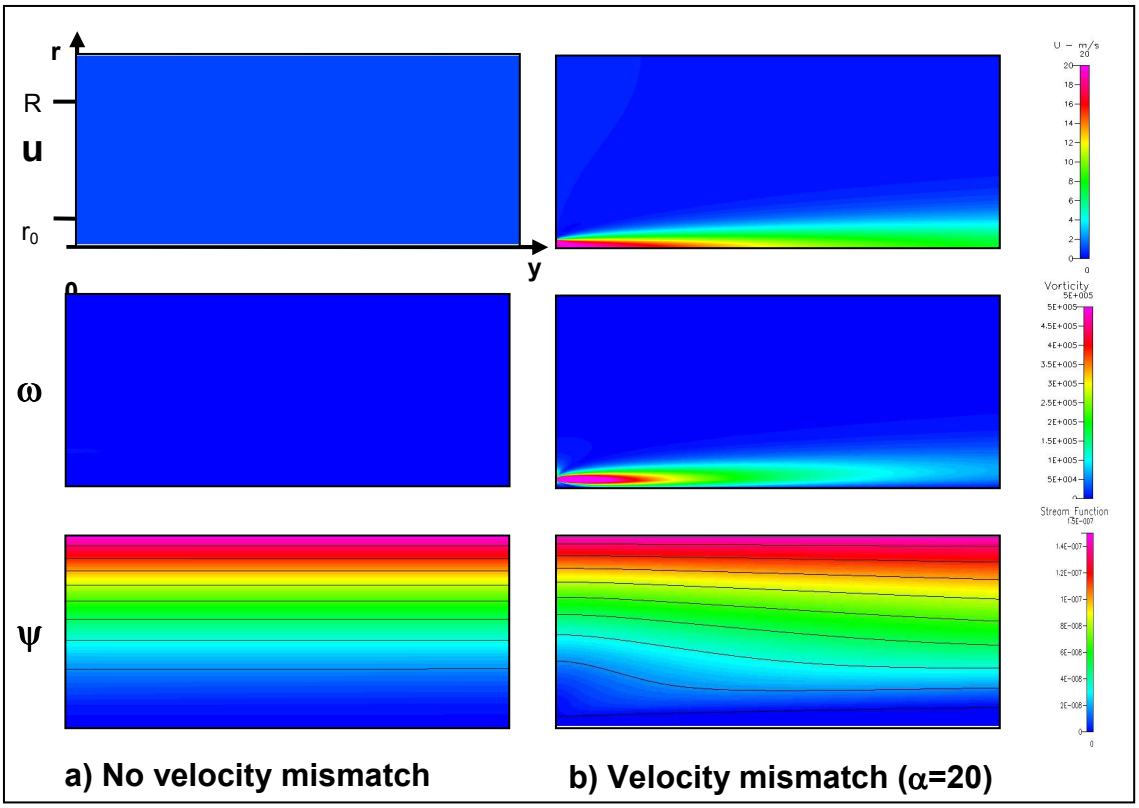

Figure 3-10. U-velocity component, vorticity and stream function contours associated with mixing of propane and air, at an equivalence ratio of 0.8, inside a mixing a passage of radius 0.5mm, for the case of a) no shear at the mixing passage walls and b) shear at the fuel-air interface. The inlet flow velocity for case a) is 1 m/s, which corresponds to a flow Reynolds number of ~30. The air inlet velocity for case b) is 1m/s. The gas temperature is 300K.

In Figure 3-10 b) shear is present at the fuel-air interface. In this situation, the u-velocity component contours reveal that a shear layer is developing at the interface between the fuel and air streams. Associated with this shear layer is a concentrated region of vorticity which is indicative of rotational flow. Moreover, the figure shows that the streamlines in the outer (air) portion of the mixing passage are converging and curving downwards towards the fuel-air interface. This indicates that the outer (air) flow is accelerating and being entrained into the core (fuel) flow and is consistent with the explanation given for the increase in mixing length with increasing velocity ratio.

3.4 Conclusions

The major conclusions reached in this chapter are summarized below:

1. The results of effectively inviscid CFD simulations were found to agree with the predictions of the axisymmetric Burke-Schumann model to within 2% for Reynolds numbers ranging between 10 and 1000 when the overall equivalence ratio is 0.8.
2. The results indicate that axial diffusion appears to have an insignificant effect on the mixing length at overall equivalence ratios near unity. It becomes more significant at low Reynolds numbers (< 50) when the overall equivalence ratio is much larger or smaller than one.
3. Viscous shear at the wall slows the outer (air) flow near the wall while slightly increasing the velocity of the fluid in the center of the mixing passage. For the overall equivalence ratio explored in this study (Φ=0.8), the mixing length was found to increase by approximately 8% percent over the entire range of Reynolds number explored ($10 \leq Re \leq 1000$).
4. Introducing a velocity mismatch between the fuel and air streams produces an increase in the mixing length which depends on the velocity ratio. At low to moderate velocity ratios ($\alpha < 10$) the increase in mixing length is as much as 10%, while at higher velocity ratios ($10 < \alpha < 60$), it can be as much as 50%. The increase in mixing length is larger at higher velocity ratios because the disparity between the fuel and air stream velocities is greater. This means that it takes longer for the high speed stream to decelerate and mix through entrainment of the low speed flow.

Chapter 4: Methods of Enhancing Fuel-air Mixing in Micro-flameholders

4.1 Introduction

The main focus of this chapter is to present various active and passive approaches which can be used to enhance fuel-air mixing in micro-flameholders. In order to understand how these enhancement techniques work it is necessary to understand the basic physics involved in mixing and to be cognizant of the dominant mixing mechanism in micro-flameholders. Chapter four therefore begins with a brief introduction to the fundamental physics governing the mixing of fuel and air in laminar and turbulent flows. It is followed by a simple first order analysis which is used to identify the dominant mixing mechanism in micro-flameholders. Next, several active and passive mixing enhancement techniques suitable for use in micro-flameholders, are presented. The chapter concludes with a brief discussion on how to quantify mixing enhancement and a summary of the major highlights of this chapter.

4.2 Physics of Fuel-air Mixing

4.2.1 Introduction

The mixing of fuel and air in any flow is a complex process. In general, mixing occurs in two main ways: via a combination of convection and molecular diffusion, or solely through molecular diffusion. In the first case mixing is generally very fast and is typified by high Reynolds number, turbulent flow, in which inertial forces dominate the flow field. In contrast, in the latter case mixing is slow and it is characterized by low Reynolds number, laminar flow, in which viscous forces

dominate. A thorough discussion of both of these mixing mechanisms is presented in the following section. In addition, based on this discussion, the dominant fuel-air mixing mechanism in micro-flameholders is identified and suitable strategies which can be used to enhance mixing are proposed.

4.2.2 Physics of Convective Fuel-air Mixing

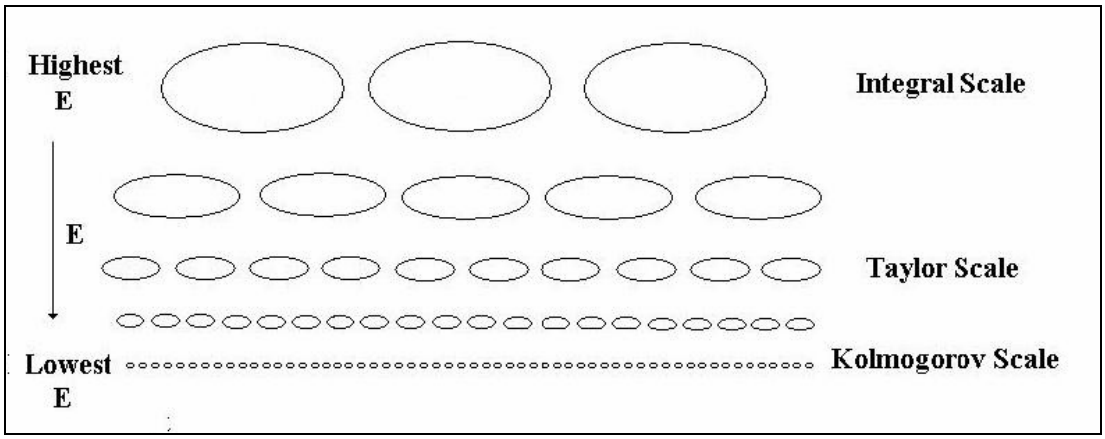

Figure 4-1: The cascade of length scales associated with mixing in a turbulent flow

Before discussing convective fuel-air mixing it is useful to first get a physical picture of a turbulent flow. Figure 4-1 shows the cascades of length scales and energy found in a turbulent flow [63]. The largest length scale, which possesses the highest energy, is called the integral scale. It is length scale at which production (i.e. extraction of energy from the mean flow) occurs, which is usually taken to be on the order of the device size. At the other extreme is the Kolmogorov scale, which is the smallest length scale and has the lowest energy in the flow. The Kolmogorov scale is the length scale at which viscous dissipation occurs. Several intermediate length scales can also be defined in between the integral and Kolmogorov scales. One such scale, which is illustrated in Figure 4-1, is the Taylor scale. With this basic physical picture in mind we can now discuss the physics of convective fuel-air mixing.

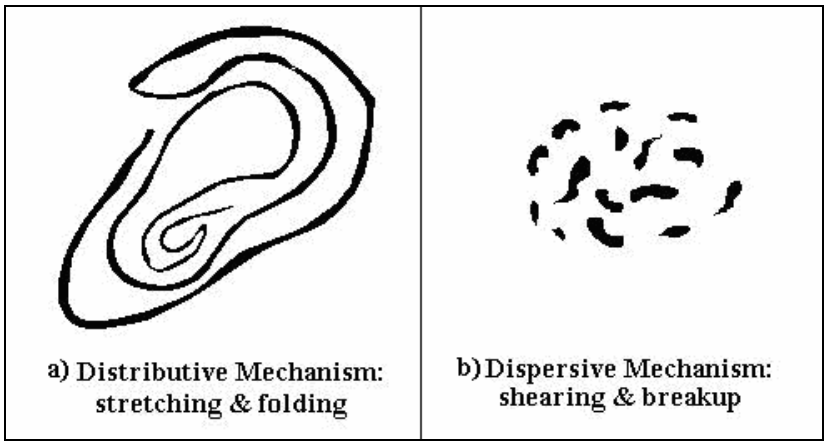

Figure 4-2: Illustration of the two main convective mixing mechanisms (Adapted from Ottino 1989 [80]).

Convective fuel-air mixing usually occurs via two distinguishable mechanisms in turbulent flows [80 & 83]. In the first or distributive mechanism, mixing takes place through the stretching and folding (i.e. roll-up) of the fluid by inertial forces, which results in the formation of large eddies (illustrated above in Figure 4-2 a). Distributive mixing provides global homogeneity on a coarse scale (i.e. at the integral scale, which is on the order of the device size), but the fuel and air molecules still remain largely unmixed.

The second convective mixing mechanism involves dispersive mixing of fuel through shearing and breakup of large eddies into numerous smaller eddies (i.e. small pockets of fuel on the order of the Taylor intermediate scale), as illustrated in Figure 4-2 b). The dispersive mechanism is also attributable to the strong inertial forces associated with turbulent flows. It produces finer scale mixing (i.e. on the order of the Kolmogorov length scale) than the distributive mechanism; however, it still does not achieve thorough mixing of the fuel and air. In order to complete the fuel-air mixing process molecular diffusion is needed. Diffusive mixing is discussed in detail in the next section.

4.2.3 Physics of Diffusive Fuel-air Mixing

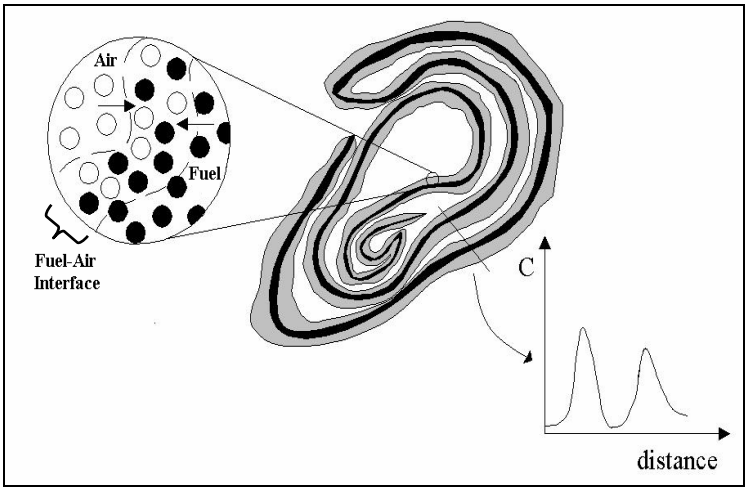

Figure 4-3: Illustration of the diffusive mixing in a turbulent flow (Adapted from Ottino 1989 [80]).

Diffusive mixing is characterized by a species concentration gradient which is established at the interface between the unmixed air and the fuel [84], as shown in Figures 4-3 and 4-4. This is governed by the diffusive flux equation [77], which can be written as:

$$\underset{=}{j} = -D \frac{\partial}{\partial x} \tag{4.1}$$

where j is the diffusive flux, D is the diffusion coefficient, C is species concentration and x is distance.

In this case, mass transfer and transport, and therefore mixing occur as a result of molecular diffusion at the fuel-air interface, where the species concentration gradient is steepest. Fluid (fuel or air) is therefore transported from regions of high species concentration to regions of lower concentration, until equilibrium is reached [77]. Initially, when the fuel and air are completely unmixed, the species concentration gradients will be very steep, and mixing is therefore very rapid.

However, as mixing progresses the species concentration field spreads out, gradients become less steep, and species transport becomes slower.

Diffusive mixing is an essential element of fuel-air mixing in both turbulent and laminar flows. In turbulent, convectively dominated flows ($Re > 10^4$) strong inertial forces cause breakup and stretching of the fluid. This speeds diffusion by creating steep species concentration gradients associated with the numerous small pockets of fuel and air that are generated by the breakup and stretching processes. However, in laminar flows ($Re < 2300$) viscous forces become significant relative to the inertial forces since the inertial forces are weaker in laminar flows, the fluid is not stretched and broken up into small pockets as in the turbulent mixing case. This slows the rate of molecular diffusion since viscous forces resist the formation of the gradients necessary to drive diffusion. Diffusive mixing should therefore be much slower in laminar flows.

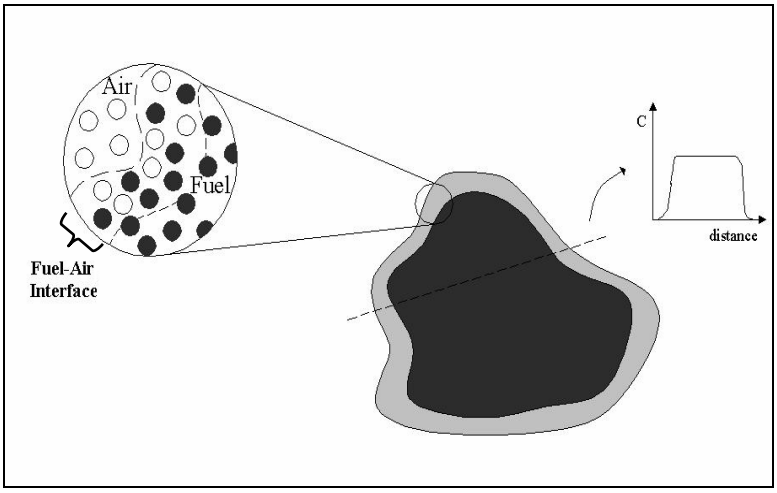

Figure 4-4: Illustration of diffusive mixing in a laminar flow.

4.3 Physics of Fuel-air Mixing in Micro-flameholders

4.3.1 Introduction

In order to gain deeper physical insight into the fuel-air mixing process in a micro-flameholder we need to determine the dominant mixing mechanism taking place. In Chapter two we estimated that the Reynolds numbers associated with fuel-air mixing in micro-flameholders fall in the laminar-transitional flow regime. This strongly suggests that at the microscale, fuel-air mixing may be difficult because it will rely heavily on molecular diffusion in the absence of strong convective forces to breakup and fold the fuel and air as they mix together. To convince ourselves that this is indeed a reasonable inference about fuel-air mixing in micro-flameholders, we can investigate how the diffusive and convective mixing times vary in micro-flameholders compared with conventional-scale flameholders.

4.3.2 Identifying the Dominant Mixing Mechanism in Micro-flameholders

4.3.2.1 Estimating the Relative Dominance of Molecular Diffusion or Convection

The first step in determining the dominant mixing mechanism in micro-flameholders is to assess the relative importance of convection verses molecular diffusion in the flow through a micro-flameholder. To do this, we use the Peclet number for mass transfer, Pe_m, which is defined below in Eq. (4.2) as the ratio of the diffusive mixing time, τ_{diff}, to the convective mixing time, τ_{conv}, in a flow.

$$Pe_m = \frac{\tau}{\tau} \qquad (4.2)$$

Low Peclet numbers are associated with good mixing because the diffusive mixing time is much shorter than the convective mixing time. This in turn means that concentration gradients cannot persist in the flow for very long, and that the flow becomes well mixed rapidly. In contrast, high Peclet numbers are associated with poor mixing, since the diffusive mixing time is much greater than the convective mixing time. This means that gradients persist in the flow and therefore that the flow is not well mixed.

Following the approach of Broadwell et al. [85], we define τ_{diff} and τ_{conv} as:

$$\tau_{diff} = \frac{\ell_{diff}}{} \tag{4.3}$$

$$\tau_{conv} = \frac{}{} \tag{4.4}$$

where ℓ_{diff}, is a characteristic length scale over which molecular diffusion occurs, D is the diffusivity, L is the characteristic device length and, U is the mean flow velocity.

Next, substituting Eqs. (4.3) and (4.4) into Eq. (4.2), and multiplying by $(\nu H^2)/(\nu H^2)$ yields the following expression for the Peclet number:

$$Pe = ReSc\left(\frac{H}{L}\right)\left(\frac{\ell_{diff}}{H}\right)^2 \tag{4.5}$$

where H is the mixing passage height, Re is the flow Reynolds number (previously defined in equation (2.1)), and Sc is the Schmidt number which is defined in terms of the diffusivity, D and the kinematic viscosity ν, as:

$$Sc = \frac{\nu}{} \tag{4.6}$$

Eq.(4.5) highlights the dependence of the Peclet number on the Schmidt number, the flow Reynolds number, the ratio of the mixing passage height to its length and the particular choice of characteristic length scale over which diffusion occurs. As a result, how mixing scales with Reynolds number depends on how ℓ_{diff} scales with Reynolds number. If it is assumed that molecular diffusion takes place over the characteristic device width or integral length scale, H, (discussed previously in Section 4.2.2) then Eq. (4.5) becomes:

$$Pe_m = \text{Re}\, Sc\left(\frac{H}{L}\right) \tag{4.7}$$

which says that mixing becomes harder with increasing Reynolds number.

If instead ℓ_{diff} is assumed to be an intermediate length scale like the Taylor scale, which is defined as $\lambda = \frac{H}{\text{Re}^{1/2}}$, then Eq. (4.5) becomes:

$$Pe_m = Sc\left(\frac{H}{L}\right) \tag{4.8}$$

and the Reynolds number dependence disappears entirely.

Finally, if the Kolmogorov length scale ($\eta = \frac{H}{\text{Re}^{3/4}}$, the smallest length scale in a flow with a Reynolds greater than unity), is used for ℓ_{diff} then the expression for the Peclet number becomes:

$$\text{Pe}_\text{m} = \text{Sc}\left(\frac{\text{H}}{\text{L}}\right)\text{Re}^{-1/2} \tag{4.9}$$

where mixing is important with increasing Reynolds number.

It is important to note here that Eqs. (4.8) and (4.9) are only valid when the Reynolds number is greater than one, since below this Reynolds number, no cascade

of length scales exists. Only the integral length scale is definable below Reynolds numbers of unity and hence only Eq. (4.7) is valid in this regime. In addition, it is crucial to note that Eq. (4.8) is essentially a constant value, independent of Reynolds number, for a particular fluid. It is therefore not useful in estimating the relative dominance of molecular diffusion or convection in a particular flow.

Using the Peclet number definitions outlined in Eqs. (4.7) and (4.9), together with the previous Reynolds number analysis from Chapter two; we can evaluate how fuel-air mixing is in micro-flameholders scales with Reynolds number using Eqs. (4.7) and (4.9).

Before continuing further, it is also important to recognize the limitations of this approach. Eqs. (4.7) through (4.9), assume that the nature of turbulence in a flow is uniform throughout the entire flow and independent of the Reynolds number. While this is useful for the present analysis it must be recognized that this is an oversimplification which is no strictly applicable to all turbulent flows.

4.3.2.2 Identifying Peclet Number Ranges Associated with Good Mixing

A plot of Peclet number divided by Schmidt number (Pe_m/Sc) as a function of crossflow Reynolds number Re_D associated with propane-air mixing in a mixing passage of height H and length L is shown in Figure 4-5. The dashed family of lines was computed using Eq. (4.7) for various mixing passage height-to-length ratios (L/H) where the length scale for diffusion is taken to be the integral length scale. The solid family of lines was computed using Eq. (4.9) for various mixing passage height to length ratios (L/H) where the diffusive length scale is taken to be the Kolmogorov length scale. The area bounded by these lines is sub-divided to show regions

associated with diffusion-dominated mixing, turbulence-dominated mixing, and intermediate regions where both turbulence and molecular diffusion may be important.

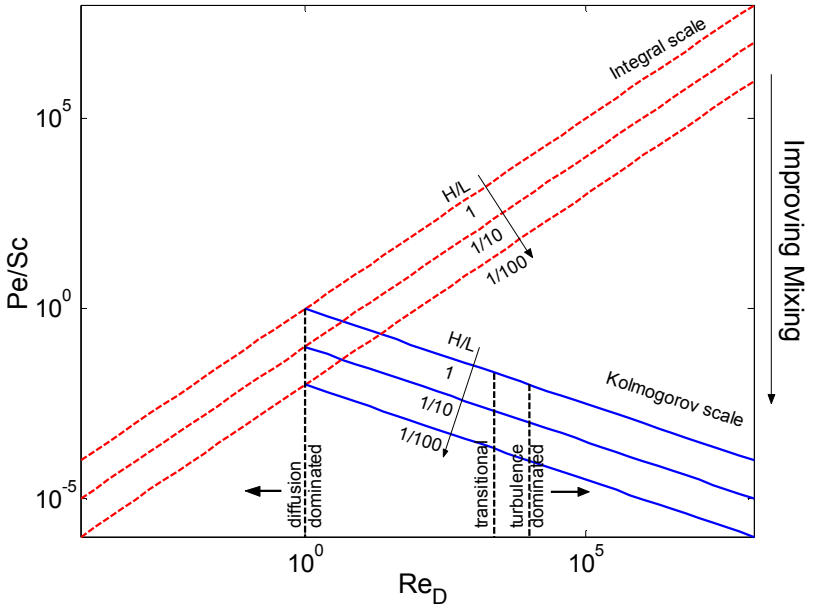

Figure 4-5: Peclet number divided by Schmidt number, Pe_m/Sc, as a function of crossflow Reynolds number, Re_D, associated with the mixing of propane and air, inside ca mixing passage of height, H, and length, L.

Since good mixing is associated with low Peclet numbers, Figure 4-5 shows that mixing can be improved by making mixing passages proportionally longer, i.e. by decreasing the mixing passage height to length ratio. In addition, the figure shows that in the turbulence dominated region, mixing can be improved (i.e. the Peclet number can be lowered) by increasing the Reynolds number. In contrast, in the diffusion-dominated region mixing can be improved by lowering the Reynolds number. Based on the Reynolds number analysis conducted in Chapter two, micro-flameholders will generally fall in the intermediate regions where both turbulence and molecular diffusion may be important. Note, however, that this is also the region with

the highest Peclet numbers indicating that mixing should be proportionally more difficult.

However, in spite of this uncertainty in these intermediate regions some inferences can still be made about the relative importance of diffusion verses convection in these regions. It can be inferred from Figure 4-4, that turbulence will likely be more important than molecular diffusion in the transitional region between laminar flow and fully turbulent flow (i.e. between $2.3x10^3 < Re_D < 10^4$). In a similar manner, we can infer that in the region between transitional flow and diffusion dominated flow (i.e. $Re_D < 1$), diffusion will likely be more important than turbulence.

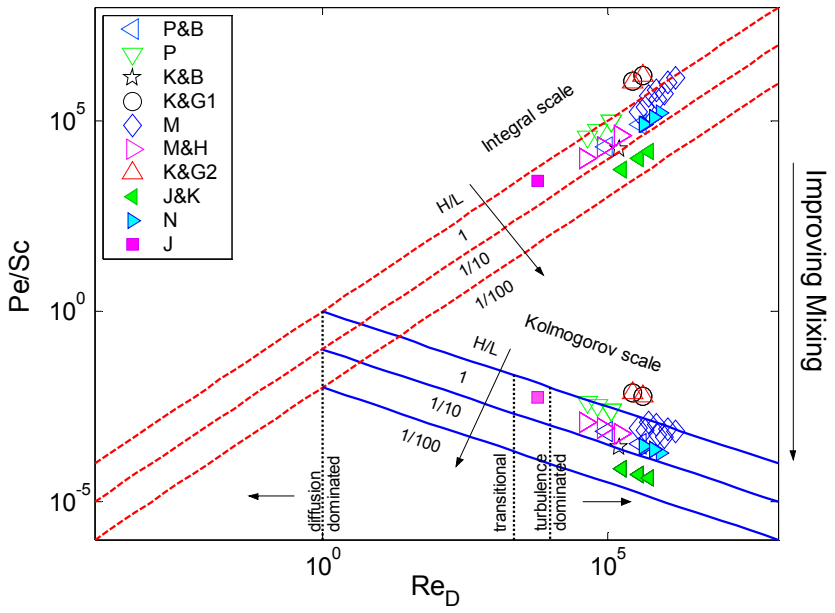

Figure 4-6: Peclet number divided by Schmidt number, Pe_m/Sc, as a function of crossflow Reynolds number, Re_D, associated with the mixing of propane and air, inside a mixing passage of height, H, and length, L. The open symbols correspond to previous experimental investigations of G-G mixing [18], [20-24] & [71] and the solid symbols correspond to L-G [26]& [30] and L-L [29] mixing studies.

If we now include data from several well-known conventional-scale mixing studies [18, 20-24, 26, 29-30 & 71] we can heuristically determine the Peclet number

range required to achieve good mixing in micro-flameholders. Figure 4-6, is the same as Figure 4-5 except that symbols corresponding to various experiments are added. The solid symbols correspond to experimental investigations of liquid-gas (L-G) and liquid-liquid (L-L) mixing while the open symbols correspond to gas-gas (G-G) mixing studies. The data corresponding to each study, along with the abbreviations used in the figure, were summarized previously in Table 2.4. Figure 4-6 shows that the majority of the data from the previous mixing studies are confined to the turbulence dominated region, and are associated with Peclet numbers, based on the Kolmogorov length scale, below 0.01, i.e. ($Pe_m/Sc \leq 0.01$).

Similar plots can also be produced using the jet and jet-interface Reynolds, respectively, as the characteristic Reynolds number associated with fuel-air mixing.

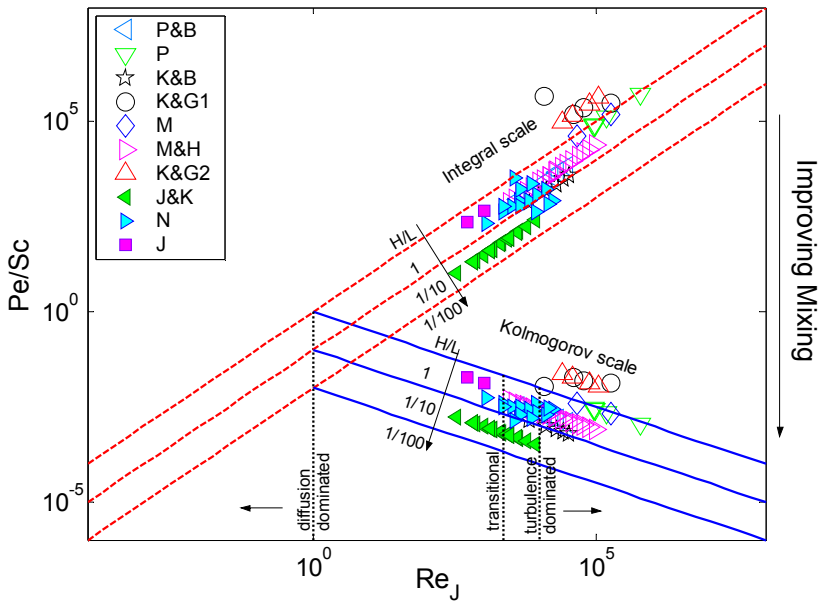

Figure 4-7: Peclet number divided by Schmidt number, Pe_m/Sc, as a function of jet Reynolds number, Re_J, associated with the mixing of propane and air, inside a mixing passage of height, H, and length, L. The open symbols correspond to previous experimental investigations of G-G mixing [18], [20-24] & [71] and the solid symbols correspond to L-G [26]& [30] and L-L [29] mixing studies.

Figure 4-7 shows a plot of Peclet number divided by Schmidt number, Pe_m/Sc, as a function of jet Reynolds number, Re_J, associated with propane-air mixing in a mixing passage of height, H, and length, L. The solid symbols correspond to experimental investigations of liquid-gas (L-G) and liquid-liquid (L-L) mixing [26& 29-30] while the open symbols correspond to gas-gas (G-G) mixing studies [18, 20-24, & 71]. The figure shows that most of the data from these mixing studies are confined to the turbulence dominated and transitional regions, and are associated with $Pe_m/Sc \leq 0.01$ based on the Kolmogorov length scale.

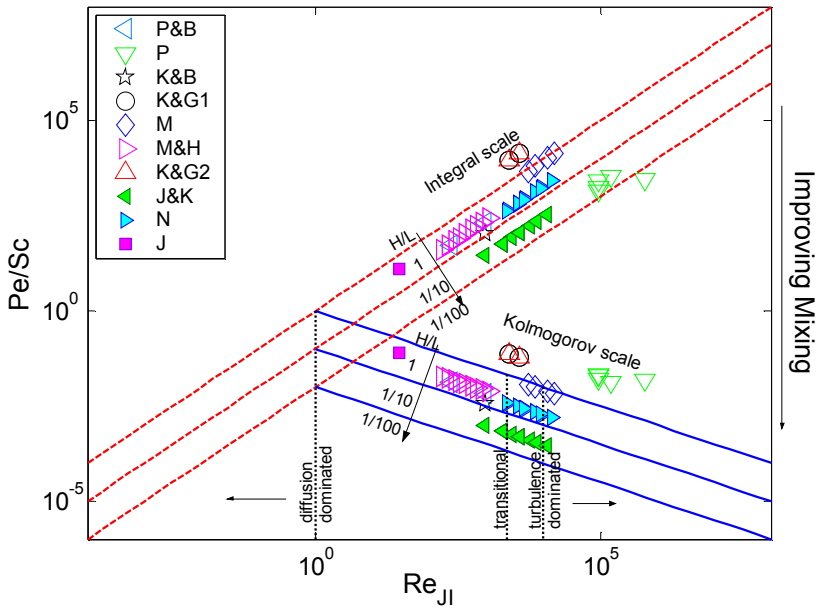

Figure 4-8: Peclet number divided by Schmidt number, Pe_m/Sc, as a function of jet-interface Reynolds number, Re_{JI}, associated with the mixing of propane and air, inside a mixing passage of height, H, and length, L. The open symbols correspond to previous experimental investigations of G-G mixing [18], [20-24] & [71] and the solid symbols correspond to L-G [26]& [30] and L-L [29] mixing studies.

Figure 4-8 shows a plot of Peclet number divided by Schmidt number (Pe_m/Sc) as a function of jet-interface Reynolds number Re_{JI} associated with the mixing of propane and air in a mixing passage of height, H, and length, L. Once again, the solid symbols correspond to experimental investigations of liquid-gas (L-

G) and liquid-liquid (L-L) mixing [26&29-30] while the open symbols correspond to gas-gas (G-G) mixing studies [18, 20-24 & 71]. The figure shows that most of the data from these mixing studies fall in the laminar to transitional regions, and are associated with Peclet numbers, based on the Kolmogorov length scale, below 0.02, i.e. ($Pe_m/Sc \leq 0.02$).

4.3.3 Conclusions about the Dominant Mixing Mechanism in Micro-flameholders

The preceding analysis has allowed us to gain some deeper insight into the physics governing fuel-air mixing in micro-flameholders. Using the Peclet number, representing the non-dimensional ratio of the diffusive mixing time to the convective mixing time, we have determined that in order to achieve levels of mixing in micro-flameholders comparable to conventional scale devices the $Pe_m/Sc < 0.02$. In order to achieve lower Peclet numbers in micro-flameholders the Peclet number analysis suggests that micro-flameholder mixing passages will need be to be proportionally longer (i.e. have lower passage height to length ratios). This suggests that fuel-air mixing in micro-flameholders can be expected to be a slower process than at that the conventional-scale, unless some form mixing enhancement is utilized. To this end, the next section presents various active and passive strategies suitable for enhancing mixing in micro-flameholders.

4.4 Mixing Enhancement Strategies

4.4.1 Introduction

Fuel-air mixing enhancement is often needed in situations in which convection is not the dominant mixing mechanism. Mixing enhancement is accomplished by stimulating the flow to become more turbulent, so that convective mixing can occur. This is generally done in three ways; by active or passive means or by some combination of these two approaches. Active mixing enhancement strategies involve actuating the fuel-air mixture through mechanical means. In contrast, passive mixing enhancement uses simple geometric means to induce the flow to become turbulent.

4.4.2 Passive Mixing Enhancement Strategies

The chief advantages of passive mixing enhancement schemes are their great simplicity (they have no moving parts) and ease of implementation. In addition, because of their lack of complexity the resulting hardware is rarely subject to failure. However, unlike active enhancement strategies they generally do not provide optimum mixing enhancement, since they must be designed to provide adequate performance over a broad operating envelope.

A wide array of passive mixing enhancement schemes exists in the open literature [16, 82 & 86-94]. However, due to the small dimensions associated with micro-flameholders and difficulties involved in fabrication/implementation, not all of the existing mixing enhancement approaches are applicable to micro-flameholders.

One common passive mixing enhancement strategy suited to micro-flameholders is surface roughening. This approach was first investigated in turbulent (liquid) pipe flows by Nikuradse et al. [86] and by Colebrook et al. [87] in the 1930's. These studies both showed that the transition to turbulence is accelerated by roughening the wall surfaces of pipes. Applying this technique to micro-flameholders could enhance mixing by causing the dominant mixing mechanism to shift from diffusion to convection. The coarsening of the mixing passage walls can be easily achieved by micro-machining or by other non-mechanical means (such as gluing sand grains to the passage walls).

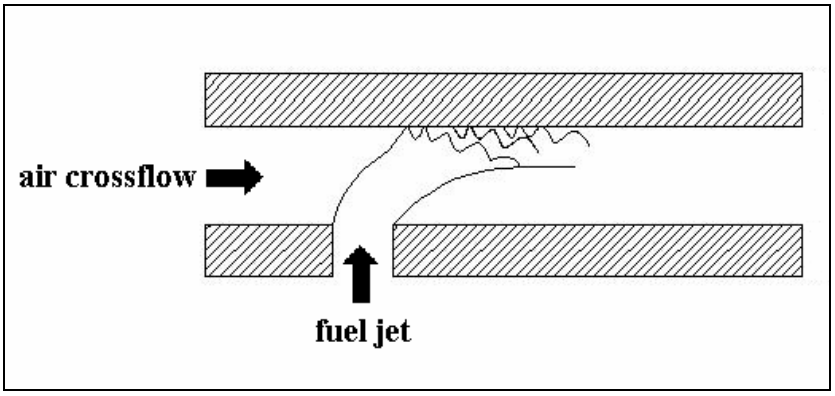

Figure 4-9: Illustration of mixing enhancement by fuel-jet wall impingement.

Wall impingement is another passive strategy that can be used to enhance mixing in micro-flameholders [16]. In this technique, which is illustrated in Fig. 4-9, the fuel jet is impinged on the mixing channel walls in order to promote more rapid breakup of the fuel jet by the air crossflow. Wall impingement mixing enhancement can be easily implemented in micro-flameholders since it simply involves increasing the jet injection velocity.

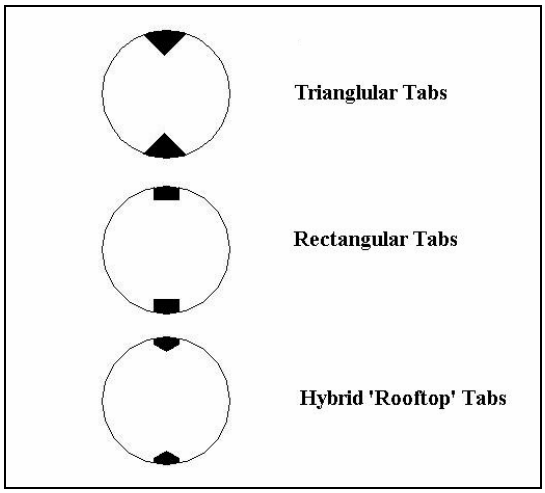

Figure 4-10: Schematic of various mechanical tabs used for mixing enhancement (Adapted from Kobyashi et al. (2000) [88]).

Another promising passive mixing enhancement technique applicable to micro-flameholders is the use of vortex generators in the form of mechanical tabs or small protrusions at the exit of the fuel injection orifices. This approach can be easily implemented in micro-flameholders through micromachining or other micro-fabrication techniques, for simple vortex generator geometries.

Passive mixing enhancement by vortex generators has been extensively investigated at the conventional scale in subsonic [88-92] and supersonic flows [93&94]. In 2000, Kobayashi et al. [88], experimentally investigated the mixing enhancement of a low speed, round jet (Re = 4,000) using delta tab vortex generators. Their results showed that tabbed jet flows have smaller spanwise Kelvin-Helmholtz vortices and earlier appearance of small scale turbulent structures when compared with un-tabbed jet flows. In addition, the length of the laminar region in the jet flow was found to be shorter when tabs are used. Zaman et al. [89] (1993) conducted a series of experiments to study the effects of various triangular and rectangular tab configurations (shown in Figure 4-10) on the evolution of free, round jets 1.27cm in

diameter, and rectangular jets measuring 1.47cm by 0.35cm. The results showed that the mechanical tabs enhanced jet mixing by generating streamwise vorticity which distorts the mixing layer around the jet. Zaman et al. also found that triangular tabs were more effective in enhancing mixing than rectangular tabs.

All of the preceding passive mixing enhancement strategies can also be collectively implemented in micro-flameholders. This collective approach may provide better overall mixing enhancement over the entire micro-flameholder operating envelope, since some strategies may work better under different flow conditions.

4.4.3 Active Mixing Enhancement Strategies

The primary advantage of active mixing enhancement techniques is their ability to provide the best possible or nearly optimum mixing enhancement over a wide range of operating conditions. However, this advantage is offset by their inherent complexity and by difficulties associated with their implementation.

A wide variety of active mixing enhancement schemes have been extensively investigated extensively over the past thirty years [95-104]. However, some of these techniques are impractical for use in micro-flameholders due to difficulties involved in fabricating complex structures at the small length scales associated with these devices. Hence, the active mixing enhancement schemes considered here are chosen because of their relative ease of implementation and fabrication compared to other methods.

One promising active mixing enhancement technique, which can be readily implemented in micro-flameholders, is pulsed or forced fuel jet injection. Pulsing of a

fluid jet at high frequencies enhances mixing by creating small-scale velocity disturbances which amplify natural (Kelvin-Helmholtz) instabilities in the jet as they progress downstream. These, in turn, cause the jet to spread and mix with the surrounding fluid [95]. Typically, jet forcing is achieved through acoustic, mechanical, or thermal means [96]. In acoustic forcing, excitation of the jet is achieved by using a sound-wave producing device while in mechanical forcing an actuator is used. In thermal forcing, the jet is excited by heating the fluid in the vicinity of the lip of the jet injection orifice which induces disturbances in the jet at frequencies as high 100 kHz [97]. However, the latter approach is impractical for micro-flameholders because of the very high temperatures and voltages needed to excite the jet sufficiently [97].

The use of acoustic forcing as a means of enhancing mixing has been extensively investigated over the past twenty years. In 1986, Raman [98] explored the effect of acoustic forcing on the mixing of an axisymmetric air jet using a single hot-wire probe to obtain turbulence levels at the nozzle exit and along the jet centerline as well as a microphone at the nozzle exit . He found that excitation at the appropriate Strouhal number ($St = \frac{fD}{U}$, where f is the driving frequency, D is the passage width and U is the characteristic velocity) resulted in a significant improvement in mixing, with the effects being most prominent in the Strouhal number range, $0.4 \leq St \leq 1.0$. More recently, in 1997, Matta et al. [99] studied the effects of modulated, transverse acoustic excitation on a subsonic round jet using image processing techniques to compute the mixing entropy. From their results they concluded that mixing enhancement is strongly dependent on Strouhal number with the greatest benefits

seen between $0.3 \leq St \leq 0.4$. Matta et al. also found that there was no strong correlation between modulating frequency and mixing enhancement over the frequency range tested (5-20 Hz).

Many studies have also considered mixing enhancement through mechanical forcing [100-104]. The most commonly investigated mechanical forcing techniques in recent years have been piezoelectric actuators and synthetic jet actuators. Piezoelectric actuators work through the electrical stimulation of a piezoelectric membrane to produce small-amplitude deflections at high frequencies which excite instabilities in a fluid jet, thereby enhancing mixing. Synthetic jet actuators, in contrast, achieve mixing enhancement through the interaction of zero-mass flux jets synthesized from the working fluid in the flow system with the main jet. These interactions are used to promote momentum transfer into the main jet.

Several studies over the last decade have explored the use of piezoelectric actuators for mixing enhancement [100&101]. In 1996, Prakesh et al. [100] examined the effects of piezoelectric excitation devices on high aspect-ratio, rectangular jets, at subsonic and supersonic jet Mach numbers. They evaluated mixing effectiveness by using pressure-probe surveys, near- and far-field acoustic surveys and by schlieren flow visualization. Prakesh et al. found that significant increases in mixing were achieved in the subsonic, transonic and supersonic flow regimes. These were attributed to the excitation of the jet flapping mode by the piezoelectric actuators. Enhanced mixing was most pronounced when the excitation Strouhal number was approximately 0.2. Moreover, in 2001, Pothos et al. [101] studied the asymmetric forcing of a turbulent, rectangular jet by a piezoelectric actuator with a maximum

displacement of 120 microns. Using hot-wire measurements they observed that actuation strongly affects both the mean and root mean squared velocity (rms) profiles downstream of the jet injection orifice. They also found that forcing the jet at Strouhal numbers less than 0.3 yielded faster decay of the centerline velocity, higher far field spreading rates, and asymmetric rms velocity profiles compared with those of unforced flows.

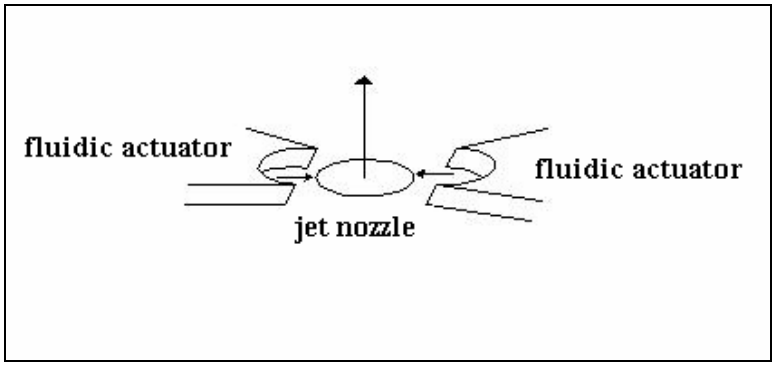

Figure 4-11: Schematic of jet mixing enhancement using two fluidic actuators. [Adapted from Freund et al. (2000)]

A number of studies have also involved the use of synthetic jet actuators to enhance mixing in jets and shear flows [102-104]. In 1997, Smith et al. [102] investigated the effects of placing miniature (millimeter-scale), high aspect ratio actuator jets near the exit plane of a large 75mm-wide rectangular air jet. They found that the action of the actuator jets greatly increased small scale motions in the primary jet and enhanced turbulent dissipation. Synthetic jet actuators have also been numerically studied by Freund et al. [103&104] for a round air jet at Mach 0.9 using the configuration shown in Figure 4-11. The numerical results of these studies were validated via comparison to the experimental results of Stromberg et al. [105] (1980) for the case of no jet forcing. Freund et al. showed that high-amplitude, low mass flux pulsed slot jets issuing normal to the jet's shear layer, near the jet nozzle, significantly

altered the jets development, by exciting a distinct jet flapping mode. They also observed that the potential core length of the jet was reduced most by forcing the jet at a Strouhal number of 0.2.

The next logical step is to find a way to evaluate the performance of a given mixing enhancement strategy when it is applied to a micro-flameholder. This brings us to the question of how to quantify mixing enhancement? This question is tackled in the next section.

4.5 Quantifying Mixing Enhancement

In order to assess the performance of the mixing enhancement schemes which were presented in the previous section, we need to devise a means of quantifying mixing enhancement. One simple way to do this is to define a mixing enhancement 'efficiency', based on the mixing length, L_m; which was defined previously in Chapter 2, as the distance (measured from the point of fuel injection) required for the fuel and air to mix to some pre-defined level of completeness. If we consider the mixing length before mixing enhancement has been applied as an un-enhanced mixing length $L_{m,UE}$, and the mixing length after enhancement has been applied as an enhance mixing length $L_{m,E}$, we can define a mixing enhancement efficiency, η_{ME}, as:

$$\eta_{ME} = \frac{L_{m,UE} - L_{m,E}}{L_{m,UE}} \text{x}100\% \tag{4.10}$$

It is important to observe here that if $\eta_{ME} = 0\%$ then the enhanced mixing length is the same as the un-enhanced mixing length, while if $\eta_{ME} = 100\%$, then the enhanced mixing length is zero which corresponds to perfect mixing.

Using equation (4.10) we can effectively quantify mixing enhancement in micro-flameholders and assess the performance of the different enhancement schemes presented in the preceding section. The best scheme or combination of schemes will result in the highest mixing enhancement efficiency.

4.6 Summary

This chapter has presented a brief introduction to the basic physics governing the mixing of fuel and air in laminar as well as turbulent flows. The Peclet number which represents the non-dimensional ratio of the diffusive mixing time to the convective mixing time, was used to characterize the relative ease of fuel-air mixing mechanism in micro-flameholders. Using this approach we have determined that levels of mixing comparable to those found in conventional devices are achieved when the Pe_m/Sc based on the Kolmogorov length scale is less than 0.02. The Peclet number analysis also suggests that mixing in micro-flameholders will rely heavily on molecular diffusion in the absence of strong inertial forces. This suggests that fuel-air mixing in micro-flameholders will be a slower process than that realized at the conventional-scale unless mixing enhancement is utilized. Several promising passive as well as active mixing enhancement strategies suitable for implementation in micro-flameholders were also presented. Finally, a method of quantifying mixing enhancement was proposed using a mixing enhancement efficiency parameter based on the mixing length.

Chapter 5: Experimental Design

5.1 Introduction

This chapter presents the basic outline of an experiment that could be constructed to verify the predictions of the analytical model and the two- as well as three-dimensional CFD simulations. In addition, the proposed experiment could be used to evaluate the effectiveness of the mixing enhancement strategies which were discussed in the previous chapter.

The specific objectives of this experiment are to:

- Simulate the flow conditions encountered in a micro-flameholder.
- Verify that fuel-air mixing is difficult in micro-flameholders.
- Investigate the effects of operational parameters (i.e. fuel type, equivalence, inlet temperature) on fuel-air mixing in micro-flameholders.
- Test and evaluate the effectiveness of various mixing enhancement strategies.
- Provide data for analytical and numerical model validation.

5.2 Experimental Details

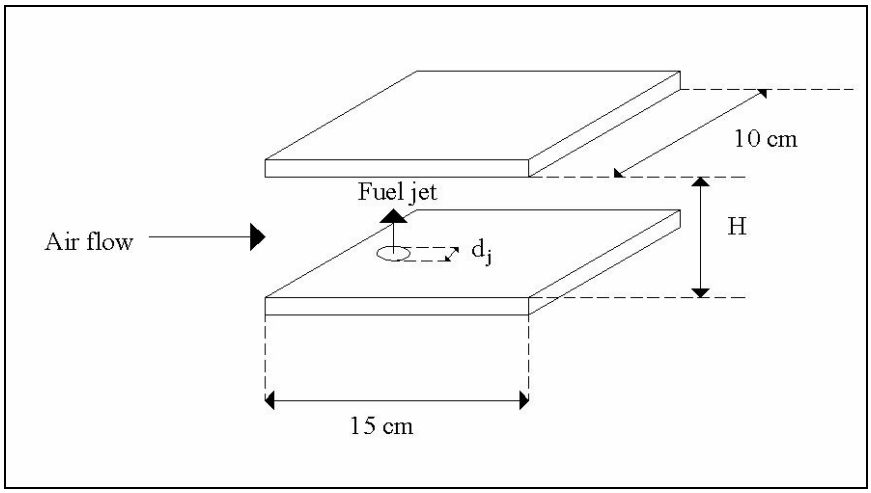

Figure 5-1: Schematic of the micro-flameholder to be used in the proposed experiment.

Figure 5-1 shows a schematic of the micro-flameholder to be used in the proposed experiment. It consists of two parallel, aluminum plates, separated by a distance, H, between which fuel and air are mixed. The plates will be 10 cm wide, 15 cm long and 1 cm thick, with an adjustable separation distance between 0.5 mm and 5 mm. The geometry of the micro-flameholder would also be varied by changing the number, shape, and size of the fuel injection ports found in the lower plate. To do this, the lower plate, would be made removable so that it could be switched with another plate with a different geometry. This will allow a wide range of flow conditions to be explored, as well as facilitate the testing of different mixing enhancement strategies.

Fuel and air will be introduced into the micro-flameholder from plenums using mass flow controllers as shown in Figure 5-2. Pressure valves will be used to regulate the flow between the plenums and the injection ports. The composition of the fuel-air mixture in the micro-flameholder can be made leaner or richer by using the

fuel or air mass flow controllers. This will be used in the tests in which the operational parameters of the micro-flameholder are varied. Moreover, in order to test the effect of preheating the air entering the flameholder on fuel-air mixing, a heating coil, wrapped around the airflow pipe, will be used to raise the air temperature up to 700 K.

Carbon dioxide (CO_2), will be used to simulate the fuel flow because its concentration can be easily measured using a wide variety of diagnostic techniques, and because it has the same molecular weight, and hence diffusive properties as propane. This will facilitate ready comparison of the experimental and numerical results. Further, in order to visualize the mixing process, two calcium fluoride windows will be installed on either side of the parallel plates, as shown in Figure 5-2. To prevent side leakage of the flow, the windows will be equipped with seals.

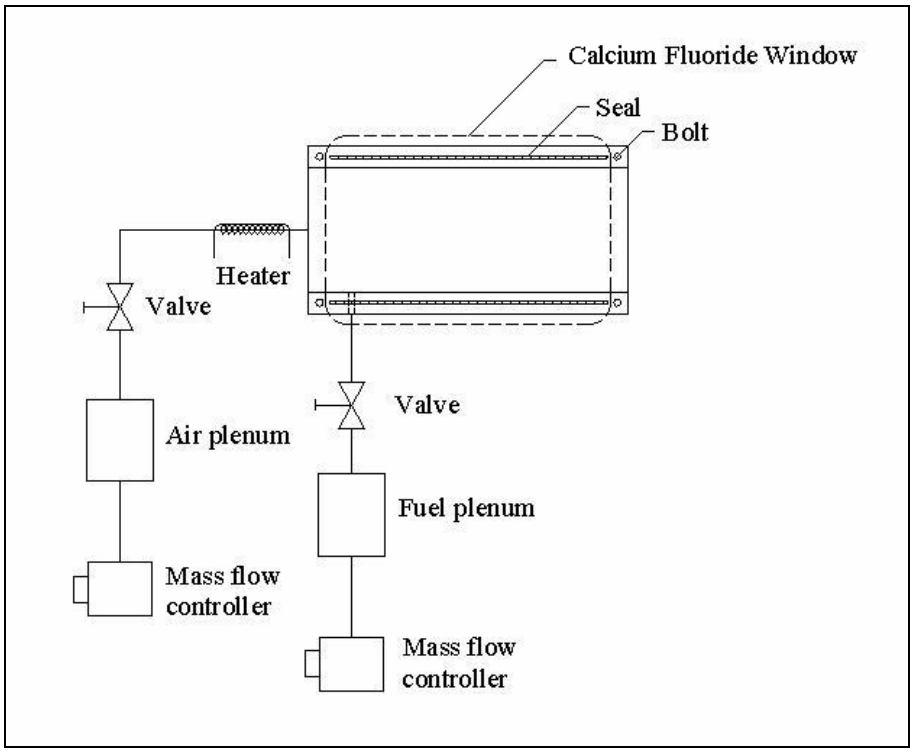

Figure 5-2: Schematic of the flow control apparatus to be used in the proposed experiment.

5.3 Experimental Diagnostics

A Fourier Transform Infrared (FTIR) spectrometer will be used to measure the concentration of carbon dioxide as it mixes with air along the length of the micro-flameholder. The progress of the mixing will be inferred by studying the evolution of these concentrations with downstream distance. This FTIR diagnostic technique, which is described in detail in Heatwole et al. [106], can also be used to measure temperature in the micro-flameholder for the tests involving preheating of the air entering the flameholder. Figure 5-3, shows a schematic of the diagnostic apparatus:

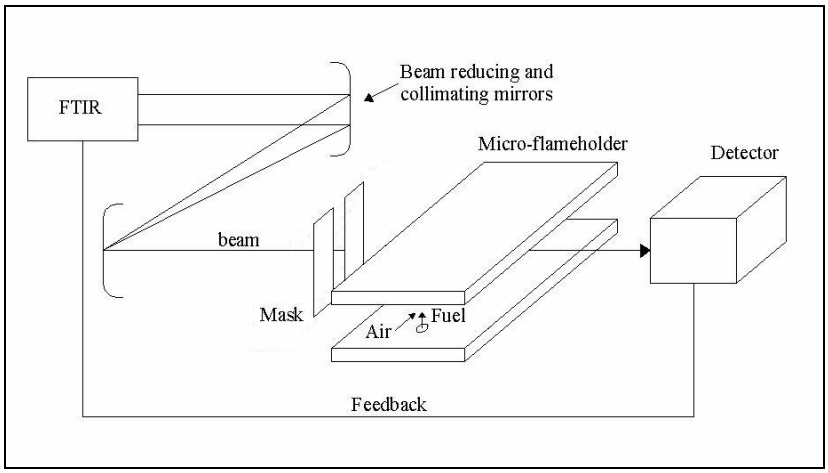

Figure 5-3: Schematic of the FTIR diagnostic apparatus.

Spatial resolution is increased by reducing the size of the interrogation area by using a mask as shown in Figure 5-4.

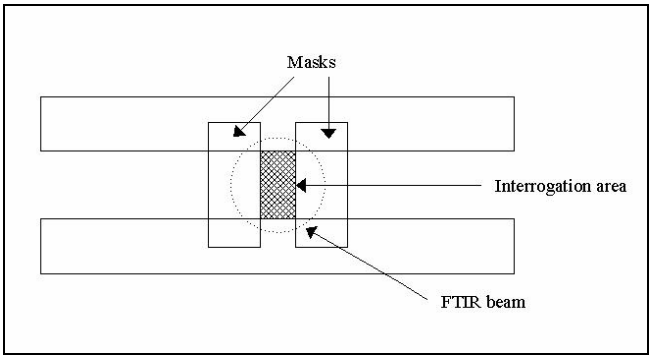

Figure 5-4: Sketch showing the use of a mask to reduce the interrogation area.

An alternative to the previously described diagnostic approach would be to use infra-red Planar Laser Induced Fluorescence (PLIF) to measure the concentration of CO_2 as it mixes with air along the length of the micro-flameholder. The mixing progress in this case would be determined by monitoring the change in CO_2 concentration with downstream distance, as schematized below in Figure 5-5. A thorough description of this diagnostic technique is given by Kirby et al. (2000) [107].

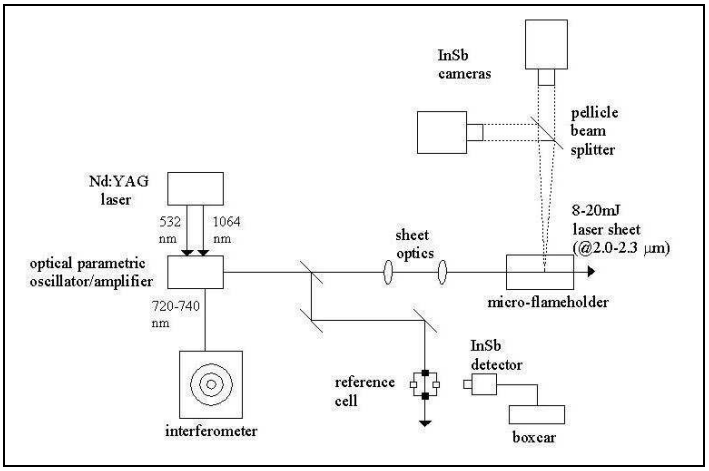

Figure 5-5: Schematic of the CO_2 PLIF diagnostic apparatus. [Adapted from Kirby et al. (1989)]

One minor shortcoming of this technique is that it will not provide gas temperature data in the micro-flameholder. In this case, a high resolution Infra-Red (IR) Camera can be used to obtain the necessary gas temperature information.

5.4 Summary

This chapter has presented a brief outline of an experiment which can be constructed to test the predictions of the analytical and numerical models. The experimental approach and diagnostic techniques presented here are only preliminary.

A lot more design work and planning needs to be done before the proposed experiment could actually be built and carried out.

Chapter 6: Conclusions

This chapter summarizes the research described in this thesis and presents the major conclusions that were found.

6.1 Research Summary

The main focus of this work was to characterize the fuel-air mixing process in a micro-flameholder. While a micro-flameholder has been previously built and tested by Mitani et al. [5], there has thus far never been a comprehensive study to investigate the nature of fuel-air mixing in such a device.

The first step in this characterization process involved the identification of the Reynolds numbers associated with fuel-air mixing in micro-flameholders using a simple, first-principles model. The Reynolds number is useful for characterizing mixing because it represents the ratio of inertial to viscous forces in a flow. Inertial forces are associated with the breakup and dispersion of fluid in a flow, while viscous forces are related to the diffusion of momentum in a flow. If the Reynolds number is large ($Re>10^5$) this implies inertial forces are dominant and therefore mixing is taking place in a turbulent environment. In contrast, if the Reynolds number is small ($Re<1$) then inertial forces are weak, and mixing is taking place in a laminar environment. Therefore, knowing the range of Reynolds numbers expected therefore gives useful first-order physical insight into the nature of the fuel-air mixing process in a micro-flameholder.

The next step was to investigate how the Reynolds number range predicted in micro-flameholders was affected by variations in micro-flameholder operating

parameters such as the inlet temperature, the equivalence ratio, and the fuel type used. Understanding how these parameters affect mixing is crucial to the fuel-air mixing characterization process since a micro-flameholder may be required to operate over a range of off-design conditions. This is also important in determining an optimum flameholder design.

To further characterize fuel-air mixing in micro-flameholders, the range of mixing lengths expected in micro-flameholders was estimated using a purely diffusive mixing model based on the Burke-Schumann diffusion flame theory. Mixing lengths were estimated using a parameter β which allowed stoichiometric fuel-air contour to be computed from the fuel and air mass fractions. For lean mixtures the mixing length is the maximum streamwise distance along the centerline of the mixing passage for which $\beta = 0$; whereas for rich mixtures the mixing length is the maximum streamwise distance near the wall of the mixing passage for which $\beta = 0$. Knowing the mixing length is useful since it influences the overall size/length of a micro-flameholder.

A more complete characterization of the fuel-air mixing process in a micro-flameholder necessitated the use of a Navier-Stokes solver which could account for convective transport, interface instability, and viscous effects. Low Reynolds number axisymmetric CFD simulations were performed using CFD-ACE+ [81], a commercial Navier-Stokes solver. The main objective in performing low Reynolds number CFD simulations was to understand the reliability of the predictions made using the simple Burke-Schumann diffusive mixing model. The CFD simulations were also useful because they allowed the effects of axial diffusion as well as viscous shear at the

walls and the fuel-air interface to be explored individually. This is helpful for understanding their individual impacts on the overall mixing problem.

The final step in the characterization process was to identify the dominant fuel-air mixing mechanism in micro-flameholders. This is important since the mixing length, and hence the overall micro-flameholder device size, depends heavily upon the dominant mechanism by which mixing occurs. If mixing occurs via a combination of convection and molecular diffusion then mixing lengths will likely be short because the strong inertial forces will cause the fluid to breakup and disperse quickly which in turn creates steep concentration gradients to drive diffusive transport. If inertial forces are weak mixing occurs solely through molecular diffusion. In this case, mixing lengths will likely be very long because the fluid will not be broken up or dispersed and the concentration gradients in the fluid will not remain steep. The Peclet number, which represents the non-dimensional ratio of the diffusive mixing time to the convective mixing time, was used to determine the relative ease of achieving mixing of fuel and air in a micro-flameholder. A heuristic approach, using data from several well known mixing studies, was employed to determine the Peclet range required to ensure good mixing in micro-flameholders.

The major conclusions derived from the analytical and numerical characterization of fuel-air mixing in micro-flameholders are summarized in the next section.

6.2 Major Conclusions

The most significant conclusions of this thesis are summarized below:

1. The range of Reynolds numbers associated with fuel-air mixing in micro-flameholders has been identified.

   a) It falls in the laminar to transitional flow regime.

   b) This Reynolds number range is much lower than that associated with mixing in conventional-scale power systems.

   c) Pre-heating of the fuel-air mixture will reduce Reynolds numbers associated with fuel-air mixing in micro-flameholders.

2. There is a dearth of experimental work in the literature that has investigated the flow regime associated with fuel-air mixing in micro-flameholders.

3. A simple model based on molecular diffusion has been developed to predict how the size of a micro-flameholder should vary with Reynolds number. The model shows that:

   a) Fuel-air mixing lengths in micro-flameholders decrease with decreasing micro-flameholder size.

   b) The shortest mixing lengths are predicted for mixing at lean and rich overall equivalence ratios ($\Phi << 1$ and $1 << \Phi$).

   c) Fuel-air mixing lengths can be minimized by pre-heating the fuel-air mixture and by minimizing the flow velocity in micro-flameholders.

4. The predictions of the simple mixing length model were compared to the results of CFD simulations.

a) The results of effectively inviscid CFD simulations agreed closely (within 2%) with the predictions of the axisymmetric Burke-Schumann model in the Reynolds numbers ranging between 10 and 1000. This suggests that the Burke-Schumann Model-based mixing length approach provides reasonable first-order estimates of fuel-air mixing lengths in micro-flameholders at low Reynolds numbers.

b) The CFD results indicate that axial diffusion appears to have an insignificant effect on the mixing length at overall equivalence ratios near unity. However, axial diffusion becomes more significant at low Reynolds numbers ($Re < 50$) when the overall equivalence ratio is much larger or smaller than one.

c) Viscous shear at the wall slightly increases the fuel-air mixing distance. Shear at the wall slows the outer (air) flow near the wall, while in turn slightly increasing the velocity of the fluid in the center of the mixing passage. For the equivalence ratio explored in this study ($\Phi=0.8$), the mixing length was found to increase by approximately 8% percent over the entire range of Reynolds numbers explored ($10 \leq Re \leq 1000$).

d) Velocity mismatch between the fuel and air streams produces an increase in the mixing length which depends on the velocity ratio. At low to moderate velocity ratios ($\alpha < 10$) the increase in mixing length is as much as 10%, while at higher velocity ratios ($10 < \alpha < 60$), it can be as much as 50%. The increase in mixing length is larger at higher velocity ratios because the disparity between the fuel and air stream velocities is greater. This, in turn,

means that it takes longer for the high speed stream to decelerate and mix through entrainment of the low speed flow.

5. The results of a simplified residence time analysis showed:

   a) Fuel-air mixing in micro-flameholders is expected to rely heavily on molecular diffusion, in the absence of strong inertial forces.

   b) To ensure ‘good’ mixing, in micro-flameholders the Peclet number based on the Kolmogorov length scale must be less than 0.02.

   c) Lower Peclet numbers in micro-flameholders can be achieved by making mixing passages proportionally longer.

Chapter 7: Future Work

The first and most important task will be to perform three-dimensional CFD simulations to examine how flow structures influence fuel-air mixing characteristics in micro-flameholders at low Reynolds number. Single jet mixing configurations will be numerically explored first, followed by more elaborate multiple jet configurations. Once these further three dimensional simulations are completed the next task will be to modify the two- and three-dimensional numerical simulations to model the effects of varying different operational parameters, such as the inlet temperature, on fuel-air mixing in a micro-flameholder. These results can then be compared with the analytical model predictions presented in Chapter 2 for verification. The third task will be to numerically model some of the mixing enhancement strategies which were proposed in Chapter 4. Passive mixing enhancement approaches will likely be the easiest to model due to their great simplicity and lack of moving parts. Moreover, these simulations should allow an optimum enhancement strategy to be identified by determining which enhancement technique yields the shortest mixing length. Fourth, the effect of using a low molecular weight fuel on fuel-air mixing in micro-flameholders can be investigated by numerically simulating the mixing of hydrogen and air. Fifth, the simple analytical model can be extended to investigate the mixing of liquid fuel and air in micro-flameholders. Finally the experiment which was proposed in Chapter 5 needs to be constructed in order to provide experimental validation of the predictions made by the analytical model and numerical simulations.

Bibliography

[1] Wu, M., Yetter, R., and Yang, V., 'Combustion in Meso-scale Vortex Combustors: Experimental Characterization,' AIAA 2004-0980, 42nd AIAA Aerospace Sciences Meeting and Exhibit, Reno, NV, Jan. 5-8th, 2004.

[2] Singh, D., Carpenter, M., and Drummond, J., 'Thrust Enhancement in Hypervelocity Nozzles by Chemical Catalysis,' Journal of Propulsion and Power, Vol. 13, No. 4, 1997, pp. 574-578.

[3] Taha, A., Tiwari, S., and Mohieldin, T., 'Pilot Injection and Flame Characteristics of Propane Combustion in Scramjet Engines,' AIAA 2002-4276, 38th AIAA/ASME/SAE/ASEE Joint Propulsion Conference & Exhibit, Indianapolis, IN, Jul. 7-10, 2002.

[4] Cheng, Z., Wehrmerer, J. and Pitz, R., 'Downstream Interaction of Lean Premixed Flame,' Proceedings of the Third Joint Meeting of the US. Sections of the Combustion Institute, Chicago, IL, March 16-19, 2003.

[5] Mitani, T. ,Kobayashi, K., and Tomioka, S., 'Ignition by an H_2/O_2 Micro-burner in a Supersonic Airflow,' AIAA 2001-1763, AIAA/NAL-NASDA-ISAS 10th International Space Planes and Hypersonic Systems and Technologies Conference, Kyoto, Japan, 2001.

[6] Mehra, A, 'Development of a High Power Density Combustion System for a Silicon Micro Gas Turbine,' Ph.D. Thesis, M.I.T., Feb. 2000.

[7] Sabel'nikov, V. and Penzin, V., 'The Enhancement of Liquid Hydrocarbon Supersonic Combustion Using Effervescent Sprays and Injectors with Noncircular Injectors' published in Scramjet Propulsion, edited by Curran, E. and Murthy, S.,

Vol. 189, Progress in Aeronautics and Astronautics, AIAA, Reston, VA, 2000, pp.310-317.

[8] Fernandez-Pello, C., 'Micro-Power Generation Using Combustion: Issues and Approaches,' presented as a Topical Review at the 29th International Symposium on Combustion, Jul. 21-26, 2002, Sapporo Japan, pp.11-14.

[9] Gruber, M., Mathur, T., Baurle, R., and Hsu, K., 'Fundamental Studies of Cavity-based Flameholder Concepts for Supersonic Combustors,' AIAA 99-2248, 35th AIAA/ASME/SAE/ASEE Joint Propulsion Conference and Exhibit, Los Angeles CA, Jun. 20-24, 1999.

[10] Yu, G., Li, J., Chang, X., Chen, L. and Sung, C., 'Investigation of Fuel Injection and Flame Stabilization in Liquid Hydrocarbon-fueled Supersonic Combustors,' AIAA 2001-34308, 37th AIAA/ASME/SAE/ASEE Joint Propulsion Conference and Exhibit, Salt Lake City, UT, Jul. 8-11, 2001.

[11] Hassa, C., Carl, M., Frodermann, M., Behrendt, T., Heinze, J., Fleing, C., Meier, U., Wolff-Gabmann, D., Hohmann, S., Zarzalis, N., 'Experimental and Numerical Investigation of a Planar Combustor Sector at Realistic Conditions,' ASME paper 2000-GT-0123, ASME Turbo Expo 2000, Munich, Germany, May 8-11, 2000.

[12] Chen, K-S., 'Materials Characterization and Structural Design of Ceramic Microturbomachinery,' Ph.D. Thesis, M.I.T., 1999.

[13] Lide, D., CRC Handbook of Chemistry and Physics, 72nd Edition, CRC Press, Cleveland, OH, 1991.

[14] Ben-Yakar, A. and Hanson, R., 'Cavity Flameholders for Ignition and Flame Stabilization in Scramjets: Review and Experimental Study,' AIAA 98-3122, 34th

AIAA/ASME/SAE/ASEE Joint Propulsion Conference & Exhibit, Cleveland, OH, Jul. 13-15, 1998.

[15] Leach, T. Jackson, G. and Cadou, C., 'Effect of Structural Conduction and Heat Losses on Combustion in Micro-Channels,' accepted for publication by the Journal of Combustion Theory and Modeling, 2005.

[16] Griffiths, J. and Barnard, J., Flame and Combustion, 3rd Ed., Chapman & Hall, New York, 1995, pp.43 & 259.

[17] Gordier, R., 'Studies on Fluid Jets Discharging Normally into Moving Liquid,' St. Anthony Falls Hyd. Lab., University of Minnesota, Tech. Paper, no. 28, Series B, 1959.

[18] Keffer, J. F, and Baines, W. D., 'The Round Turbulent Jet in a Cross-wind', J. Fluid Mech., Vol. 8, 1963, pp.481-496.

[19] Alderberg, M., 'Breakup Rate and Penetration of a Liquid Jet in a Gas Stream,' AIAA Journal, Vol. 5, Feb. 1967, pp.1408-1415.

[20] Pratte, B. D., and Baines, W. D., 'Profiles of the Round Turbulent Jet in a Crossflow', Journal of the Hydraulics Division, ASCE, Vol. 92, 1967, pp.53-64.

[21] Margason, R.J., 'The Path of a Jet Directed at Large Angles to a Subsonic Free Stream', NASA TN D-4919, 1968.

[22] Patrick, M. A., 'Experimental Investigation of the Mixing and Penetration of a Round Turbulent Jet Injected Perpendicularly into a Transverse Stream', Transactions of the Institution of Chemical Engineers, Vol. 45, 1967, T16-T31.

[23] Greber, I. and Kamotani, Y., 'Experiments on a Turbulent Jet in a Cross Flow,' AIAA Journal, Vol.10, no. 11, Nov. 1972, pp. 1425-1429.

[24] Greber, I. and Kamotani, Y., 'Experiments on Confined Turbulent Jets in Crossflow,' NASA CR-2392, 1974.

[25] Kelso, R. and Smits, A., 'Horseshoe Vortex Systems Resulting from the Interaction between a Laminar Boundary Layer and a Transverse Jet,' Physics of Fluids, Vol. 7, no.1, Jan. 1995, pp153-158.

[26] Nejad, A., Fuller, R., and Kirkendall, K., 'Breakup Processes of Liquid Jets in Subsonic Crossflows,' AIAA 96-3024, 32nd AIAA/ASME/SAE/ASEE Joint Propulsion Conference and Exhibit, Lake Buena Vista, FL, Jul. 1-3, 1996.

[27] Faeth, G., Dai, Z., and Mazallon, J., 'Primary Breakup of Non-turbulent Round Liquid Jets in Gas Crossflows,' Atomization and Sprays, Vol. 9, 1999, pp.291-311.

[28] Gonçalves, J., Martins-Costa, M. and Coury, J., 'Trajectory of a Liquid Jet Transversally Injected into a Subsonic Gas Stream,' Enpromer'99- II Congresso de Engenharia de Processos do MERCOSUL, 30 Aug.- 2 Sept., 1999.

[29] Johari, H., Hermanson, J. and Pacheco-Tougas, M., 'Penetration and Mixing of Fully Modulated Turbulent Jets in Crossflow,' AIAA Journal Vol. 37, No. 7, Jul. 1999, pp.842-850.

[30] Kennedy, K., Jackson, T. and Lin, K., 'Spray Structures of Aerated-liquid Jets in Subsonic Crossflows,' AIAA 2001-0330, 39th AIAA Aerospace Sciences Meeting and Exhibit, Reno, NV, Jan. 8-11, 2001.

[31] Aso, S., Yamane, Y., Ando, Y., Umii, K., Tokunaga, K. and Sakata, K., 'A Study on Supersonic Mixing Flowfield with Swept Ramp Injectors,' AIAA 97-0397, 35th AIAA Aerospace Sciences Meeting and Exhibit, Reno, NV, Jan. 6-9, 1997.

[32] Mathur, T., Gruber, M., Donbar, J., Jackson, T., Eklund, D., and Billig, F., 'Performance of an Aerodynamic Ramp Fuel Injector in a Scramjet Combustor,' AIAA 2000-3708, 36th AIAA/ASME/SAE/ASEE Joint Propulsion Conference and Exhibit, Huntsville, AL, Jul. 16-19, 2000.

[33] Nishioka, M., Wendt, M. and Sunami, T., 'Supersonic Mixing and Combustion Control Using Streamwise Vortices,' AIAA 98-3271, 34th AIAA/ASME/SAE/ASEE Joint Propulsion Conference & Exhibit, Cleveland, OH, Jul. 13-15, 1998.

[34] Chen, T., Creese, A., Dasgupta, S., Fuller, R. and Wu, P., 'Combustion and Mixing Studies in Compressible Flows,' WL-TR-96-2129, Taitech Inc., Sept., 1996.

[35] Burnes, R., Parr, T. and Wilson, K., 'Investigation of Supersonic Mixing Control Cavities: Effect of Fuel Injection Location,' AIAA 2000-3618, 36th AIAA/ASME/SAE/ASEE Joint Propulsion Conference, Huntsville, AL, Jul. 16-19, 2000.

[36] Yu, K. and Nenmeni, V., 'Cavity-Induced Mixing Enhancement in confined Supersonic Flows,' AIAA 2002-1010, 40th Aerospace Sciences Meeting and Exhibit, Reno, NV, Jan. 14-17,2002.

[37] Seiner, J., Dash, S. and Kenzakowski, D., 'Historical Survey on Enhanced Mixing in Scramjet Engines,' AIAA 99-4869, 9th International Space Planes and Hypersonic Systems and Technologies Conference and 3rd Weakly Ionized Gases Workshop, Norfolk, VA, Nov. 1-5, 1999.

[38] Miyake, R., Lammerink, T., Elwenspoek, M. and Fluitman, J., 'Micro Mixer with Fast Diffusion,' Proc. IEEE MEMS Workshop, Fort. Lauderdale, FL, 1993, pp. 248-253.

[39] Whitesides, G. 'Chaotic Mixer for Micro-channels,' Science, Vol. 295, 25 Jan., 2002, pp.647-651.

[40] Beebe, D., Aref, H., Adrian, R., Santiago, J., Olsen, M., Sharp, K., Stremler, M. and Liu, R., 'Passive Mixing in a 3-D Serpentine Micro-channel,' Journal of Microelectromechanical Systems, Vol. 9, No. 2, June 2000.

[41] Evans, J. Liepmann, D. and Pisano, A., 'Planar Laminar Mixer,' Proc. IEEE MEMS Workshop, Nagoya, Japan, 1997, pp. 96-101.

[42] Branebjerg, J., Gravesen, P., Krog, J. and Nielsen, C., 'Fast Mixing by Lamination,' Proceedings of the IEEE MEMS Workshop, San Diego, CA, 1996, pp. 441-446.

[43] Betz, D., 'Physical Mechanisms of Mixing,' Ph.D. Thesis, UCSB, June 2001.

[44] Choudhuri, A., Camacho, J., Wicker, R., and Gollahalli, S., "Characteristics of Microjet Diffusion Flames," AIAA 2002-4019, 38th AIAA/ASME/SAE/ASEE Joint Propulsion Conference and Exhibition, Indianapolis, IN, Jul. 7-10, 2002.

[45] Anchondo, I. and Choudhuri, A., "An Investigation on the Mixing and Flame Behavior of Microcombustors," AIAA. 2003-4635, 39th AIAA/ASME/SAE/ASEE Joint Propulsion Conference and Exhibit, Huntsville, AL, Jul. 20-23, 2003.

[46] Ahmed, M., Anchondo, I., and Choudhuri, A., "Mixing Dynamics of a Channel Type Micro-combustor," AIAA. 2004-3711, 40th AIAA/ASME/SAE/ASEE Joint Propulsion Conference and Exhibit, Fort Lauderdale, FL, Jul. 11-14, 2004.

[47] Cornell W. and Ohio, E., 'The Flow in a Vee-Gutter Cascade,' Transactions of the ASME, Vol. 78, 1956, pp.573-580.

[48] Ames, L., 'Interference Effects between Multiple Bluff-body Flameholders,' Engineer's Thesis, Caltech, Jan. 1956.

[49] Potter, A. and Wong, E., 'Effect of Pressure and Duct Geometry on Bluff Body Flame Stabilization,' NASA TN-4381, 1958.

[50] Bardon, M., Carrier, D., and De Champlain, A., 'Direct Fuel Injection for Bluff Body Flame Stabilization,' AIAA 96-3032, 32nd AIAA/ASME/SAE/ASEE Joint Propulsion Conference and Exhibit, Lake Buena Vista, FL, Jul. 1-3, 1996.

[51] Roquemoore, W., Shouse, D., Hancock, R., Ehret, J. and Zelina, I., 'Ultra-compact Combustion Technology Using High Swirl for Enhanced Burning Rate,' AIAA 2002-3725, 38th AIAA/ASME/SAE/ASEE Joint Propulsion Conference and Exhibit, Indianapolis, IN, Jul. 7-10, 2002.

[52] Hanson, R. and Ben-Yakar, A., 'Supersonic Combustion of Cross-flow Jets and the Influence of Cavity Flame Holders,' AIAA 1999-0484, 37th Aerospace Sciences Meeting and Exhibit, Reno, NV, Jan.11-14, 1999.

[53] Mathur, T., Streby, G., Gruber, M., Jackson, K., Donbar, J., Donaldson, W., Jackson, T., Smith, C., and Billig, F., 'Supersonic Combustion Experiments with a Cavity-Based Fuel Injector,' AIAA 99-2102, 35th AIAA/ASME/SAE/ASEE Joint Propulsion Conference and Exhibit, Jun. 20-23, 1999.

[54] Sung, C., Li, J., Chang, X., Chen, L. and Yu, G., 'Investigation of Fuel Injection and Flame Stabilization in Liquid Hydrocarbon-Fueled Combustors,' AIAA 2001-3608, 37th AIAA/ASME/SAE/ASEE Joint Propulsion Conference and Exhibit, Salt Lake City, UT, Jul. 8-11, 2001.

[55] Bowersox, R., and Davis, D., 'Stirred Reactor Analysis of Cavity Flame Holders for Scramjets,' AIAA 97-3274, 33rd AIAA/ASME/SAE/ASEE Joint Propulsion Conference and Exhibit, Seattle, WA, Jul. 6-9, 1997.

[56] Mohieldin, T., Tiwari, S., and Taha, A., 'Pilot Injection and Flame Characteristics of Propane Combustion in Scramjet Engines,' AIAA 2002-4276, 38th AIAA/ASME/SAE/ASEE Joint Propulsion Conference and Exhibit, Indianapolis, IN, Jul. 7-10, 2002.

[57] Fernandez-Pello, C., Fu, K., Knobloch, F., Martinez, F., Walther, D., Pisano, A., Liepmann, D., Miyaska, K., and Maruta, K., "Design and Experimental Results of Small-scale Rotary Engines," Proc. 2001 International Mechanical Engineering Congress and Exposition, IMECE2001/MEMS-2394, New York, Nov. 11-16, 2001.

[58] Dahm, W., Ni, J., Mijit, K., Mayor, R., Qiao, G., Benjamin, A., Gu, Y., Lei, Y. and Papke, M., "Micro Internal Combustion Swing Engine (MISCE) for Portable Power Generation Systems," AIAA 2002-0722, 40th Aerospace Sciences Meeting, Jan. 14-17, 2002, Reno., NV.

[59] Faulkner, J., Scarborough, D. and Jagoda, J., 'A Study of Ignition and Flame Propagation in a Small, High Surface-to-Volume Ratio Combustor,' AIAA 2000-0591, 38th Aerospace Sciences Meeting and Exhibit, Reno, NV, Jan. 10-13, 2000.

[60] Gollahalli, S., Choudhuri, A., Camacho, J. and Wicker, R., 'Characteristics of Microjet Diffusion Flames', AIAA 2002-4019, 38th AIAA/ASME/SAE/ASEE Joint Propulsion Conference and Exhibition, Indianapolis, Jul. 7-10, 2002.

[61] Lee, D. and Kwon, S., 'Heat Transfer and Quenching Analysis of Combustion in a Micro-combustion Vessel,' Journal of Micromechanics and Microengineering, Vol. 12, pp.670-676, 2002.

[62] Leach, T. and Cadou, C., 'The Role of Structural Heat Exchange and Heat Loss in the Design of Efficient Silicon Micro-Combustors,' Proceedings of the Combustion Institute, Vol. 30, 2005, pp. 2437-2444.

[63] Tennekes, H. and Lumley, J., A First Course in Turbulence, MIT Press, Cambridge, MA, 1973, pp. 8-10.

[64] White, F., Fluid Mechanics, 4th Ed., Mc Graw-Hill, New York, 1999, pp.330-349.

[65] Morini, G., 'Laminar-to-turbulent Flow Transition in Micro-channels,' presented at the International Symposium on Micro/Nano-scale Energy Conversion and Transport Phenomena, Antalya, Turkey, Apr. 14-19, 2002.

[66] Peng, X., Peterson, G. and Wang, B., 'Frictional Flow Characteristics of Water Flowing Through Micro-channels,' Exp. Heat Transfer, Vol. 7, 1994, pp. 249-264.

[67] Choi, S., Barron, R. and Warrington, R., 'Liquid Flow and Heat Transfer in Micro-tubes,' Micromechanical Sensors, Actuators and Systems, ASME DSC, Vol. 32, 1991, pp. 123-128.

[68] Ismagilov, R., Lyon, A., Song, H. and Tice, J., 'Formation of Droplets and Mixing in Multiphase Microfluidics at Low Values of the Reynolds and the Capillary Numbers,' Langmuir, Vol.19, 2003, pp.9127-9133

[69] Purcell, E., 'Life at Low Reynolds Number,' American Journal of Physics, Vol. 45, pp. 3-11, 1977.

[70] Platten, J. L. and Keffer, J. F., 'Deflected Turbulent Jet Flows', Transactions of the ASME, Journal of Applied Mechanics, 1971, pp. 756-758.

[71] Smith, S., Hasselbrink, E., Mungal, M. and Hanson, R., "The Scalar Concentration Field of the Axisymmetric Jet in Crossflow," AIAA 96-0198, 34th Aerospace Sciences Meeting and Exhibit, Reno, NV, 15-18 Jan., 1996.

[72] Holdemann, J. and Walker, R., 'Mixing of a Row of Jets with a Confined Crossflow,' AIAA Journal Vol. 15, no. 2, Feb. 1977, pp.243-249.

[73] Samuelsen, D., Leong, M. and Mc Donnell, V., 'Effect of Ambient Pressure on an Airblast Spray Injected into a Crossflow,' AIAA 98-3903, 34th AIAA/ASME/SAE/ASEE Joint Propulsion Conference and Exhibit, Cleveland, OH, Jul. 13-15, 1998.

[74] Schetz, J. and Padhye, A., 'Penetration and Breakup of Liquids in Subsonic Airstreams,' AIAA Journal Vol. 15, No. 10, Oct. 1977, pp.1385-1390.

[75] Lefebvre, A., Gas Turbine Combustion, Taylor & Francis Pub., 1983, pp. 117-120.

[76] Mattingly, J. D., Heiser, W. H. and Daley, D. H., Aircraft Engine Design, AIAA Education Series, AIAA, Washington DC, 1987, pp.301-303.

[77] Bird, B., Stewart, W. and Lightfoot, E., Transport Phenomena, John Wiley and Sons, 1960, pp.495-546.

[78] Burke, S. and Schumann, T., 'Diffusion Flames,' Combustion Institute, 1st Symposium on Combustion, 1928, pp. 2-11.

[79] Kuo, K., Principles of Combustion, John Wiley & Sons, Inc., New York, NY, 1986, pp. 347-356.

[80] Ottino, M., The Kinematics of Mixing: Stretching, Chaos and Transport, Cambridge University Press, New York, 1989, pp.1-15.

[81] ESI U.S. R&D, Inc., 'CFD-ACE+ V2004 Modules Manual- Volume 1,' ESI U.S. R&D, May 2004.

[82] Schlichting, H., Boundary-Layer Theory, 7th Ed., McGraw-Hill, New York, 1979, pp.47-69.

[83] Oldshue, J., Fluid Mixing Technology, Mc Graw-Hill, New York, 1983, pp. 224-229.

[84] Brasoveanu, D., 'Analysis of Gaseous Fuel-air Mixing and Flame Stability,' Ph.D. Thesis University of Maryland, 1997.

[85] Broadwell, J., and Briedenthal, R., 'A Simple Model of Mixing and Chemical Reaction in a turbulent Shear Layer,' Journal of Fluid Mechanics, Vol. 125, 1982, pp. 397-410.

[86] Nikuradse, J., 'Strömungsgestze in Rauhen Rohren,' VDI Forschungsh, Vol. 361, 1933; English translation, NACA TM 1292.

[87] Colebrook, C., 'Turbulent Flow in Pipes, with Particular Reference to Transition between Smooth and Rough Pipe Laws,' Journal of the Institution of Civil Engineering, London, Vol. 11, 1938-1939, pp. 133-156.

[88] Kobayashi, T., Hu, H., Saga, T. and Taniguchi, N., 'Passive Control on Jet Mixing Flows by Using Vortex Generators,' Proceedings of the Sixth Triennial International Symposium on Fluid Control, Measurement and Visualization, Sherbrooke, Canada, Aug. 13-17, 2000.

[89] Zaman, K., 'Stream-wise Vorticity Generation and Mixing Enhancement in Free Jets by Delta-Tabs,' NAS 1.15:106235, 1993.

[90] Brown, W., 'Enhancement of Mixing in a Rectangular Jet by Mechanical Tabs,' NAS 1.26: 185207, Apr., 1990.

[91] Kobayashi, T., Hui, H., Wu, S. and Shen, G., 'Changes to the Vortical and Turbulent Structure of Jet Flows Due to Mechanical Tabs,' Proceedings of the Institution of Mechanical Engineers Part C, Journal of Mechanical Engineering Science, Vol. 213, 1999, pp.321-329.

[92] Yu, S., Hou, Y. and Low, S., 'The Flow Characteristics of a Confined Square Jet With Mixing Tabs,' Proceedings of the Institution of Mechanical Engineers Part C, Journal of Aerospace Engineering, Vol. 212, 1998, pp.63-76.

[93] Schadow, K., Sabel'nikov, V. and Koronstvit, Y., 'Investigation of Supersonic Combustion Using Barbotage and Injectors with Non-Circular Nozzles,' AIAA 98-1516, 8th AIAA International Space Planes and Hypersonic Systems and Technologies Conference, Norfolk, VA, Apr. 27-30, 1998.

[94] Reeder, M., Samimy, M., and Elliott, G., 'Investigation of The Effect of Tabs on Supersonic Jets Using Advanced Diagnostics,' Journal of Propulsion and Power, Vol.12, No. 4, 1996, pp. 742-751.

[95] Peacock, T., Bradley, E., Hertzberg, J., and Lee, Y., 'Forcing A Planar Jet Flow Using MEMS,' Experiment in Fluids, Vol. 37, No. 1, 2004, pp. 22-28.

[96] Gad-el-Hak, 'Modern Developments in Flow Control,' Applied Mechanics Review, Vol. 49, No. 7, 1996, pp. 365-380.

[97] Corke, T., and Cavalieri, D., 'Mode Excitation in a Jet at Mach 0.85,' 49th American Physical Society Meeting, DFD, Syracuse, NY, 1996.

[98] Raman, G., 'Enhanced Mixing of an Axisymmetric Jet by Aerodynamic Excitation,' Masters Thesis, Cleveland State University, Mar. 1986.

[99] Matta, L., Johnson, C., Jagoda, J. and Zinn, B., 'Jet Mixing Enhancement Using Acoustically Induced Swirling Bifurcation,' AIAA 97-0148, 35th AIAA Aerospace Sciences Meeting and Exhibit, Reno, NV, Jan. 6-9, 1997.

[100] Prakesh, D., Kibens, V., Glezer, A., Wiltse, J. and Smith, D., 'Innovative Jet Flow Control- Mixing Enhancement Experiments,' AIAA 96-0308, 34th AIAA Aerospace Sciences Meeting and Exhibit, Reno, NV, Jan. 15-18, 1996.

[101] Pothos, S., and Longmire, E., 'Asymmetric Forcing of a Turbulent Rectangular Jet with a Piezoelectric Actuator,' Physics of Fluids, Vol. 13, No. 5, May, 2001, pp. 1480-1491.

[102] Smith, B. and A. Glezer, 'Vectoring And Small-Scale Motions Effected In Free Shear Flows Using Synthetic Jet Actuators,' AIAA 97-0213, 35th Aerospace Sciences Meeting, Reno NV, January 1997.

[103] Freund, J., and Moin, P., 'Jet Mixing enhancement by High-Amplitude Fluidic Actuation: Direct Numerical Simulations,' Proceedings of the ASME Fluids Engineering Division Summer Meeting, Washington, DC, June 21st-25th, 1998.

[104] Freund, J., and Moin, P., 'Jet Mixing Enhancement by High-Amplitude Fluidic Actuation,' AIAA Journal, Vol. 38, No. 10, Oct. 2000.

[105] Stromberg, J., McLaughlin, D. and Troutt, T., 'Flowfield and Acoustic Properties of a Mach Number 0.9 Jet at Low Reynolds Number,' Journal of Sound and Vibration, Vol. 72, No. 2, 1980, pp. 159-176.

[106] Heatwole, S., Veeraragavan, A., Buckley, S. and Cadou, C., 'In-situ Diagnostic Measurements in Micro-combustors,' submitted to Combustion and Flame 2005.

[107] Kirby, B. J., and Hanson, R. K., 'Imaging of CO and CO2 Using Planar Laser-Induced Fluorescence,' Proc. of the Combustion Institute, Vol. 28, 2000, pp. 253-259.